DESIGN AND IMPLEMENTATION OF A FREE PISTON COMPRESSOR

By

José A. Riofrío

Thesis

Submitted to the Faculty of the

Graduate School of Vanderbilt University

in partial fulfillment of the requirements

for the degree of

MASTER OF SCIENCE

in

Mechanical Engineering

December, 2005

Nashville, Tennessee

Approved:

Professor Eric J. Barth

Professor Robert W. Pitz

Professor Michael Goldfarb

ACKNOWLEDGMENTS

First and foremost I would like to express my most sincere gratitude and appreciation to my advisor, Dr. Eric Barth, for giving me this opportunity. His constant guidance throughout this work was both challenging and inspiring. I am also grateful for all the help provided by Dr. Michael Goldfarb, Dr. Kevin Fite, Dr. Bobby Shields, and Dr. Robert Pitz, who patiently shared their expertise in various aspects relating to this work.

My learning experience at Vanderbilt has been greatly influenced by professors, peers, and staff members. Special thanks go to Dr. Ken Frampton, Dr. Nilanjan Sarkar, Yong Zhu, Dr. Navneet Gulatti, Joshua Schultz, Mark Adams, Tyler Li, Amit Bohara, Xiangrong Xen, Peter Schmidt, Chakradhar Byreddy, Bibhrajid Halder, Steve Williams, Jason Mitchell, Myrtle Daniels, Jean Miller, and Walt Bieschke.

Finally, I'd like to especially thank the Vanderbilt University Discover Grant for its financial contribution.

TABLE OF CONTENTS

LIST OF FIGURES

LIST OF TABLES

CHAPTER I

INTRODUCTION AND BACKGROUND

Introduction

The need for an effective portable power supply for human-scale robots has increasingly become a matter of interest in robotics research. Current prototypes of humanoid robots, such as the Honda P3, Honda ASIMO and the Sony QRIO, show significant limitations in the capacity of their power sources in between charges (the operation time of the humanoid-size Honda P3, for instance, is only 25 minutes). This limitation becomes a strong motivation for the development and implementation of a more adequate source of power. Moreover, the power density of the actuators coupled to the power source needs to be maximized such that, on a systems level evaluation, the combined power supply and actuation system is both energy and power dense. Put simply, state-of-the-art batteries are too heavy for the amount of energy they store, and electric motors are too heavy for the mechanical power they can deliver, in order to present a viable combined power supply and actuation system capable of delivering human-scale mechanical work in a human-scale self contained robot package, for a useful duration of time. The motivation details are discussed more thoroughly in [4].

The total energetic merit of an untethered power supply and actuation system is a combined measure of 1) source energy density of the energetic substance being carried, 2) efficiency of conversion to controlled mechanical work, 3) energy converter mass, and 4) power density of the actuators. With regard to a battery powered electric motor

actuated system, the efficiency of conversion from stored electrochemical energy to shaft work after a gear head can be high (~50%) with very little converter mass (e.g. PWM amplifiers); however, the energy density of batteries is relatively low (about 180 kJ/kg for NiMH batteries), and the power density of electrical motors is not very high (on the order of 50 W/kg), rendering the overall system heavy in relation to the mechanical work that it can output. With regard to the hydrocarbon-pneumatic power supply and actuation approach presented here relative to the battery/motor system, the converter mass is high and the total conversion efficiency is shown to be low. However, the energy density of hydrocarbon fuels, where the oxidizer is obtained from the environment and is therefore free of its associated mass penalty, is in the neighborhood of 45 MJ/kg, which is more than 200 times greater than the energy density of state of the art electrical batteries. This implies that even with poor conversion efficiency (poor but within the same order of magnitude), the available energy to the actuator per unit mass of the energy source is still at least one order of magnitude greater than the battery/motor system. Additionally, linear pneumatic actuators have roughly one order of magnitude greater power density than state of the art electrical motors. Therefore, the proposed technology yields an increased energetic merit on an overall systems level.

The free piston compressor (FPC) presented in this work serves the function of converting chemically stored energy of a hydrocarbon into pneumatic potential energy of compressed air. More specifically, it extracts the energy by producing combustion of a stoichiometric mixture of propane and air, and the combustion-driven free piston acts as an air pump to produce the compressed air.

Previous Work

The idea of using a free piston combustion-based device as a pump has been around since the original free-piston patent by Pescara in 1928 [7]. The automotive industry conducted a large amount of research in the 1950's. Ford Motor Company considered the use of a free piston device as a gasifier in 1954 [5]. General Motors presented the "Hyprex" engine in 1957 [8]. Such endeavours were aimed at an automotive scale engine and were largely unsuccessful. In more recent times, the free piston engine concept has been considered for small-scale power generation. Aichlmayr, et. al. [1, 2] have considered the use of a free piston device as an electrical power source on the 10 W scale meant to compete with batteries. Beachley and Fronczak [3], among others, have considered the design of a free-piston hydraulic pump. McGee, et. al. have considered the use of a monopropellant-based catalytic reaction as an alternative to combustion, as applied to a free piston hydraulic pump [6].

Contribution

Even though free piston devices have been studied in the past, none of these previous designs explicitly featured what is perhaps the main advantage of a free piston, which is its capability to offer a purely inertial load. The main focus of this work is to exploit the fact that a free piston can present a purely inertial load to the combustion, and as a result, desirable operational characteristics can be obtained, such as high efficiency, low noise, and low temperature operation. Additionally, this work aims to demonstrate that a free piston compressor stands as a strong candidate for a portable power supply system for untethered human-scale pneumatic robots.

Overview

The work presented here is comprised of four independent manuscripts (Chapter II through Chapter V). The first three manuscripts are currently published in conference proceedings, and the last one was written for submission to a journal archival . Chapter II (Manuscript 1) introduces the FPC design concept and presents an analytical model with regard to general design considerations. Figure 1-1 shows a schematic of the generalized FPC concept. The model obtained in Chapter II was derived from both a thermodynamic and a dynamic analysis, with the main goal of finding a theoretical overall system efficiency (with and without heat losses). Another important feature presented in Chapter II is the effect of inertial loading in terms of the theoretical efficiency of converting chemically stored energy of a hydrocarbon into kinetic energy of the free piston. Additionally, other characteristics of the FPC were analyzed, such as: Reinvestment of air mass from the air tank for combustion, injection pressure, and efficiency of converting kinetic energy of the free piston into potential energy of compressed air.

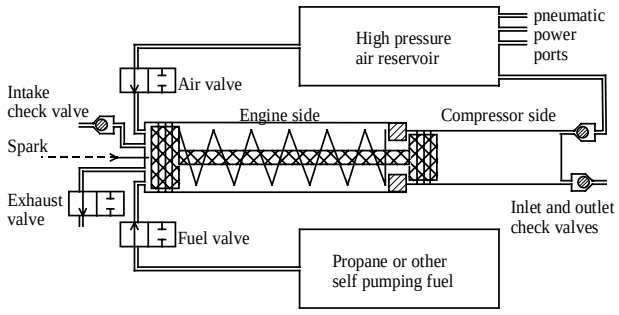

Figure 1-1. Schematic of the free piston compressor system.

Chapter III (Manuscript 2) presents the first hardware prototype of an FPC. This design featured a ‘pump on return’ mechanism, as seen in Figure 1-2, where combustion

and compression occurred in separate cylinders and on adverse strokes. This chapter focuses mainly on the combustion portion of the process, and presents in detail all the main features of the free piston engine, such as efficiency, low noise, self-cooling mechanism, start on demand, and simplicity. It also addresses important practical issues such as air/fuel mixture, injection pressure, inertia, and thermal management. Experimental results showed a nearly adiabatic expansion of the combustion gases, and a respectable efficiency converting chemically stored energy of propane into kinetic energy of the free piston. However, this prototype showed significant limitations in the pumping phase. Specifically, these were due mostly to frictional losses and hardware non-idealities, all which suggested a different configuration altogether.

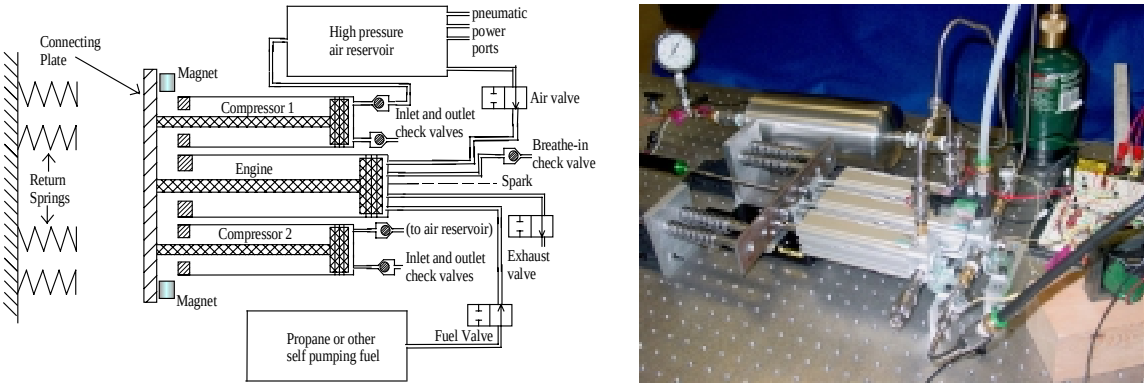

Figure 1-2: Schematic (left) and picture (right) of 'pump on return' FPC prototype.

Chapter IV (Manuscript 3) addresses the limitations presented in Chapter III, and presents a new version of an FPC. This new prototype features combustion and pumping within the same stroke, and the experimental setup, shown in Figure 1-3, is very similar to the generalized schematic shown in Figure 1-1. The use of more adequate hardware components minimized inertial resistances such as frictional losses and flow obstructions,

and successful pumping was obtained up to 310 kPa. This chapter also presents a more effective way of measuring the mass of propane for each combustion cycle, and experimentally calculates the overall efficiency of the system. Finally, based on the experimentally obtained efficiency, a numerical analysis comparing the FPC to state-of-the art systems is presented.

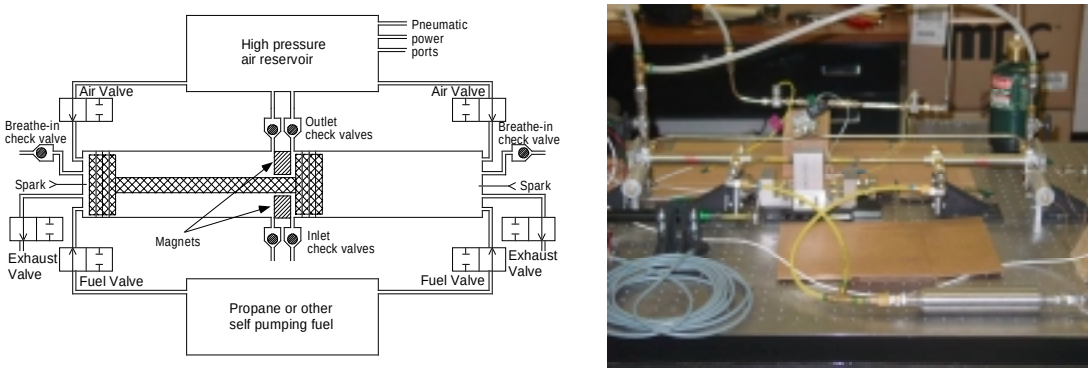

Figure 1-3: Schematic (left) and picture (right) of new version of FPC.

Lastly, Chapter V (Manuscript 4) was written in the format of an independent journal article, and combines the work presented in Chapters II through IV.

References

[1] Aichlmayr, H. T., Kittelson, D. B., and Zachariah, M. R., "Miniature free-piston homogenous charge compression ignition engine-compressor concept – Part I: performance estimation and design considerations unique to small dimensions," *Chemical Engineering Science*, 57, pp. 4161-4171, 2002.

[2] Aichlmayr, H. T., Kittelson, D. B., and Zachariah, M. R., "Miniature free-piston homogenous charge compression ignition engine-compressor concept – Part II: modeling HCCI combustion in small scales with detailed homogeneous gas phase chemical kinetics," *Chemical Engineering Science*, 57, pp. 4173-4186, 2002.

[3] Beachley, N. H. and Fronczak, F. J., "Design of a Free-Piston Engine-Pump," *SAE Technical Paper Series*, 921740, pp. 1-8, 1992.

[4] Goldfarb, M., Barth, E. J., Gogola, M. A., Wehrmeyer, J. A., "Design and Energetic Characterization of a Liquid-Propellant-Powered Actuator for Self-Powered Robots". *IEEE/ASME Transactions on Mechatronics*, vol. 8, no. 2, pp. 254-262, June 2003.

[5] Klotsch, P., "Ford Free-Piston Engine Development," *SAE Technical Paper Series*, 590045, vol. 67, pp. 373-378, 1959.

[6] McGee, T. G., Raade, J. W., and Kazerooni, H., "Monopropellant-Driven Free Piston Hydraulic Pump for Mobile Robotic Systems," *ASME Journal of Dynamic Systems, Measurement, and Control*, vol. 126, pp. 75-81, March 2004.

[7] Pescara, R. P., "Motor Compressor Apparatus," U.S. Patent No. 1,657,641, Jan. 31, 1928.

[8] Underwood, A. F., "The GMR 4-4 'Hyprex' Engine: A Concept of the Free-Piston Engine for Automotive Use," *SAE Technical Paper Series*, 570032, vol. 65, pp. 377-391, 1957.

CHAPTER II

MANUSCRIPT 1

DYNAMIC CHARACTERISTICS OF A FREE PISTON COMPRESSOR

Eric J. Barth and José Riofrio

Department of Mechanical Engineering

Vanderbilt University

Nashville, TN 37235

(Accepted by *ASME International Mechanical Engineering Congress and Exposition (IMECE)*, Anaheim, CA, November 2004)

Abstract

The design and dynamic characterization of a free piston compressor is presented in this paper. The free piston compressor is a proposed device that utilizes combustion to compress air into a high-pressure supply tank. The device is configured such that the transduction from thermal energy to stored energy, in the form of compressed gas, is efficient relative to other small-scale portable power supply systems. This efficiency is achieved by matching the dynamic load of the compressor to the ideal adiabatic expansion of the hot gas combustion products. It is shown that a load that is dominantly inertial provides a nearly ideally matched load for achieving high thermodynamic efficiency in a heat engine. The device proposed exploits this fact by converting thermal energy first into kinetic energy of the free piston, and then compressing air during a separate compressor phase. The proposed technology is intended to provide a compact pneumatic power supply source appropriate for human-scale robots. The combined factors of a high-energy density fuel, the efficiency of the device, the compactness and low weight of the device, and the use of the device to drive lightweight linear pneumatic actuators (lightweight as compared with power comparable electric motors) is projected to provide at least an order of magnitude greater total system energy density (power supply and actuation) than state of the art power supply (batteries) and actuators (electric motors) appropriate for human-scale power output. An analytical model of the proposed device is developed and simulation results are discussed.

Introduction

The idea of using a free piston combustion-based device as a pump has been around since the original free-piston patent by Pescara in 1928 [7]. The automotive industry

conducted a large amount of research in the 1950's. Ford Motor Company considered the use of a free piston device as a gasifier in 1954 [5]. General Motors presented the "Hyprex" engine in 1957 [8]. Such endeavors were aimed at an automotive scale engine and were largely unsuccessful. In more recent times, the free piston engine concept has been considered for small-scale power generation. Aichlmayr, et. al. [1, 2] have considered the use of a free piston device as an electrical power source on the 10 W scale meant to compete with batteries. Beachley and Fronczak [3], among others, have considered the design of a free-piston hydraulic pump. McGee, et. al. have considered the use of a monopropellant-based catalytic reaction as an alternative to combustion, as applied to a free piston hydraulic pump [6].

Following from the motivations outlined in [4], the free piston compressor presented here is intended as a power supply for a mobile robotic system of human comparable power, mass and size. In this paper it is shown that the use of a free piston engine as a direct air compressor offers nearly ideal loading characteristics necessary for high efficiency, in a simple and small package. Indeed the original patent by Pescara [7] intended the free piston engine foremost as a compressor. It is additionally shown that such a device can run at low temperatures and with low noise relative to other internal combustion devices.

An outline of this paper is as follows. Section 2 describes the proposed device and its operation. Section 3 presents an idealized thermodynamic analysis of the engine side and the compressor side separately. This analysis yields a set of relationships that are useful for design specifications regarding, among other things, the selection of a propellant, the required mass of combustion gasses, the combustion chamber volume, and the required compressor chamber volume, for nominal operation at maximum efficiency. Section 4

presents a dynamic model of the system that more accurately models the interaction of the engine side and the compressor side, in addition to providing the capability of modeling the effects of heat losses, friction, valve losses, and other influences.

The Free Piston Compressor

A schematic of the free piston compressor system is shown in Figure 2-1. As shown in its original position, the device operates by first opening the air and fuel valves to allow the proper mixture and amount of air and fuel into the combustion chamber of the engine side. Once the proper air/fuel mixture is inside, the valves close and a spark initiates the combustion. Upon combustion, the free piston moves to the right as the combustion gases expand, converting the energy of combustion into kinetic energy of the free piston. The compressor side of the device is configured such that the piston sees a negligible compressive force for a distance greater than required for the combustion chamber to both expand down to atmospheric pressure, and allowed to intake fresh cool air to cool the exhaust products through the intake check valve. After this point the kinetic energy of the free piston is converted into the work required to compress and then pump the gasses in the compressor chamber into the high-pressure reservoir. The cycle is completed when the light return spring moves the piston to the left pushing out the diluted exhaust products of the engine side, and refilling the compressor side with air drawn in through an inlet check valve.

Besides advantages regarding efficiency, the free piston compressor offers on-demand start and stop (since there is no compression stroke in the engine side), cool operation (given that the combustion products are greatly diluted with air after expanding

down below atmospheric pressure), quiet operation (given that there is no exhaust of high-pressure gasses), and simple.

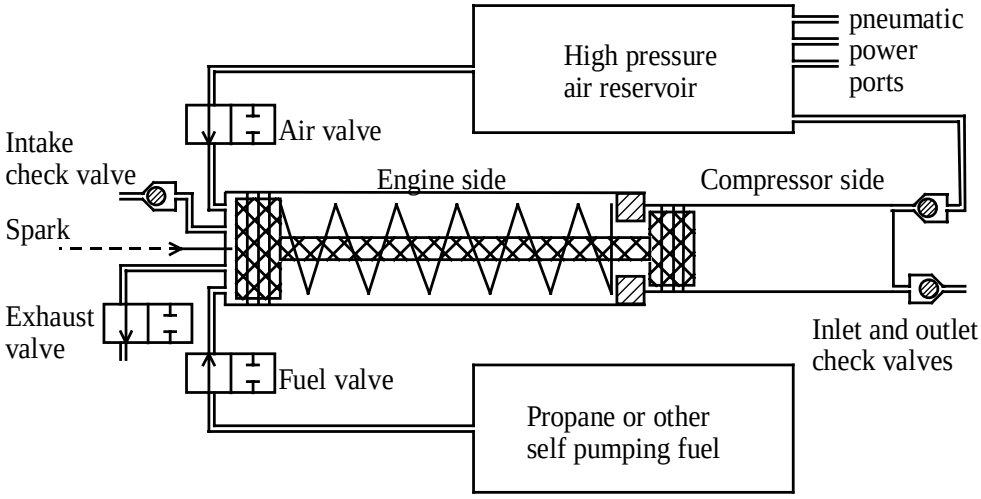

Figure 2-1: Schematic of the free piston compressor system.

Thermodynamic Model

The thermodynamic analysis below reveals a number of design constraints and key relationships regarding the dependency of efficiency on certain design variables.

Engine side

The engine side of the free piston compressor converts the energy of combustion into kinetic energy of the free piston, while the compressor side then converts this kinetic energy into stored compressed gas in the high-pressure reservoir. Presenting a purely inertial load during the expansion of the combustion products allows the right loading characteristics such that the high-pressure combustion products are allowed to fully expand down to atmospheric pressure. When this is the case, and assuming an adiabatic

process in the combustion chamber, the work done on the inertial load will be equal to the following,

$$W_e = \frac{P_{e0}V_{e0}^{\gamma_e}}{1-\gamma_e}\left(V_{ef}^{1-\gamma_e} - V_{e0}^{1-\gamma_e}\right) - P_{atm}\left(V_{ef} - V_{e0}\right) \tag{1}$$

where P_{e0} is the initial combustion pressure, V_{e0} and V_{ef} is the initial and final volume of the combustion chamber respectively, and γ_e is the ratio of specific heats of the combustion gases (products of combustion). Assuming losses associated with friction are negligible, the kinetic energy of the piston will be equal to the work done W_e, when reaching the position associated with the final volume V_{ef}. The combustion chamber volume required such that the combustion gases are allowed to fully expand down to atmospheric pressure under adiabatic conditions can be found as:

$$V_{ef} = \left(\frac{P_{e0}}{P_{atm}}\right)^{1/\gamma_e} V_{e0} \tag{2}$$

Taking the initial combustion pressure P_{e0} as a specifiable quantity (design specification), the required mass of the fuel/air mixture can be found using the ideal gas law as,

$$m_{e0} = \frac{P_{e0}V_{e0}}{R_e T_{AFT}} \tag{3}$$

where R_e is the average gas constant associated with the combustion products, and T_{AFT} is the adiabatic flame temperature.

The efficiency of conversion from the energy available in the combustion products to kinetic energy of the piston is then given by,

$$\eta_{KE} = \frac{W_e}{m_{e0}e} = \left(\frac{R_e T_{AFT}}{e}\right)\left(\frac{\gamma_e P_{e0}^{1/\gamma_e} P_{atm}^{(\gamma_e-1)/\gamma_e} - P_{e0} + (1-\gamma_e)P_{atm}}{(1-\gamma_e)P_{e0}}\right) \tag{4}$$

where Equations (1-3) have been used, and where e is the mass specific energy of the fuel/air mixture computed as the following for the air supported combustion of propane:

$$e = \frac{46350\,\text{kJ}}{\text{kg fuel}} \times \frac{1\,\text{kg fuel}}{16.63\,\text{kg fuel/air mixture}} = 2{,}787{,}000\ \frac{\text{J}}{\text{kg fuel/air mixture}} \tag{5}$$

It is important to note that, for a given fuel, the theoretical adiabatic efficiency of conversion to kinetic energy given by Equation (4) is dependent only on the initial combustion pressure. This relationship for the combustion of propane is shown in Figure 2-2. The dependence on only the initial combustion pressure is markedly different from the Otto cycle's efficiency dependence on the compression ratio. In effect, the free piston compressor establishes an expansion ratio of V_{ef} / V_{e0}, given by Equation (2), based on the initial combustion pressure.

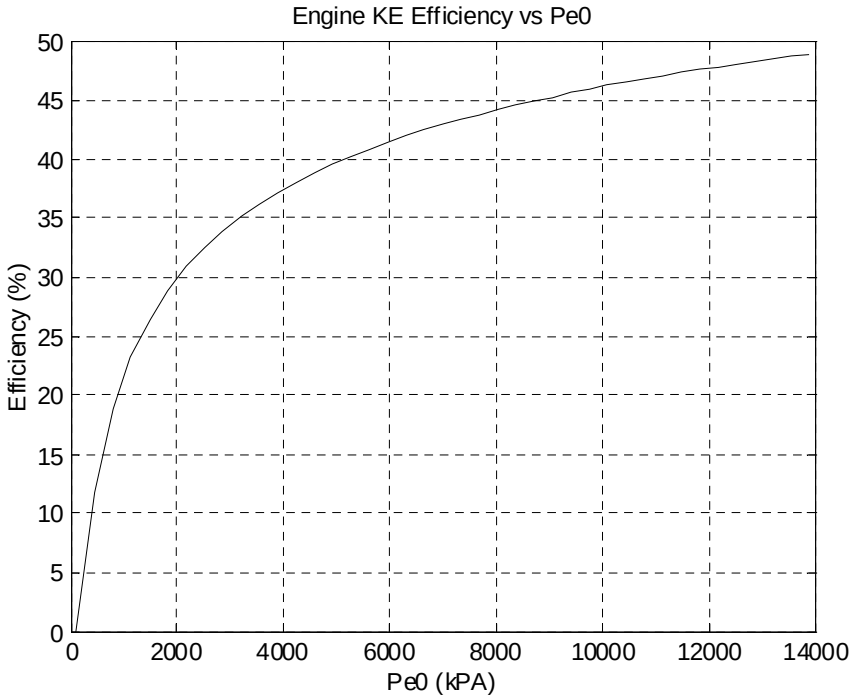

Figure 2-2: The efficiency of converting energy of combustion into kinetic energy of the free piston as a function of the initial combustion pressure.

In order to establish the target initial combustion pressure, the free piston compressor as proposed requires that both the fuel pressure and pressure of the air reservoir are adequate enough to inject the fuel and air mixture into the combustion chamber before combustion occurs. This minimum pressure requirement is given by,

$$P_{inj} = \left(\frac{R_{reac} T_{amb}}{R_e T_{AFT}} \right) P_{e0} \tag{6}$$

where R_{reac} and T_{amb} is the average gas constant of the reactants and the ambient temperature, respectively.

Compressor Side and Reservoir

The theoretical operation of the compressor side can be considered as two processes: firstly, the adiabatic (or polytropic) compression of a gas, and secondly, the constant pressure process of pumping the gas into the high-pressure air reservoir. The work required for these two processes will be provided by the kinetic energy of the free piston as established by the combustion side. Here it is assumed that the length of the device is such that the pressure in the compressor side is negligible until the pressure has reduced to atmospheric and the kinetic energy of the free piston has reached its maximum.

The work associated with the adiabatic compression process is given by the following,

$$W_{c1} = \frac{P_{atm} V_{c0}^{\gamma}}{1-\gamma} \left(V_{ci}^{1-\gamma} - V_{c0}^{1-\gamma} \right) - P_{atm} \left(V_{ci} - V_{c0} \right) \tag{7}$$

where γ is the ratio of specific heats of air, V_{c0} and V_{ci} is the initial volume of the compression chamber where compression begins, and the intermediary volume where pumping begins, respectively. The analysis can be extended to include heat losses in the

compressor by considering a polytropic process whereby γ is reduced but remains greater than unity. The intermediary volume V_{ci} is given by,

$$V_{ci} = \left(\frac{P_{atm}}{P_s} \right)^{1/\gamma} V_{c0} \tag{8}$$

where P_s is the pressure of the high-pressure reservoir. The volume of this air reservoir is assumed to be large enough such that the pressure does not change appreciably over a single stroke of the free piston compressor. The work associated with the constant pressure process of pumping is given by the following:

$$W_{c2} = (P_s - P_{atm})(V_{cf} - V_{ci}) \tag{9}$$

where V_{cf} is the final volume of the compressor side (i.e. the dead volume of the cylinder not able to be pumped out).

For efficient operation of the engine side together with the compressor side, it is assumed that all of the kinetic energy stored in the free piston as a consequence of the combustion is utilized to perform the required work on the compressor side:

$$W_e = -W_{c1} - W_{c2} \tag{10}$$

By using Equation (10), and approximating the dead volume of the compressor side as zero, the following relationship between V_{c0} and V_{e0} is obtained:

$$\frac{V_{e0}}{V_{c0}} = \frac{\dfrac{\gamma P_{atm}}{(1-\gamma)} \left[1 - \left(\dfrac{P_{atm}}{P_s} \right)^{\frac{1-\gamma}{\gamma}} \right]}{\dfrac{P_{e0}}{(1-\gamma_e)} \left[\gamma_e \left(\dfrac{P_{atm}}{P_{e0}} \right)^{\frac{\gamma_e - 1}{\gamma_e}} - 1 + (1-\gamma_e) \left(\dfrac{P_{atm}}{P_{e0}} \right) \right]} \tag{11}$$

Effectively, Equation (11) related the initial volume and pressure of the engine side to the volume and pressure to be compressed and pumped in the compressor side. Using Equations (1) and (7-11), the efficiency of the compressor can thus be found as:

$$\eta_{comp'} = \frac{-W_{c2}}{W_e} = \left(\frac{(1-\gamma)}{\gamma}\right)\left(\frac{\left(\frac{P_{atm}}{P_s}\right)^{\frac{1-\gamma}{\gamma}} - \left(\frac{P_{atm}}{P_s}\right)^{\frac{1}{\gamma}}}{1-\left(\frac{P_{atm}}{P_s}\right)^{\frac{1-\gamma}{\gamma}}}\right) \tag{12}$$

This analysis assumes that the air pumped into the reservoir is at some temperature, higher than the ambient temperature, reached when the volume in the compressor is reduced to V_{ci}. Once the air is in the reservoir, and assuming that the reservoir is large, at constant pressure, and that the residence time of the air is large, this air will cool to the ambient temperature. This heat loss that occurs in the reservoir has an associated efficiency since the energy stored reduces from $(P_s - P_{atm})V_{ci}$ to $(P_s - P_{atm})V_s$, where V_s is the final volume the pumped air eventually takes on in the reservoir. Therefore the efficiency of the initial energy storage to the final is:

$$\eta_{res} = \frac{(P_s - P_{atm})V_s}{(P_s - P_{atm})V_{ci}} = \frac{T_{amb}}{T_{ci}} \tag{13}$$

According to the ideal gas law, the temperature T_{ci} can be found in terms of the mass pumped m_c:

$$T_{ci} = \frac{P_s V_{ci}}{m_c R} \tag{14}$$

where *R* is the gas constant of air. The mass pumped can in turn be written as:

$$m_c = \frac{P_{atm} V_{c0}}{R T_{amb}} \tag{15}$$

Substitution of Equations (14), (15) and (8) into (13) yields the following expression for the efficiency of energy storage of the reservoir:

$$\eta_{res} = \left(\frac{P_{atm}}{P_s} \right)^{\frac{\gamma-1}{\gamma}} \tag{16}$$

The combined efficiency of the compressor converting kinetic energy and the reservoir storing pneumatic energy is thus:

$$\eta_{comp} = \eta_{comp'} \eta_{res} \tag{17}$$

The overall efficiency of the compressor is shown in Figure 2-3. It is important to note that the efficiency is enhanced if heat losses occur in the compressor. This is intuitive considering the compressor must fight against the heat during the compression phase from V_{c0} to V_{ci}. On a design level, this indicates that cooling fins should be placed on the compressor side of the device to promote as much heat loss as possible.

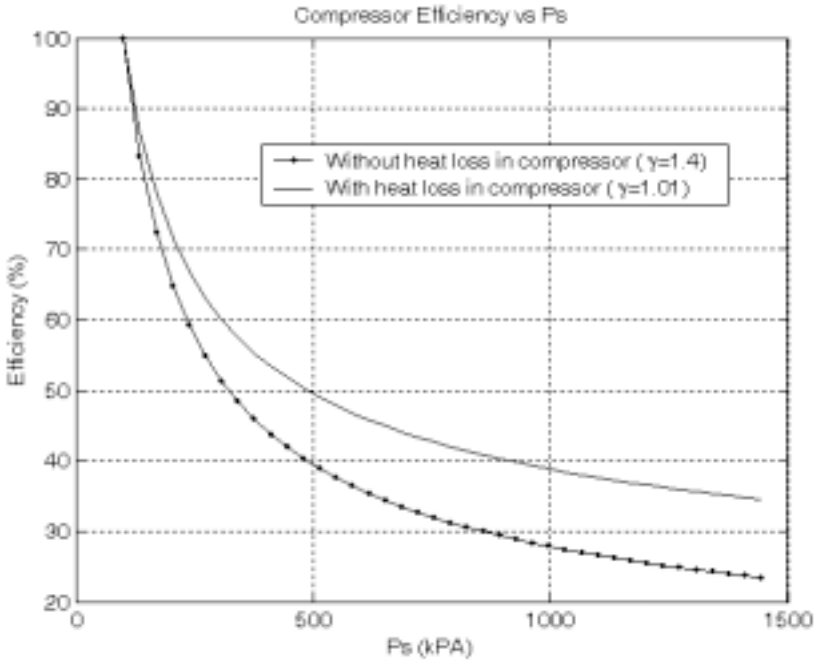

Figure 2-3: The efficiency of converting kinetic energy of the free piston into stored energy in the reservoir as a function of the reservoir pressure.

Mass Investment

Finally, to complete the cycle, the mass of air utilized from the reservoir to support the combustion process must be taken into account. Given that the energy stored in the reservoir is equal to $(P_s - P_{atm})V_s$, and using the ideal gas law for V_s, it can be shown that the energy stored (relative to atmospheric pressure at ambient temperature) in the reservoir is equal to the following:

$$\text{Energy Stored} = \frac{(P_s - P_{atm})}{P_s} m_c R T_{amb} \tag{18}$$

Therefore the energy stored is proportional to the mass in the reservoir. The investment of air mass needed for the combustion can therefore be expressed as the following efficiency, for air supported propane combustion:

$$\eta_{invest} = \frac{m_c - \frac{15.63}{16.63} m_{e0}}{m_{e0}} \tag{19}$$

Using the ideal gas law, this can be expressed as the following:

$$\eta_{invest} = 1 - \frac{15.63}{16.63} \frac{P_{e0} V_{e0} R T_{amb}}{P_{atm} V_{c0} R_e T_{AFT}} \tag{20}$$

where the functionally constrained volume ratio V_{e0} / V_{c0} is given by Equation (11). The efficiency related to the investment of reservoir air mass for the combustion event is shown in Figure 2-4, for a reservoir pressure of 653 kPa (80 psig), as a function of the initial combustion pressure P_{e0}. If heat loss occurs in the compressor chamber, the efficiency associated with the mass investment is enhanced.

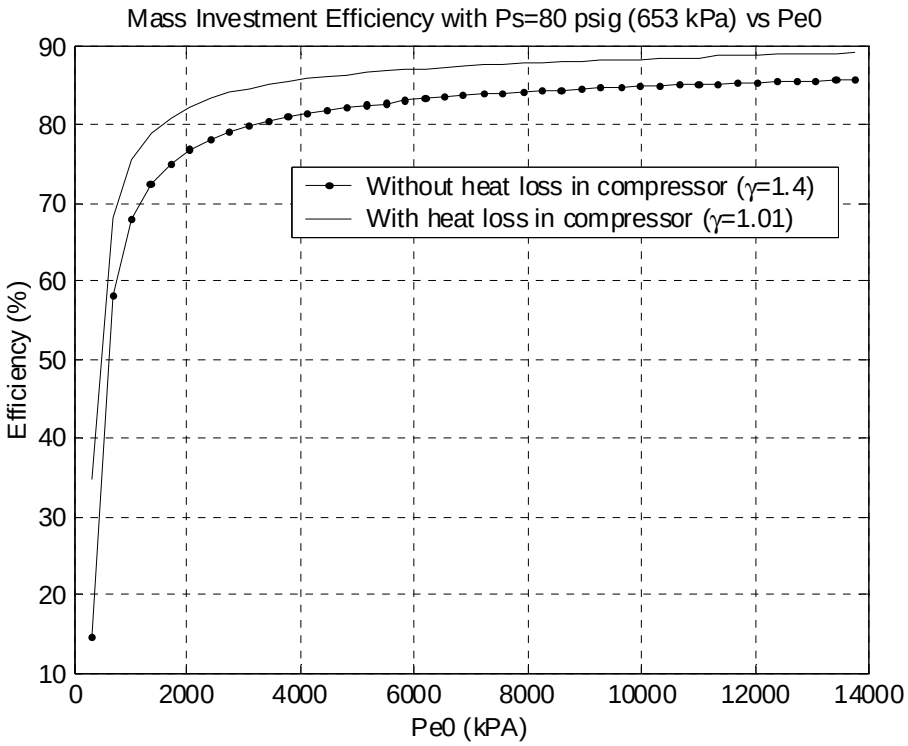

Figure 2-4: Efficiency associated with the investment of reservoir air for the combustion of propane as a function of the initial combustion pressure (and with P_s = 653 kPa).

System Efficiency

The overall efficiency of the system can be found by multiplying the individual efficiencies regarding the conversion of energy released in combustion to kinetic energy of the free piston, η_{KE}, the conversion of kinetic energy to energy stored in the reservoir at ambient temperature, η_{comp}, and the efficiency related to the required investment of reservoir air to the combustion event, η_{invest}. By multiplying Equations (4), (12), (16) and (20), the overall system efficiency is found in closed-form shown in Equation (21).

$$\eta_{sys} = \left(\frac{1}{e}\right)\left(1-\frac{P_{atm}}{P_s}\right)\left[\left(\frac{(1-\gamma)}{\gamma(1-\gamma_e)}\right)\left(\frac{\gamma_e\left(\frac{P_{atm}}{P_{e0}}\right)^{\frac{(\gamma_e-1)}{\gamma_e}}+(1-\gamma_e)\left(\frac{P_{atm}}{P_{e0}}\right)-1}{1-\left(\frac{P_{atm}}{P_s}\right)^{\frac{(1-\gamma)}{\gamma}}}\right)R_eT_{AFT}-\frac{15.63}{16.63}RT_{amb}\right] \quad (21)$$

Figure 2-5 shows the overall system efficiency as a function of the initial combustion pressure for a reservoir pressure of 653 kPa (80 psig). It should again be noted that heat losses, if present, in the compressor chamber enhance the efficiency.

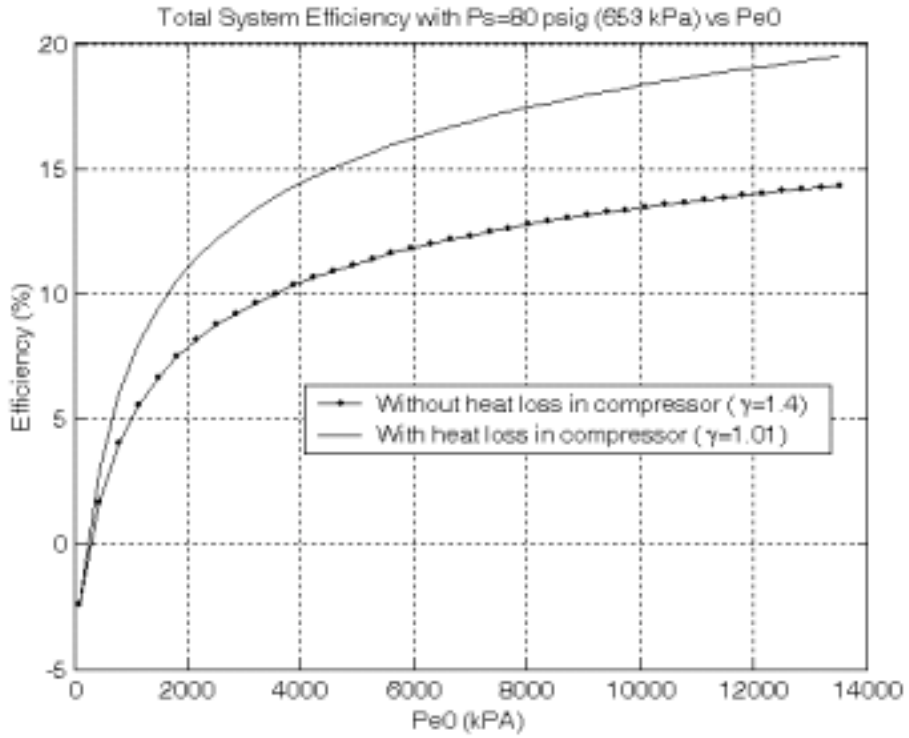

Figure 2-5: The overall system efficiency as a function of the initial combustion pressure (and with P_s = 653 kPa).

Dynamic Model

The thermodynamic model of the free piston compressor presented above reveals several fundamental dependencies regarding the efficiency and configuration of the device. However, the thermodynamic analysis cannot evaluate the effect of several influences. The effect of the return spring and the effect of diluting the exhaust gasses and therefore lowering the temperature as the engine side intakes air is not included in the thermodynamic model above. Other influences capable of being included in a dynamic

model can include: the temperature dependence of specific heat, and losses due to check valves, friction, and leakage, among others. Most importantly, the thermodynamic model cannot accurately model the interaction between the engine side and the compressor side (they were modeled separately in Section 3) Lastly, a dynamic model can offer a time-based evaluation of the system.

Dynamic Model of the Engine Side

Immediately following combustion, the pressure and temperature dynamics in the combustion side are determined by the following power balance,

$$\dot{U}_e = \dot{H}_e + \dot{Q}_e - \dot{W}_e \tag{22}$$

where $\dot{U}_e$ is the rate of internal energy stored in the control volume comprising the combustion chamber, $\dot{H}_e$ is the rate of enthalpy crossing the CV boundary, $\dot{Q}_e$ is the heat flux rate into or out the CV, and $\dot{W}_e$ is the work rate. Assuming an ideal gas, the rate of internal energy storage is given by the following two relationships,

$$\dot{U}_e = \dot{m}_e c_{ve} T_e + m_e c_{ve} \dot{T}_e = \frac{1}{\gamma_e - 1}(\dot{P}_e V_e + P_e \dot{V}_e) \tag{23}$$

where $\dot{m}_e$ is the mass flow rate of gas entering (positive values) or exiting (negative values) the combustion chamber, c_{ve} and γ_e are the constant-volume heat capacity and ratio of specific heats, respectively, of the gas in the combustion chamber, and P_e, V_e and T_e are the pressure, volume, and temperature, respectively, of the combustion chamber. The values of c_{ve} and γ_e must in general be found from the appropriately weighted average of the temperature dependent values of c_p of the species contained

within the chamber. The enthalpy rate of energy entering or exiting the control volume is given by,

$$\dot{H}_e = \dot{m}_e c_{p,in/out} T_{in/out} \tag{24}$$

where $c_{p,in/out}$ is the constant-pressure heat capacity of the gas entering or exiting the combustion chamber, and $T_{in/out}$ is the temperature of the mass entering or exiting the chamber. If it is assumed that the engine side is adiabatic, then $\dot{Q}_e = 0$. The work rate is given as:

$$\dot{W}_e = P_e \dot{V}_e \tag{25}$$

The operation of the "engine side" of the device can be considered in three phases: the work phase, the intake phase, and the exhaust phase.

Work Phase

During work phase, no mass flow occurs and Equations (21-25) reduce to the following relationships regarding the pressure and temperature dynamics inside the combustion chamber:

$$\dot{P}_e = \frac{-\gamma_e P_e \dot{V}_e}{V_e} \tag{26}$$

$$\dot{T}_e = \frac{-P_e \dot{V}_e}{m_{e0} c_{ve}} \tag{27}$$

The work phase persists while $P_e > P_{atm} - P_{cvd}$ where P_{cvd} represents the minimum pressure difference necessary to open the intake check valve.

Intake Phase

If the device is configured such that the free piston is allowed to travel further than the distance corresponding to a volume of V_{ef} as given by Equation (2), and if the

combustion chamber is fitted with a check valve, the combustion chamber will draw in fresh air to cool the combustion products. It is assumed that the check valve selected offers little resistance to the otherwise free motion of the free piston.

The intake phase is initiated when the pressure in the combustion chamber drops below $P_{atm} - P_{cvd}$ whereupon the intake check valve opens to allow ambient temperature air to enter the combustion chamber. The pressure and temperature dynamics are therefore given by the following relationships,

$$\dot{P}_e = \frac{(\gamma_{air} - 1)\dot{m}_e c_{p,air} T_{in} - \gamma_{air} P_e \dot{V}_e}{V_e} \tag{28}$$

$$\dot{T}_e = \frac{\dot{m}_e (c_{p,air} T_{in} - c_{v,air} T_e) - P_e \dot{V}_e}{m_e c_{v,air}} \tag{29}$$

where the mass flow rate through the check valve is given by the following commonly accepted mass-flow rate equation:

$$\dot{m}_e = A_{check} \Psi(P_{atm} - P_{cvd}, P_e) \tag{30}$$

It is assumed that the check valve opens completely with an orifice area of A_{check}. The area normalized mass-flow rate Ψ resides in a choked or unchoked flow regime according to the following relationship:

$$\Psi(P_u, P_d) = \begin{cases} \dfrac{C_1 C_f P_u}{\sqrt{T_{in}}} & \text{if } \dfrac{P_d}{P_u} \le C_r \text{ (choked)} \\ \dfrac{C_2 C_f P_u}{\sqrt{T_{in}}} \left(\dfrac{P_d}{P_u}\right)^{(1/\gamma,air)} \sqrt{1 - \left(\dfrac{P_d}{P_u}\right)^{(\gamma,air-1)/\gamma,air}} & \text{otherwise (unchoked)} \end{cases} \tag{31}$$

where C_f is the discharge coefficient of the check-valve, P_u and P_d are the upstream and downstream pressures, respectively, T_{in} is the air temperature, C_r is the pressure ratio that divides the flow regimes into unchoked and choked flow, and C_1 and C_2 are constants defined as:

$$C_1 = \sqrt{\frac{\gamma_{air}}{R_{air}}\left(\frac{2}{\gamma_{air}+1}\right)^{(\gamma,air+1)/(\gamma,air-1)}} \tag{32}$$

$$C_2 = \sqrt{\frac{2\gamma_{air}}{R_{air}(\gamma_{air}-1)}} \tag{33}$$

It should be noted that in Equations (28-33) it has been approximated that once the intake phase begins, the gas in the combustion chamber behaves as air (with regard to thermodynamic quantities c_v, c_p and γ). This approximation is justified by the relatively large mass of air drawn in compared the small mass of combustion gases that exist during the work phase.

Regardless of the actual mechanism of mass-flow through the check valve, Equations (28) and (29) relate the state variables of interest regarding the operation of the free piston compressor. Therefore, for purposes of this paper, Equation (30) may be replaced by the following pressure-difference driven linear mass-flow rate approximation:

$$\dot{m}_e \approx k_{check}(P_{atm} - P_{cvd} - P_e) \tag{34}$$

where the coefficient k_{check} is set such that the mass-flow rate is of a magnitude similar to that given by Equation (30). It should be noted that the check valve should be selected with a low minimum pressure to open (the “cracking pressure”) and with a large enough flow area so as to generate minimal resistive forces on the piston.

Exhaust Phase

The exhaust phase is initiated when the direction of the piston changes and the return spring pushes it toward the original starting position. This phase needs to be detected by monitoring the position and/or velocity of the piston such that an actuated valve can be opened to allow the mixture of combustion gases and air resulting from the intake phase to leave the combustion chamber. The resulting pressure and temperature dynamics

inside the combustion chamber during this phase are similar to those given by Equations (28) and (29) in the intake phase,

$$\dot{P}_e = \frac{(\gamma_{air} - 1)\dot{m}_e c_{p,air} T_e - \gamma_{air} P_e \dot{V}_e}{V_e} \tag{35}$$

$$\dot{T}_e = \frac{\dot{m}_e (c_{p,air} T_e - c_{v,air} T_e) - P_e \dot{V}_e}{m_e c_{v,air}} \tag{36}$$

where T_{in} of Equation (28) and (29) has been replaced with T_e in Equation (35) and (36). It is again approximated that the behavior of the gasses in the combustion chamber at this point is dominated by the thermodynamic characteristics of air. The mass-flow rate through the actuated outlet valve is given by:

$$\dot{m}_e = -A_{out} \Psi(P_e, P_{atm}) \tag{37}$$

where A_{out} is the flow orifice area of the outlet valve and Ψ is the area normalized mass flow given by Equations (31), (32) and (33). Similar to Equation (34), this may be approximated by the following linear mass-flow rate equation:

$$\dot{m}_e \approx -k_{out} (P_e - P_{atm}) \tag{38}$$

Dynamic Model of the Compressor Side

The compressor side of the device can be modeled using an energetic approach similar to that used to model the engine side. The compressor side undergoes three distinct phases: compression, pump, and draw-in.

Compression Phase

During the compression phase, there is no mass-flow and the pressure and temperature dynamics are similar to those given by Equations (26) and (27):

$$\dot{P}_c = \frac{-\gamma_{air} P_c \dot{V}_c}{V_c} \tag{39}$$

$$\dot{T}_c = \frac{-P_c \dot{V}_c}{m_{c0} c_{v,air}} \tag{40}$$

Note that $\dot{V}_c$ is negative in this phase as the piston moves to the right, as shown in Figure 2-1. The compression phase persists while $P_c < P_s + P_{cvd}$, where P_s represents the pressure in the high-pressure supply reservoir and P_{cvd} represents the minimum pressure difference necessary to open the reservoir check valve. The initial mass of air in the compressor chamber m_{c0} may be calculated from the ideal gas law,

$$m_{c0} = \frac{(P_{atm} - P_{cvd})V_{c0}}{R_{air} T_{amb}} \tag{41}$$

where it is assumed that upon returning to the original position, the pressure in the compressor chamber will be equal to $(P_{atm} - P_{cvd})$ with a temperature T_{amb} equal to the ambient temperature, and a volume of V_{c0}.

Pump Phase

The pump phase begins when the pressure becomes large enough to promote mass flow through the reservoir check valve: $P_c \geq P_s + P_{cvd}$. The resulting pressure, temperature and mass-flow dynamics are given by the following:

$$\dot{P}_c = \frac{(\gamma_{air} - 1)\dot{m}_c c_{p,air} T_c - \gamma_{air} P_c \dot{V}_c}{V_c} \tag{42}$$

$$\dot{T}_c = \frac{\dot{m}_c (c_{p,air} T_c - c_{v,air} T_c) - P_c \dot{V}_c}{m_c c_{v,air}} \tag{43}$$

$$\dot{m}_c \approx -k_{res}(P_c - P_s - P_{cvd}) \tag{44}$$

Draw-in Phase

The draw-in phase begins after the direction of the free piston reverses and begins to head toward the device's original position under influence of the return spring. Mass-flow of ambient temperature air into the compressor chamber is promoted when the pressure in the chamber is low enough to open the draw-in check valve: $P_c < P_{atm} - P_{cvd}$. The resulting pressure and temperature dynamics are given by Equations (42) and (43), and the mass-flow is given by the following:

$$\dot{m}_c \approx k_{draw}(P_{atm} - P_{cvd} - P_c) \tag{45}$$

Inertial Dynamics of the Free Piston

The dynamics in the engine side and the compressor side are related to each other through the movement of the free piston. Neglecting friction (although such effects could be included here), the dynamics of motion of the free piston are given by,

$$M\ddot{x} = (P_e - P_{atm})A_e - (P_c - P_{atm})A_c - F_s \tag{46}$$

where M is the mass of the free piston, A_e and A_c are the areas on the piston on the engine and compressor side respectively, x is the displacement of the piston assembly as denoted in Figure 2-1, and F_s is the return spring force. The volumes of the combustion chamber and compressor chamber, and their associated derivatives, are given by the following:

$$V_e = A_e x \tag{47}$$

$$V_c = A_c(l_c - x) \tag{48}$$

where l_c is the length of the combustion chamber when $x = 0$.

Dynamic Simulation

A dynamic simulation of the system was performed using Simulink. The following parameters were used for the simulation: mass of free piston M = 250 g, area of engine side $A_e = 5.07\,\text{cm}^2 = 5.07$ (a diameter of 1 in.), area of compressor side $A_c = 2.85\,\text{cm}^2$ (a diameter of 0.75 in.), initial combustion pressure $P_{e0} = 3548\,\text{kPa}$ (500 psig), a constant-force spring with $F_s = 0.09\,\text{N}$, a check valve cracking pressure $P_{cvd} = 2.3\,\text{kPa}$ (1/3 psi), and a reservoir pressure $P_s = 653\,\text{kPa}$ (80 psig).

A dead space of 2 mm was selected, corresponding to $V_{e0} = 1.013\,\text{cm}^3$. Equation (11) resulted in a required compressor volume of $V_{c0} = 22.04\,\text{cm}^3$ with a resulting compressor length of 7.73 cm. Figures 2-6 and 2-7 show the pressure and temperature in the engine side, respectively, as a function of time. Note that the combustion gasses are allowed to expand all the way down to atmospheric pressure whereupon the intake check valve opens allowing the mixture to dilute with cool air. The temperature in the combustion chamber therefore drops quickly from 2250 K to a final temperature of 387 K (238 ^{o}F).

Figures 2-8 and 2-9 show the pressure and temperature in the compressor side of the device, respectively, as it pumps and returns to the original position. A comparison of the dynamic simulation and the thermodynamic model yields comparable overall efficiencies. The thermodynamic model estimates an overall system efficiency of $\eta_{sys} = 10.02\,\%$ while the dynamic simulation estimates an overall system efficiency of $\eta_{sys} = 9.56\,\%$ based on the total mass of air pumped into the reservoir:

$$\eta_{sys} = \frac{(P_s - P_{atm})(m_c - \frac{15.63}{16.63} m_{e0}) R_{air} T_{amb}}{P_s m_{e0} e} \tag{49}$$

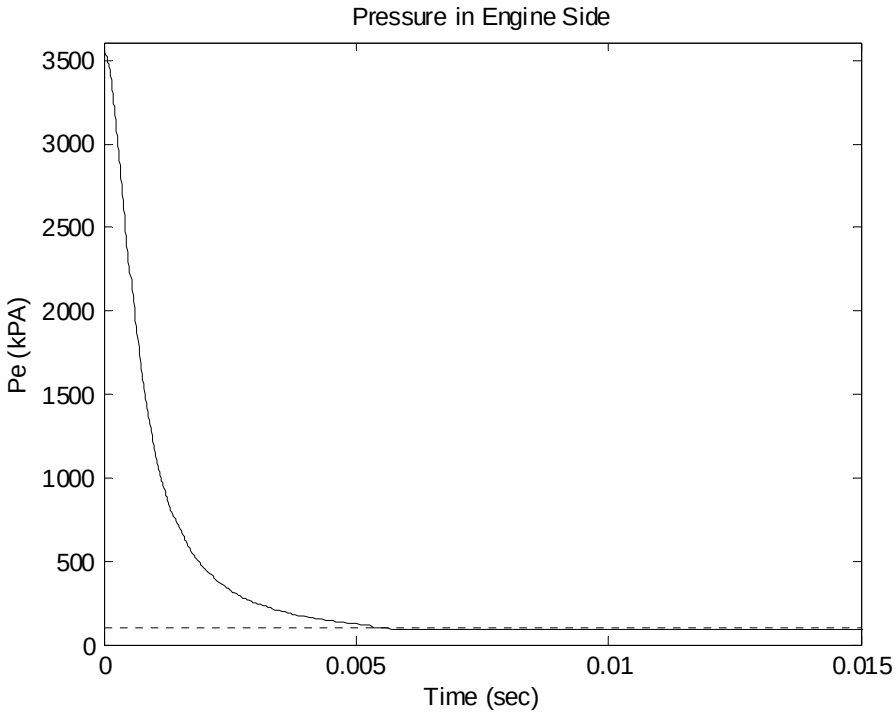

Figure 2-6: Pressure in the Engine Side.

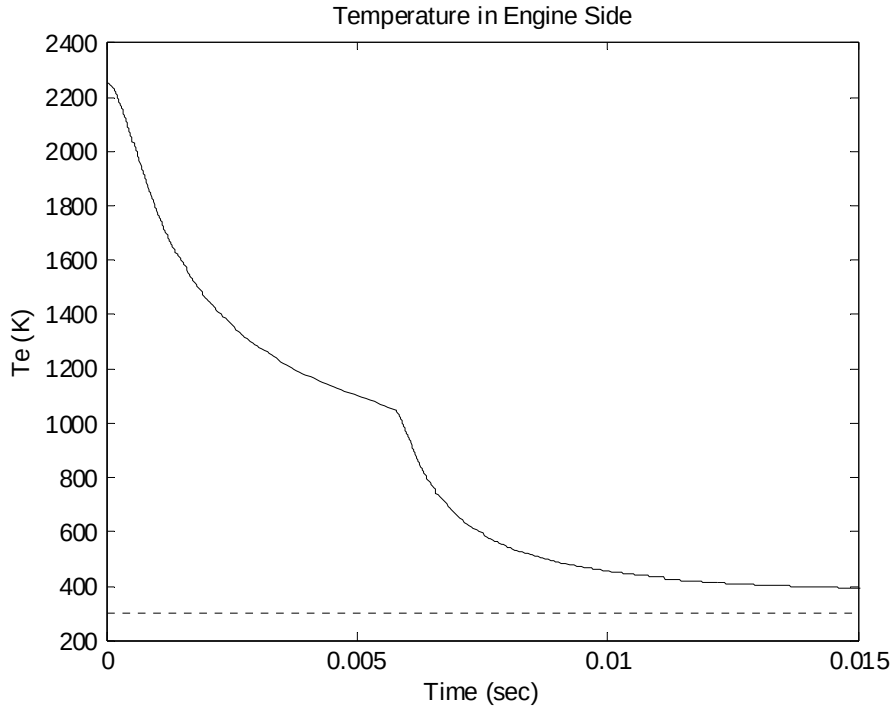

Figure 2-7: Temperature in the Engine Side.

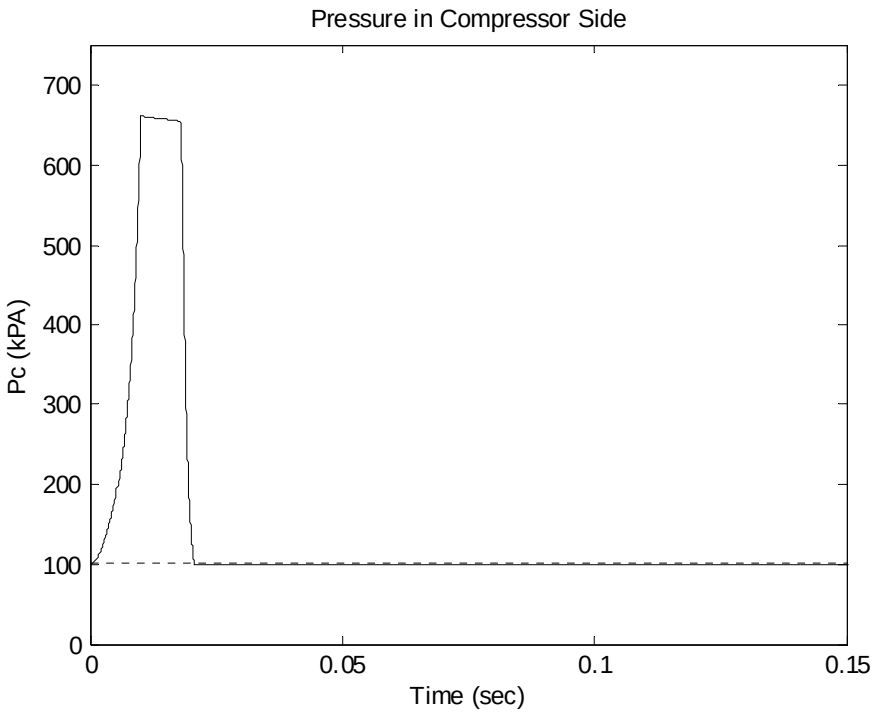

Figure 2-8: Pressure in the Compressor Side.

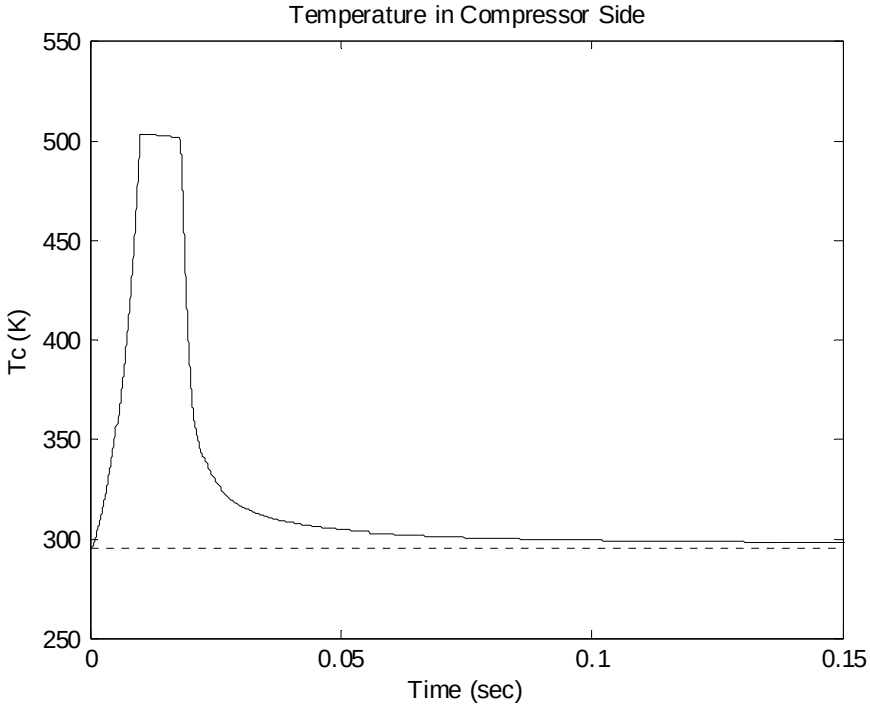

Figure 2-9: Temperature in the Compressor Side.

Likewise, the efficiencies of converting the energy of combustion into kinetic energy for the two models are comparable. Given that the device is based to a large degree on the notion of using an inertia to efficiently convert the energy of combustion, a close correlation between the models in part verifies that the coupling between the two sides of the device takes advantage of the notion of an inertially dominated load. The thermodynamic model estimates $\eta_{KE} = 36.2\,\%$ and the dynamic model estimates $\eta_{KE} = 34.6\,\%$. The thermodynamic model also estimates the following: $\eta_{comp} = 34.3\,\%$ and $\eta_{invest} = 80.6\,\%$. The differences between the models originate from the interaction of the engine side with the compressor side, which for this chosen configuration has a small contribution.

Conclusions

A thermodynamic model and a dynamic model of a free piston compressor were presented. The thermodynamic model yields a key design parameter regarding the ratio of the initial combustion chamber volume to the maximum compressor volume necessary for maximum efficiency. The thermodynamic model also shows that η_{KE} is a function only of the properties of the fuel and the initial combustion pressure, while η_{KE} is a function only of the reservoir pressure. The thermodynamic model also revealed that heat loss occurring in the compressor chamber enhances the efficiency of the device.

The dynamic model is able to offer a time-based analysis of the system that includes the interaction of the engine side with the compressor side. This interaction is useful in designing the piston areas of the engine and combustion side as well as the return spring. Additionally, the dynamic model is capable of capturing the effects of losses due to check valves, friction and leakage.

References

[1] Aichlmayr, H. T., Kittelson, D. B., and Zachariah, M. R., "Miniature free-piston homogenous charge compression ignition engine-compressor concept – Part I: performance estimation and design considerations unique to small dimensions," *Chemical Engineering Science*, 57, pp. 4161-4171, 2002.

[2] Aichlmayr, H. T., Kittelson, D. B., and Zachariah, M. R., "Miniature free-piston homogenous charge compression ignition engine-compressor concept – Part II: modeling HCCI combustion in small scales with detailed homogeneous gas phase chemical kinetics," *Chemical Engineering Science*, 57, pp. 4173-4186, 2002.

[3] Beachley, N. H. and Fronczak, F. J., "Design of a Free-Piston Engine-Pump," *SAE Technical Paper Series*, 921740, pp. 1-8, 1992.

[4] Goldfarb, M., Barth, E. J., Gogola, M. A., Wehrmeyer, J. A., "Design and Energetic Characterization of a Liquid-Propellant-Powered Actuator for Self-Powered Robots". *IEEE/ASME Transactions on Mechatronics*, vol. 8, no. 2, pp. 254-262, June 2003.

[5] Klotsch, P., "Ford Free-Piston Engine Development," *SAE Technical Paper Series*, 590045, vol. 67, pp. 373-378, 1959.

[6] McGee, T. G., Raade, J. W., and Kazerooni, H., "Monopropellant-Driven Free Piston Hydraulic Pump for Mobile Robotic Systems," *ASME Journal of Dynamic Systems, Measurement, and Control*, vol. 126, pp. 75-81, March 2004.

[7] Pescara, R. P., "Motor Compressor Apparatus," U.S. Patent No. 1,657,641, Jan. 31, 1928.

[8] Underwood, A. F., "The GMR 4-4 'Hyprex' Engine: A Concept of the Free-Piston Engine for Automotive Use," *SAE Technical Paper Series*, 570032, vol. 65, pp. 377-391, 1957.

CHAPTER II

MANUSCRIPT 1

ADDENDUM

Thermodynamic Efficiency

Upon revision of the thermodynamic efficiency presented in this manuscript, a more adequate formulation was conceived. Particularly, the pneumatic potential energy of the compressed air in the reservoir was originally taken as $(P_s - P_{atm})V_s$ (page 17), which is associated with the constant-pressure process of pumping the air into the reservoir (Equation 9). This is incompatible with the requirement that the energy stored in the reservoir must equal its capacity to perform adiabatic work in a pneumatic actuator (adiabatic if considering worst case scenario, isothermal if considering best case scenario). Hence, the stored energy in the air reservoir should be given by,

$$E_{stored} = \frac{P_s V_f}{1-\gamma}\left[\left(\frac{P_s}{P_{atm}}\right)^{\frac{1-\gamma}{\gamma}} - 1\right] \tag{50}$$

Since the mass of air is the same at V_{c0}, V_{ci} and V_f, and noting that the pressure and temperature at V_{c0} are P_{atm} and T_{amb}, respectively, we can use ideal gas law expressions to derive the following relationship:

$$V_f = \left(\frac{P_{atm}}{P_s}\right)V_{co} \tag{51}$$

The total efficiency of converting kinetic energy of the free piston into stored potential energy of compressed air can be given by,

$$\eta_{PE} = \frac{E_{stored}}{W_e} \tag{52}$$

Finally, the total thermodynamic efficiency of the system can be found by multiplying the individual efficiencies regarding the conversion of energy released in combustion to kinetic energy of the free piston, η_{KE}, the conversion of kinetic energy to energy stored

in the reservoir at ambient temperature, η_{PE}, and the efficiency related to the required investment of reservoir air to the combustion event, η_{invest}. By multiplying Equations (4), (51) and (19), and substituting Equations (50), (51) and (11), the overall thermodynamic system efficiency is found in closed-form as follows:

$$\eta_{sys} = \left(\frac{1}{e}\right)\left(\frac{1}{1-\gamma}\right)\left[\left(\frac{P_s}{P_{atm}}\right)^{\frac{1-\gamma}{\gamma}} - 1\right]\left[\frac{\left(\frac{1}{1-\gamma_e}\right)\left[\left(\frac{P_{atm}}{P_{e0}}\right)^{\frac{\gamma_e - 1}{\gamma_e}} - 1 + (1-\gamma_e)\left(\frac{P_{atm}}{P_{e0}}\right)\right]}{\gamma\left(\frac{P_{atm}}{1-\gamma}\right)\left[1 - \left(\frac{P_{atm}}{P_s}\right)^{\frac{1-\gamma}{\gamma}}\right]} - \frac{15.63}{16.63} R_{air} T_{amb}\right] \tag{53}$$

Figure 2-10 shows the overall system efficiency as a function of the initial combustion pressure for various reservoir pressure values.

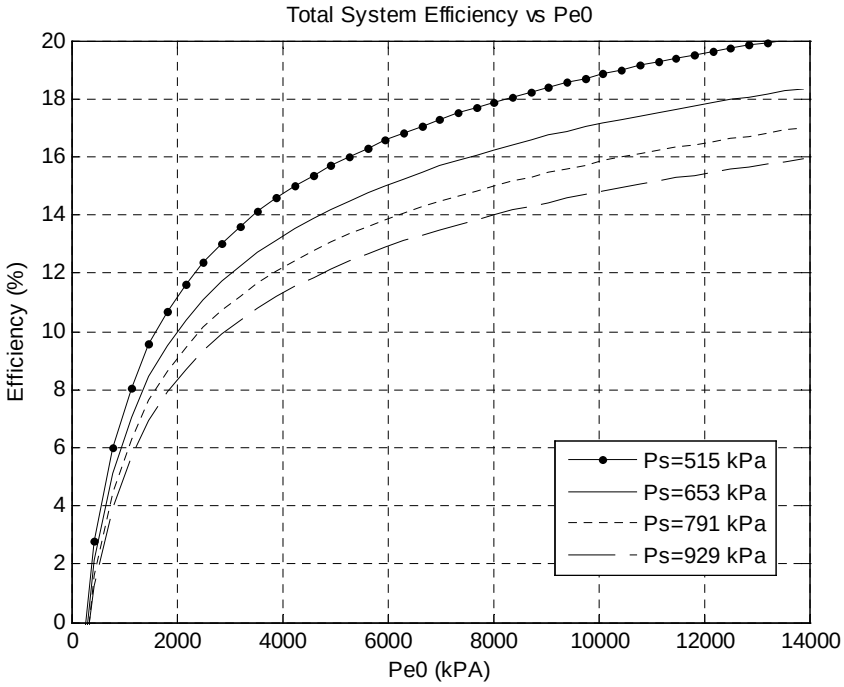

Figure 2-10: The overall system efficiency as a function of the initial combustion pressure (for various values of Ps).

CHAPTER III

MANUSCRIPT 2

DESIGN OF A FREE PISTON PNEUMATIC COMPRESSOR AS A MOBILE ROBOT POWER SUPPLY

José A. Riofrio and Eric J. Barth

Department of Mechanical Engineering

Vanderbilt University

Nashville, TN 37235

(Accepted by *IEEE International Conference on Robotics and Automation (ICRA),* Barcelona, Spain, April 2005)

Abstract

The design of a free piston compressor (FPC) intended as a pneumatic power supply for pneumatically actuated autonomous robots is presented in this paper. The FPC is a proposed device that utilizes combustion to compress air into a high-pressure supply tank by using the kinetic energy of a free piston. The device is configured such that the transduction from thermal energy to stored energy, in the form of compressed gas, is efficient relative to other small-scale portable power supply systems. This efficiency is achieved by matching the dynamic load of the compressor to the ideal adiabatic expansion of the hot gas combustion products. The device proposed exploits this fact by first converting thermal energy into kinetic energy of the free piston, and then compressing air during a separate compression phase. The proposed technology is intended to provide a compact pneumatic power supply source appropriate for human-scale robots. The design and implementation of the FPC is shown, and preliminary experimental results are presented and discussed with regard to efficiency and energetic characteristics of the device. Most significantly, the device is shown to operate nearly adiabatically.

Introduction

The need for an effective portable power supply for human-scale robots has increasingly become a matter of interest in robotics research. Current prototypes of humanoid robots, such as the Honda P3, Honda ASIMO and the Sony QRIO, show significant limitations in the duration of their power sources in between charges (the operation time of the humanoid-size Honda P3, for instance, is only 25 minutes). This limitation becomes a strong motivation for the development and implementation of a more adequate source of power. Moreover, the power density of the actuators coupled

to the power source need to maximized such that, on a systems level evaluation, the combined power supply and actuation system is both energy and power dense. Put simply, state-of-the-art batteries are too heavy for the amount of energy they store, and electric motors are too heavy for the mechanical power they can deliver, in order to present a combined power supply and actuation system that can deliver human-scale mechanical work in a human-scale self contained robot package. The motivation details are discussed more thoroughly in [4].

To address this current limitation in small-scale power supply systems appropriate for untethered robot actuation, the design of a free piston compressor (FPC) is presented in this paper. A schematic of the device is shown in Figure 3-1. The device is configured to be compact, efficient, operate with low noise and at a low temperature (relative to conventional small-scale engines), capable of on-demand start/stop operation without a separate starting mechanism, and provide a power output (compressed gas) that can be coupled to power dense pneumatic actuators (relative to electromagnetic actuators).

The idea of using a free piston combustion-based device as a pump has been around since the original free-piston patent by Pescara in 1928 [7]. The automotive industry conducted a large amount of research on free-piston engines in the 1950's. Ford Motor Company considered the use of a free piston device as a gasifier in 1954 [5]. General Motors presented the "Hyprex" engine in 1957 [8]. Such endeavours were aimed at an automotive scale engine and were largely unsuccessful. In more recent times, the free piston engine concept has been considered for small-scale power generation. Aichlmayr, et. al. [1, 2] have considered the use of a free piston device as an electrical power source on the 10 W scale meant to compete with batteries. Beachley and Fronczak [3], among others, have considered the design of a free-piston

hydraulic pump. McGee, et. al. have considered the use of a monopropellant-based catalytic reaction as an alternative to combustion, as applied to a free piston hydraulic pump [6].

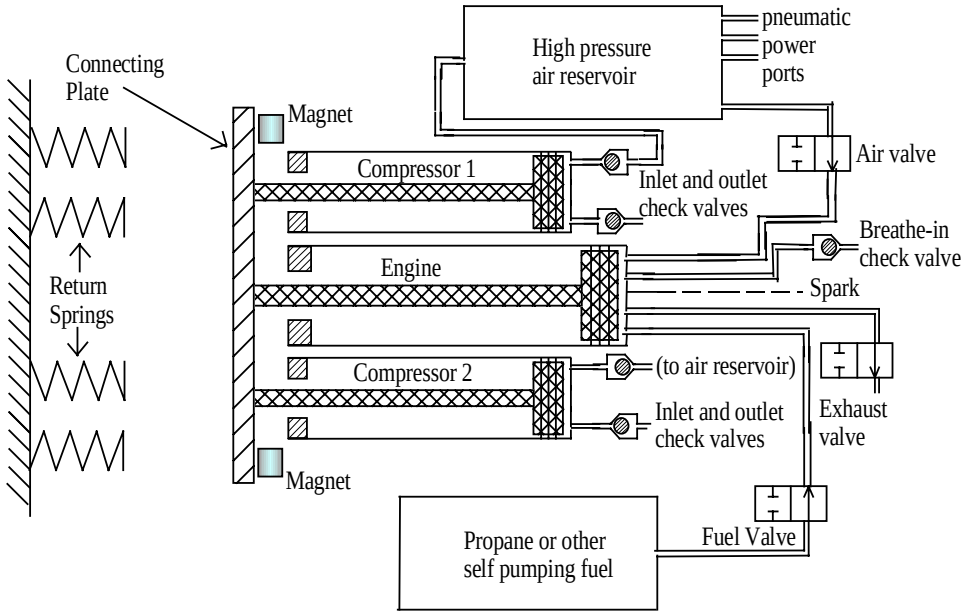

Figure 3-1: Schematic of the Free Piston Compressor.

The FPC presented here is intended as a power supply for a mobile pneumatic robotic system of human comparable power, mass and size. It is shown analytically in [9] that the use of a free piston engine as a direct air compressor offers nearly ideal loading characteristics necessary for high efficiency, in a simple and small package.

The Free Piston Compressor

The FPC is an internal combustion engine that uses its mechanical power output to pump air into a pressurized reservoir. The main idea is that the pressurized air reservoir will serve as a power supply for pneumatic systems, by using its high

pressure for pneumatic actuation. The FPC will automatically turn on and off as needed, maintaining the reservoir at the desired actuation supply pressure.

A typical 4-stroke engine cycle has a power stroke, exhaust stroke, intake stroke and compression stroke. A typical 2-stroke engine combines the power and intake stroke and combines the exhaust and compression stroke. The FPC shares some aspects of both a 4-stroke engine as well as a 2-stroke engine, but also has aspects unlike either conventional engine design.

Referring to Figure 3-1, the FPC operates by first opening the air and fuel valves for the proper durations to allow the proper mixture and amount of air and fuel into the combustion chamber of the engine cylinder. Using a self-pumping gaseous fuel such as propane, methane, or butane, and utilizing the high- pressure air in the reservoir, the injection of air and fuel effectively replaces the functions of the intake and compression strokes in a 4-cycle engine. Once the proper air/fuel mixture is inside, the valves close and a spark initiates the combustion. Upon combustion, the free piston moves to the left as the combustion gases expand, converting the energy of combustion into kinetic energy of the free piston. The travel of the free piston is configured such that the combustion products are able to fully expand down to atmospheric pressure. Once this full expansion has occurred, the kinetic energy stored in the free piston allows it to continue its motion to the left such that the pressure in the engine cylinder drops below atmospheric pressure. Given this pressure gradient, a breathe-in check valve opens and cool air from the outside environment enters the combustion cylinder to dilute and cool the combustion gasses. Continuing its motion to the left, the free piston subsequently hits and compresses the return springs, which will invert its direction of motion without absorbing energy. Upon return, the kinetic energy of the free piston is then transformed into the work required to compress and

then pump the gasses in the compressor chambers into the high-pressure reservoir. Also upon return, an electrically actuated exhaust valve opens to allow the diluted combustion gasses to be pushed out of the engine cylinder.

Features

The design and operation of the FPC addresses significant features of critical importance in IC engine design:

Efficiency

The efficiency of converting thermal energy into mechanical work through the expansion of a gas in a heat engine is related to the initial pressure of the gas as well as the amount of PV work that is delivered outside the cycle. The central feature of the FPC is that it presents an inertial load, due to the fact that the free piston is absent of any connecting rod, during the expansion of the combustion gasses. An inertial load is ideal for completely extracting work done by a pressurized gas since the pressure of the gas can decrease to atmospheric pressure while still still storing the work done as kinetic energy of the inertia. In the FPC as designed, the energy released at combustion is converted into kinetic energy of the free piston before the end of its stroke, leading to no high-pressure exhaust gasses. This avoids the wasteful exhaust of high pressure gasses typical found in an Otto cycle running at high load and thus increases the total efficiency of the system (Figure 3-2). The kinetic energy stored by the free piston will then subsequently provide the total work required to compress and pump air into a high-pressure reservoir. As configured, the FPC does not immediately reinvest mechanical work to promote the next cycle as does a conventional engine. Although a compression “stroke” is not explicitly present, it should be pointed out that the FPC does reinvest a portion of the work used to pump gas into the reservoir

since it does use the air from the reservoir during the injection of air and fuel. Therefore the portion of the curve in Figure 3-2 under the compression "stroke" of a 4-stroke engine, represents the energy stored in the reservoir from the mass pumped into the reservoir minus the mass of air used in the next injection cycle.

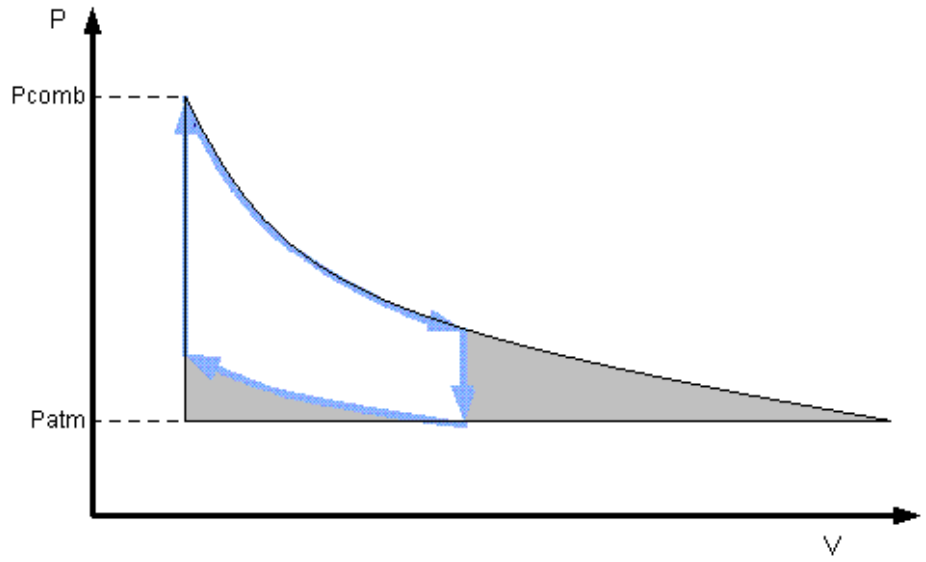

Figure 3-2: P-V diagram of FPC cycle superimposed on a P-V diagram of the Otto cycle. The shaded region to the right represents the additional work extracted in the FPC cycle that is not extracted in the Otto cycle.

Simplicity and Compactness

The FPC was built with standard cylinders, valves, and electronic components. It does not require any high-power electric signals, or electric calibration of any kind. General maintenance required is minimum to none, since no lubrication or cooling fluids need to be added. The fuel, propane as used here, is conventional, low cost and readily available.

The FPC can be easily downscaled to the size of a shoebox (plus the propane tank) while outputting an average power in the neighborhood of 200-500 W of pneumatic

power, which would be very appropriate as a portable power supply for human-scale mobile robots.

Cooling Mechanism

Overheating is a general concern in the design of any internal combustion device. By exploiting the inertial loading concept, the FPC allows for cool air to be drawn into the combustion chamber, via a check valve, before the end of the combustion stroke. This will rapidly cool the inside of the chamber, thus avoiding both the exhaust of hot gasses to the atmosphere and any significant transfer of heat to other hardware components through convection.

Start on Demand

Since the intake valves and spark plug are electrically actuated, and the free piston rods are not rigidly attached to any sort of crankshaft, the FPC does not require the implementation of a starter. This allows the engine to start on demand, without the need for a separate starting cycle. The start-on-demand feature highlights the compatibility between the FPC and a pneumatic robotic system, since they can be tied together by implementing a simple on/off control loop to regulate the pressure in the high-pressure pneumatic supply reservoir. The FPC would receive a signal and start operating as soon as the actuation pressure drops, and likewise turn off once reaching the desired pressure.

Low Noise

Due to the fact that the combustion pressure drops to atmospheric before the exhaust cycle, there are no high-pressure exhaust gasses, and therefore no exhaust noise. Other mechanical noises will be minimal, especially since the FPC will be enclosed in its respective device. Noises related to asymmetric loads and vibrations are addressed ahead.

Cost

All the components needed to build the FPC are standard and easy to find. The FPC shown in this paper can be built for under $1000. Additionally, since the FPC requires no maintenance, subsequent expenses will be limited to the replacement of the $2 bottle of propane.

Emissions

The breathe-in mechanism of the FPC will contribute to the dilution of harmful combustion products. These could be unburned hydrocarbons (HC), carbon monoxide (CO), and oxides of nitrogen (NO_x). However, the dilution of these gases does not address the real issue of emissions reduction. If emission regulations were to apply to an eventually commercial version of an FPC, the implementation of a small catalytic converter would be feasible.

Design

Figure 3-3 shows a picture of the current FPC prototype, and Figure 3-4 shows an exploded view of all the main hardware components of the FPC. The setup of the FPC consists of one 6-inch stroke combustion cylinder and two 4-inch compressor cylinders. These cylinders are the tie-rod type, and have a 1¼-inch bore. The cylinders are arranged side-to-side, with the combustion cylinder in the middle (to avoid asymmetric loads) and 2 inches behind, such that the 3 piston rods line up at their ends. A connecting plate is fixed at the end of the piston rods, ensuring that the rod ends remain in-line at all times. Opposing the cylinders are two end plates, each with 2 rods press fit unto them. These rods serve as guides to the 4 return springs, which will act upon the connecting plate after the power stroke, thus initiating the pump-on-return mechanism. Two neodymium-iron-boron magnets lock the ferrous connecting

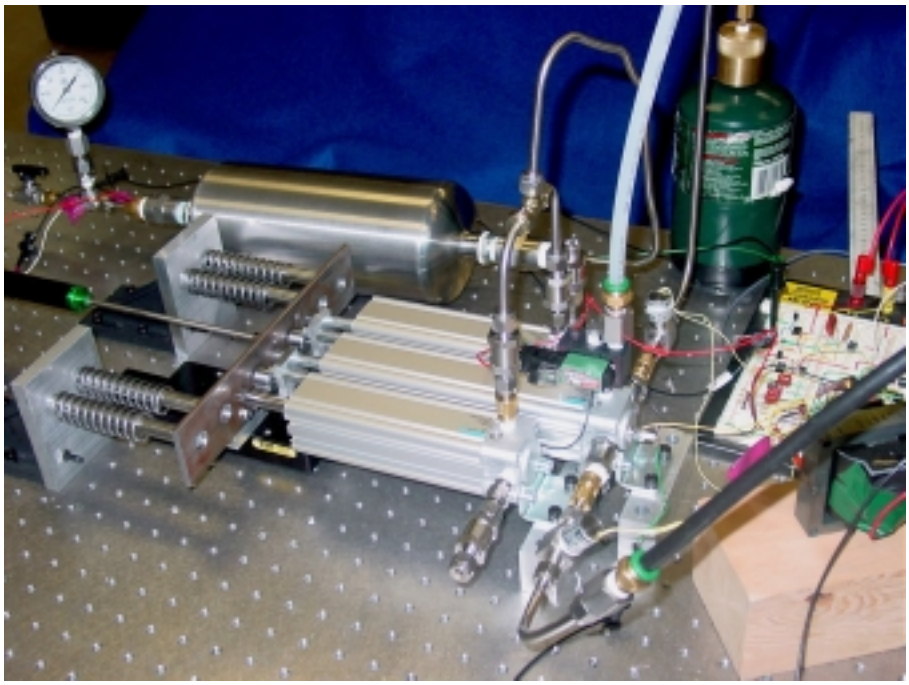

Figure 3-3: Picture of Free Piston Compressor.

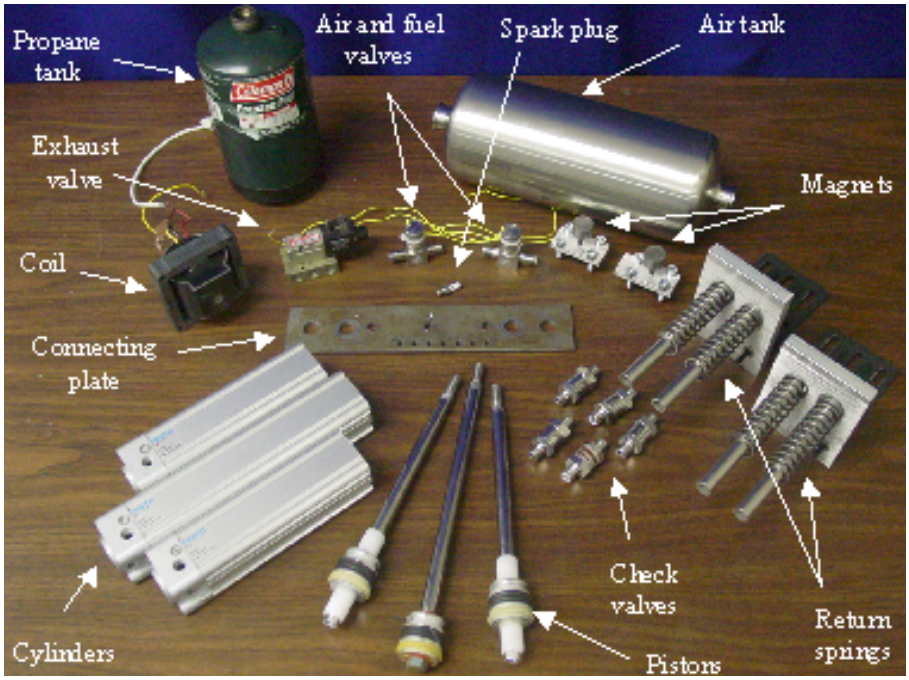

Figure 3-4: Exploded view of FPC hardware.

plate in place while the combustion cylinder is injected with a high-pressure air-fuel mixture, before combustion. The end caps of the tie-rod cylinders were ported appropriately to implement all necessary hardware. The combustor end cap needed ports for air/fuel mixture, exhaust, air breathe-in, pressure sensor, and spark plug; while the compressor end caps needed ports for breathing in and pumping out. The fuel in use is a bottle of COLEMAN® propane, available at most convenience stores for very low price. Finally, the spark plug is an NGK ME-8, normally used for model aircraft.

Several problems had to be overcome through different stages of the design process. It is mentioned in [9] that the injection pressure of the air/fuel mixture needs to be adequate enough to achieve the target initial combustion pressure. This minimum injection pressure requirement is given by,

$$P_{inj} = \left(\frac{R_{reac} T_{amb}}{R_e T_{AFT}} \right) P_{e0} \tag{1}$$

where R_{reac} and R_e are the average gas constants of the reactants and combustion products, respectively; T_{amb} and T_{AFT} are the ambient temperature and adiabatic flame temperature, respectively; and P_{e0} is the initial combustion pressure needed such that the FPC extracts enough work to pump all the air drawn into the compressor cylinders into the high-pressure reservoir. In order to obtain the appropriate injection pressure that corresponds to such an initial combustion pressure, the free piston needs to be locked in its initial position during injection. A sufficiently stiff spring could serve this purpose, but would offer so much resistance upon the combustion stroke that the desired inertial loading would not be easily obtained. To overcome this, two neodymium-iron-boron magnets were installed to hold the connecting plate at its

starting position before combustion. The gap between the magnets and the connecting plate is adjustable by the turn of a screw, such that their bonding magnetic force can be set just slightly higher than the force exerted on the free piston by the injection pressure. Since magnetic force is conservative, whatever amount of work done to overcome it will be retrieved at the end of the piston's pump stroke. Additionally, this magnetic force acts over such a small portion of the total stroke length that its effect against the inertial loading is negligible.

Another issue of considerable effect is the quality of the air/fuel mixture. Ideally, this mixture should match the stoichiometric mass ratio for combustion, namely 15.67 for air and propane. For complete combustion, it is also imperative that the mixture is uniform. This type of mixing is not instantaneous, and occurs by diffusion and any flow mixing present. By injecting the air and propane into the chamber through separate ports, it would take an uncertain amount of time for the two substances to uniformly mix, thus affecting the cycle rate of the system and making it less reliable. As a solution, a premix chamber was implemented, in order to give the air and fuel more mixing time an addition to enhancing the active mixing. The stoichiometric ratio is approximated by treating both air and propane as ideal gasses, and calculating the amount of mass of each entering the chamber based on pressure changes.

It is also important that the combustion and compression chambers are sealed properly, to avoid any unwanted leakage or blow-by that could reduce the total efficiency of the system. However, there is always a trade off between good sealing and friction between the piston and the cylinder wall. On top of that, temperature ratings play an important factor as well, though not so much in our case thanks to the cooling mechanism of the FPC. Proper sealing through the ports and through the valves are also a matter of consideration, as well as pressure ratings in the valves. The

cylinders in use have two lubricated rubber piston seals each, which, in addition to their end cap sealing, added up to a significant amount of friction, large enough to prevent us from exploiting the inertial loading effect. Since the only chambers that need proper sealing are the ones to the right, the left end caps were removed, as well as the left piston rings in all three cylinders (Figure 3-5). This greatly reduced the total amount of friction, and our PV curve in the combustion chamber began to exhibit the desired behaviour, as shown in Figure 3-6.

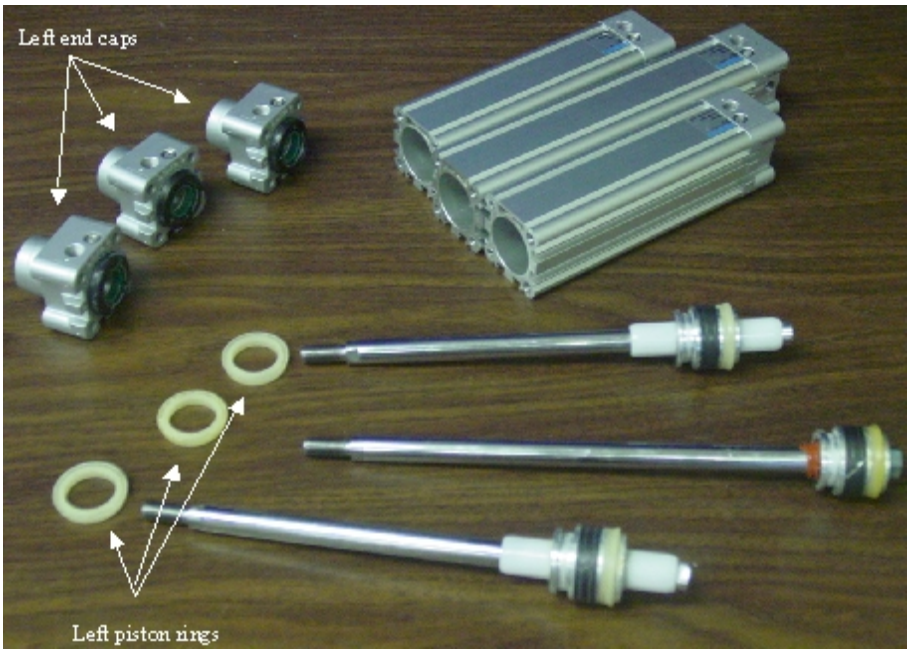

Figure 3-5: Removal of left piston seals and end caps.

For the compression (or pumping) cycle, the return springs are placed far enough to the left so that the piston fully loads up with kinetic energy just before coming into contact with them. The springs need to be stiff enough to be able to store all of the piston's energy before fully compressing. Additionally, the breathe-in check valve in the combustion side needs to be sufficiently light (crack pressure selected as 1/3 PSI =

2.3 kPa) and large enough to allow for the appropriate breathe-in air flow without presenting any significant restriction. Due the springs' efficient energy storage capacity, the piston will effectively fully regain its kinetic energy, which will become the work needed for the compression stroke. As the compression stroke reaches completion, the magnets will return the work done against them (back in the combustion stroke), and snap the plate back to its initial position while contributing work to the highest-pressure portion of pumping.

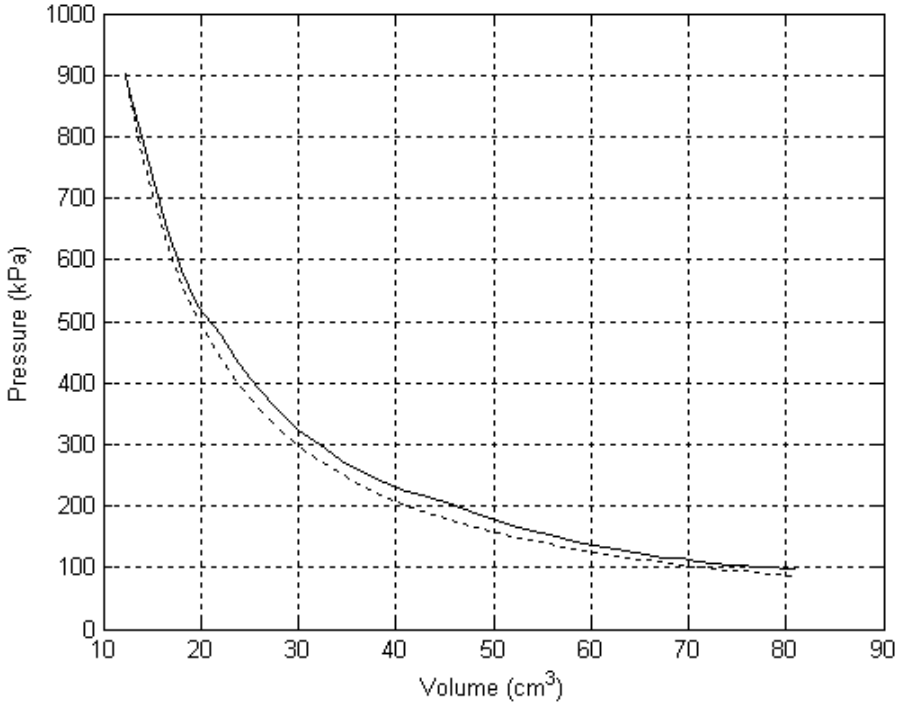

Figure 3-6: P-V curve in the combustion chamber. The solid line shows the experimentally measured P-V curve, and the dashed line shows the ideal adiabatic P-V curve.

As far as thermal management goes, it is desired to minimize energy losses through heat in the combustion chamber, and approach an adiabatic expansion of the hot gasses. Conversely, as shown in [9], heat losses are desired in the compression chambers to maximize the overall compressor efficiency. This should be intuitive

considering the compressors must fight against the heat during the compression phase. On a design level, this suggests that the walls of the compressor chambers should be of a high index of heat transfer (such as aluminum), and that cooling fins should be added to promote as much heat loss as possible.

The current FPC prototype is capable of operating at 2 Hz. Its cycle-rate is limited by the rate of flow through the valves and by the valves' opening times. Standard available valves offer a trade off between precision and flow capacity. Also, higher flow valves take longer times to open and close. The cycle rate of the FPC could be increased by implementing higher flow valves, but at the risk of losing air/fuel mixture consistency, and thus total efficiency.

Additional Design Considerations

The possibility of making the combustion chamber out of glass is currently being considered. Borosilicate glass has a very low coefficient of heat transfer, which would be ideal for a close match to an adiabatic expansion of the hot gasses in the combustion chamber. A thick enough piece of borosilicate glass tubing is capable of withstanding the peak pressures of the FPC, and can be obtained at low cost. Additionally, a glass combustion chamber would allow for the spark to be seen, which would make it very easy to achieve the stoichiometric air/fuel ratio by adjusting the mixture based on the color of the flame. Finally, with a piston made out of graphite or ground glass, the energy losses through friction would be greatly reduced, without sacrificing any significant sealing properties.

Another design consideration suitable for a commercial version of an FPC is to make it symmetrically dual sided (i.e. two 'back-to-back' FPCs). By doing so, the power-to-mass ratio would increase, since both FPCs would share combustion and

compressor chambers, and their respective valves. Additionally, the dual sidedness would reduce the vibration level and the physical noise associated with it.

Experimental Evaluation and Results

Experimental data was taken with the injection of 2.03×10^{-6} kilograms of fuel and 35.5×10^{-6} kilograms of air, in a dead volume of 11.11×10^{-6} cubic meters. The mass of air and fuel was estimated by observing the pressure in the cylinder during injection and assuming ideal gas behavior. The average combustion pressure peaked at 901 kPa, yielding a maximum speed of 2.9 meters per second of the 1.66 kilogram free piston (7.0 Joules of kinetic energy). The total efficiency of converting stored chemical energy of propane into kinetic energy of the free piston is given by,

$$\eta_{KE} = \frac{0.007\,\text{kJ}}{\frac{46350\,\text{kJ}}{\text{kg fuel}}\times(2.03\times10^{-6})\,\text{kg fuel}}\times100 = 7.4\,\% \qquad (2)$$

An adiabatic thermodynamic analysis [9] indicates that this efficiency is given analytically as:

$$\eta_{KE} = \left(\frac{R_e T_{AFT}}{e}\right)\left(\frac{\gamma_e P_{e0}^{1/\gamma_e} P_{atm}^{(\gamma_e-1)/\gamma_e} - P_{e0} + (1-\gamma_e)P_{atm}}{(1-\gamma_e)P_{e0}}\right) \qquad (3)$$

where $\gamma_e = 1.249$ is the average ratio of specific heats of the combustion products, and other variables were previously defined. Equation (3) yields a predicted efficiency of 20%. The difference between the predicted and measure transduction efficiency from the lower heating value of the fuel to kinetic energy can most likely be attributed to three unaccounted losses in the thermodynamic analysis. First, the air to fuel mass ratio achieved experimentally was 17.4 (lean) whereas the stoichiometric ratio is 15.67. Second, the thermodynamic analysis does not account for frictional losses. This

friction was measured to be about 13 N. This loss, if found to be significant, would serve to further motivate a design change of the cylinder walls to precision glass and the piston to either graphite or precision ground glass to reduce friction. Third, the thermodynamic analysis assumed adiabatic conditions. However, an evaluation of the experimentally obtained P-V curve, shown in Figure 3-6, indicates that the experimental prototype device exhibits nearly adiabatic behavior of $PV^{\gamma_e} = \text{constant}$. In fact, the experimentally obtained curve becomes flat at atmospheric pressure as hoped and indicates that the device is capable of both fully expanding the combustion products as well as being able to intake cool air from the environment to dilute the exhaust products. In light of the comparison of the experimentally obtained P-V curve as compared with the adiabatic P-V curve, heat loss appears to be minimal. It should be noted that the curve shown is from the device firing the first time when the device is cold and when heat losses would be at a maximum.

Figures 3-7, 3-8 and 3-9 show the pressure in the combustion chamber, the position of the free piston, and its velocity as a function of time. Notice in Figure 3-7 that the injection pressure right before ignition is about 267 kPa and requires that the magnetic holding force is sufficient to prevent motion of the free piston. Figure 3-7 also shows that the combustion pressure quickly rises to about 900 kPa after the spark occurs at 0 msec (spark not shown in Figure). The shape of the pressure profile after the peak pressure indicates that the combustion gasses were able to fully expand down to atmospheric pressure (101 kPa).

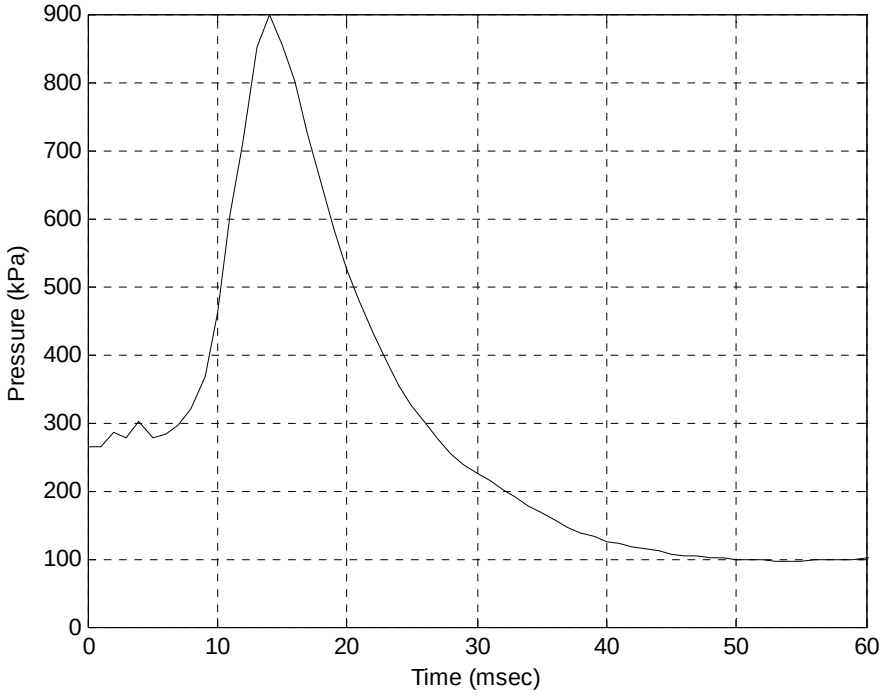

Figure 3-7: Pressure in the combustion chamber.

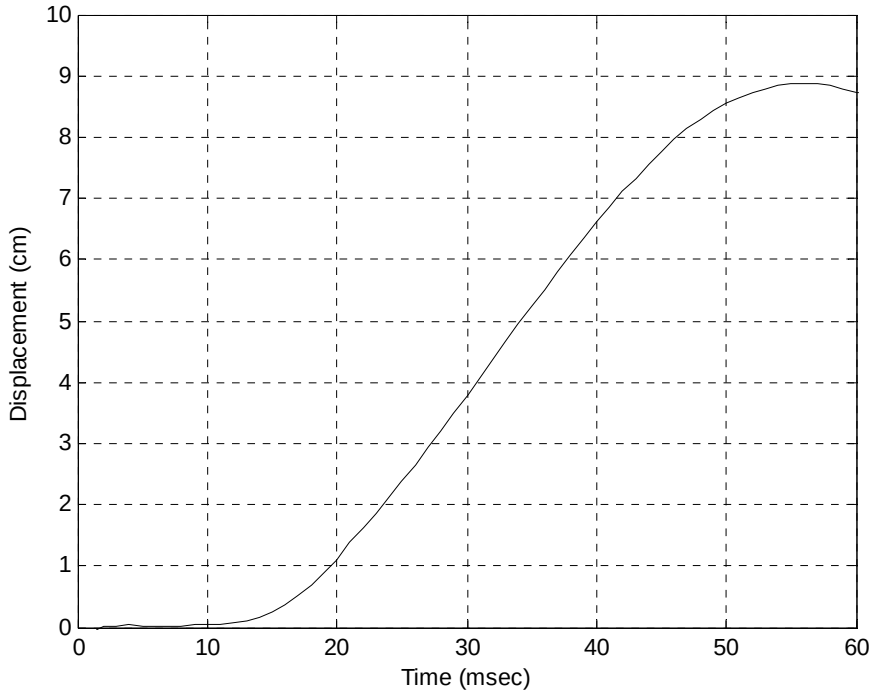

Figure 3-8: Position of the free piston.

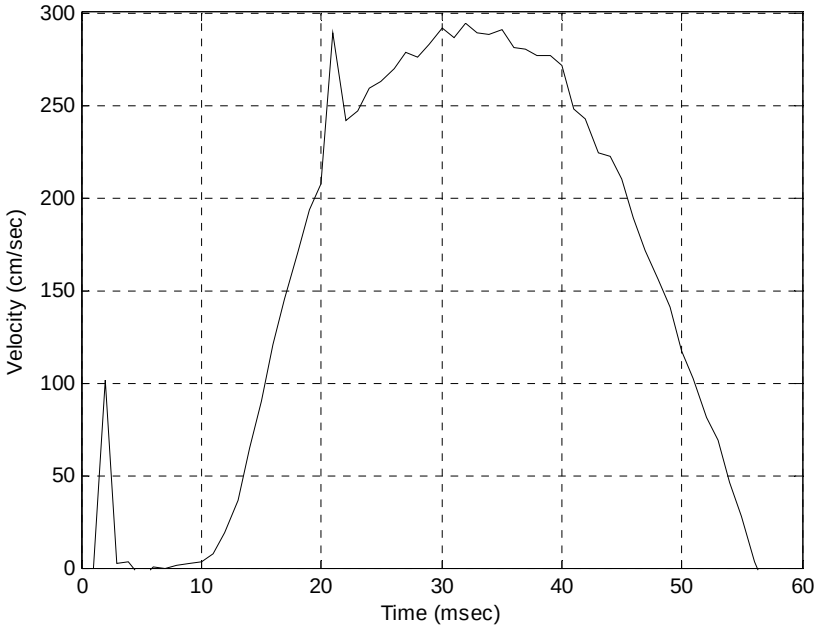

Figure 3-9: Velocity of the free piston.

Figures 3-8 and 3-9 show the displacement and velocity respectively of the free piston. The free piston begins to accelerate smoothly immediately following the rise in combustion pressure, indicating that the magnetic holding force was properly set. The velocity shows that the peak velocity occurs before the combustion pressure has dropped to atmospheric pressure, indicating that the beginning of the return springs were not place far enough along the stroke. This as well can contribute to a lower conversion efficiency as it represents a departure from the assumptions of the thermodynamic analysis. It does however indicate that a design change in the device needs to be made with respect to its length.

Conclusions

The design and construction of a Free Piston Compressor (FPC) was presented. Experimental results showed a respectable efficiency that demonstrates promise of

such a device as a small scale power supply for untethered pneumatically actuated robots. The combined factors of a high-energy density fuel, the efficiency of the device, the compactness and low weight of the device, and the use of the device to drive lightweight linear pneumatic actuators (lightweight as compared with power comparable electric motors) is projected to provide at least an order of magnitude greater total system energy density (power supply and actuation) than state of the art power supply (batteries) and actuators (electric motors) appropriate for human-scale power output.

Preliminary experimental results regarding the transduction of thermal energy into kinetic energy of the free piston demonstrate that the device is capable of fully expanding the combustion products down to atmospheric pressure as designed and demonstrates the merits of presenting a purely inertial load in a combustion process. Such dynamic loading serves to increase efficiency, allows the device to operate with low noise due to not having a high pressure exhaust “pop”, and allows the combustion products to be diluted with cool external air to contribute toward a low operating temperature compared to more conventional internal combustion engines. Most significantly, the device is shown to operate nearly adiabatically. Experimental results also demonstrated that the device is capable of start on demand, making it well suited to a pressure regulation control loop in a portable pneumatic power supply system.

Acknowledgements

This work was supported through the Vanderbilt Discovery Grant program and gifts in kind from Festo Corporation.

References

[1] Aichlmayr, H. T., Kittelson, D. B., and Zachariah, M. R., "Miniature free-piston homogenous charge compression ignition engine-compressor concept – Part I: performance estimation and design considerations unique to small dimensions," *Chemical Engineering Science*, 57, pp. 4161-4171, 2002.

[2] Aichlmayr, H. T., Kittelson, D. B., and Zachariah, M. R., "Miniature free-piston homogenous charge compression ignition engine-compressor concept – Part II: modeling HCCI combustion in small scales with detailed homogeneous gas phase chemical kinetics," *Chemical Engineering Science*, 57, pp. 4173-4186, 2002.

[3] Beachley, N. H. and Fronczak, F. J., "Design of a Free-Piston Engine-Pump," *SAE Technical Paper Series*, 921740, pp. 1-8, 1992.

[4] Goldfarb, M., Barth, E. J., Gogola, M. A., Wehrmeyer, J. A., "Design and Energetic Characterization of a Liquid-Propellant-Powered Actuator for Self-Powered Robots". *IEEE/ASME Transactions on Mechatronics*, vol. 8, no. 2, pp. 254-262, June 2003.

[5] Klotsch, P., "Ford Free-Piston Engine Development," *SAE Technical Paper Series*, 590045, vol. 67, pp. 373-378, 1959.

[6] McGee, T. G., Raade, J. W., and Kazerooni, H., "Monopropellant-Driven Free Piston Hydraulic Pump for Mobile Robotic Systems," *ASME Journal of Dynamic Systems, Measurement, and Control*, vol. 126, pp. 75-81, March 2004.

[7] Pescara, R. P., "Motor Compressor Apparatus," U.S. Patent No. 1,657,641, Jan. 31, 1928.

[8] Underwood, A. F., "The GMR 4-4 'Hyprex' Engine: A Concept of the Free-Piston Engine for Automotive Use," *SAE Technical Paper Series*, 570032, vol. 65, pp. 377-391, 1957.

[9] Barth, E. J., and Riofrio, J., "Dynamic Characteristics of a Free Piston Compressor," *2004 ASME International Mechanical Engineering Congress and Exposition (IMECE)*, IMECE2004-59594, November 13-19, 2004, Anaheim, CA.

CHAPTER III

MANUSCRIPT 2

ADDENDUM

Notes on Efficiency

The total efficiency of converting stored chemical energy of propane into kinetic energy of the free piston, as shown in Equation (2), was estimated by observing the pressure in the cylinder during injection and assuming ideal gas behavior. It was also assumed that the temperature in the chamber remained constant at ambient temperature. A better way to determine the mass of air and fuel used for combustion was devised in Manuscripts 3 and 4 (Chapters IV and V, respectively).

CHAPTER IV

MANUSCRIPT 3

EXPERIMENTAL OPERATION AND CHARACTERIZATION OF A FREE PISTON COMPRESSOR

José A. Riofrio and Eric J. Barth

Department of Mechanical Engineering

Vanderbilt University

Nashville, TN 37235

(Submitted to *ASME International Mechanical Engineering Congress and Exposition (IMECE),* Orlando, FL, November 2005)

Abstract

The ongoing design evolution of a free piston compressor (FPC) is presented in this paper. The FPC is a proposed device that utilizes combustion of a hydrocarbon fuel to compress air into a high-pressure supply tank. This device is designed to extract chemically stored energy from the fuel and convert it to potential energy of compressed air, while achieving high conversion efficiency relative to other small-scale portable power supply systems. The chemically stored energy of the hydrocarbon fuel is first converted into kinetic energy of the free piston by the end of the combustion phase. Subsequently, the moving piston acts as a pump and air compressor during a compression phase. The proposed technology is intended to provide a compact and efficient pneumatic power supply source appropriate for human-scale robots. The design and implementation of this version of the FPC is shown, and experimental results relating all phases (combustion, expansion and pumping) are discussed. The total efficiency of the system is experimentally measured and compared to its theoretical prediction.

Introduction

The need for an effective portable power supply for untethered human-scale robots has increasingly become a matter of interest in robotics research. Current prototypes of humanoid robots, such as the Honda P3, Honda ASIMO and the Sony QRIO, show significant limitations in the duration of their power sources in between charges (the operation time of the Honda P3, for instance, is only 25 minutes). This becomes a strong motivation for the implementation of a more adequate source of power. The motivation details are discussed more thoroughly in [1].

This paper presents the design of a free piston compressor (FPC) as a power supply for pneumatically actuated systems. The FPC serves the function of converting chemically stored energy of a hydrocarbon fuel into pneumatic potential energy of compressed air. More specifically, it extracts the energy by producing combustion of a stoichiometric mixture of propane and air, and the combustion-driven free piston acts as an air pump to produce the compressed air. The FPC, coupled with pneumatic actuators, is intended as an alternative to electrical batteries coupled with electrical motors. The main objective of this idea is to exploit the high mass specific energy density of hydrocarbon fuels and the high mass specific power density of linear pneumatic actuators, in order to provide at least an order of magnitude greater combined energy and power density (power supply and actuation) than state of the art electrical power supply and actuation systems.

Given their inherent penalization for carrying their own mass, the total energetic merit of an untethered power supply and actuation system is a combined measure of the source energy density of the energetic substance being carried, the efficiency of conversion to controlled mechanical work, the energy converter mass, and the power density of the actuators. With regard to a battery powered electric motor actuated system, the efficiency of conversion from stored electrochemical energy to shaft work after a gear head can be high (~ 50% to 80%) with very little converter mass (e.g. PWM amplifiers); however, the energy density of batteries is relatively low (about 180 kJ/kg for NiMH batteries), and the power density of electrical motors is not very high (on the order of 50 W/kg) rendering them heavy in relation to the mechanical work that they can output. With regard to the hydrocarbon-based pneumatic power supply and actuation approach

presented here, the converter mass is high relative to a battery/motor system, and the total conversion efficiency is shown in [2] to be low in relative terms. However, the energy density of hydrocarbon fuels is in the neighborhood of 45 MJ/kg (where the oxidizer is obtained from the environment and therefore has no associated mass penalty), which is more than 200 times greater than the energy density of conventional electrical batteries. This implies that even with poor conversion efficiency (< 10%), and with only mild expectations of miniaturizing the energy converter, the available energy to the actuator per unit mass of the energy source (mass of fuel plus mass of energy converter) is still at least one order of magnitude greater than the battery/motor system. Additionally, linear pneumatic actuators have roughly one order of magnitude greater power density than traditional electrical motors. Therefore, the proposed technology offers the potential of greatly increased energetic characteristics over state-of-the-art electrical power supply and actuation systems.

The idea of using a free piston combustion-based device as a pump has been around since the original free-piston patent by Pescara in 1928 [3]. The automotive industry conducted a large amount of research in the 1950s. Ford Motor Company considered the use of a free piston device as a gasifier in 1954 [4]. General Motors presented the “Hyprex” engine in 1957 [5]. Such endeavours were aimed at an automotive scale engine and were largely unsuccessful. In more recent times, the free piston engine concept has been considered for small-scale power generation. Aichlmayr, et. al. [6, 7] have considered the use of a free piston device as an electrical power source on the 10 W scale meant to compete with batteries. Beachley and Fronczak [8], among others, have considered the design of a free-piston hydraulic pump. McGee, et. al. have considered the

use of a monopropellant-based catalytic reaction as an alternative to combustion, as applied to a free piston hydraulic pump [9].

The FPC presented here is intended as a power supply for a mobile pneumatic robotic system of human comparable power, mass and size. It is shown analytically in [2] that the use of a free piston engine as a direct air compressor offers nearly ideal loading characteristics necessary for high efficiency (relative to similar scale combustion based devices), in a simple and small package.

A first design of the FPC was presented in [10]. In this previous design, particular emphasis was placed into the combustion portion of the device, and it outlined the main features of the FPC concept and design considerations of that particular prototype. The main features should be re-stated here, since they constitute the essence of the FPC idea:

Inertial Loading – The free piston is not rigidly attached to a crankshaft or any timing linkage alike, so it offers purely inertial loading to the expanding combustion gases. This allows the free piston to load up with kinetic energy resulting from the work done by the ideal adiabatic expansion [10] of the combustion gases. The combustion gases are allowed to expand until they reach atmospheric pressure, all while still contributing to the inertial loading. This full expansion contributes to a higher efficiency than if full expansion were not allowed, as is the case with most small-scale IC engines. As an additional consequence, the FPC has a quiet exhaust, since no high-pressure gases will be exhausted into the atmosphere.

Breathe-in Mechanism – When the combustion gases reach atmospheric pressure, the free piston will still be traveling (with maximum kinetic energy), and thus will induce a drop of pressure in the combustion chamber as the motion continues. This pressure drop

will cause an intake check valve to open and allow fresh atmospheric air to enter the chamber. This fresh air will both cool down and dilute the combustion products. The breathe-in mechanism ensures a low temperature operation of the device.

Start on Demand – Since the intake valves and spark plug are electrically actuated, and since high-pressure injection of air and fuel eliminate the need for a conventional intake and compression stroke, the FPC does not require the implementation of a starter. This allows the engine to start on demand, without the need for a separate starting cycle. This feature highlights the compatibility between the FPC and a pneumatic robotic system, since they can be tied together by implementing a simple control loop to maintain a particular pressure in a supply reservoir. The FPC would receive a signal and start operating as soon as the actuation pressure supply drops, and likewise turn off once reaching the desired pressure.

The features outlined above, among others, are discussed more in detail in [10], and become the platform for the work presented in this paper. What follows is an introduction of the new FPC prototype and some new design considerations, a comprehensive analysis of the design evolution, analysis of new experimental data showing combustion and pumping, and a calculation of the total efficiency of the system.

New Version of FPC

The previous prototype of the FPC [10] consisted of one combustion cylinder and two pumping cylinders. The three cylinders were aligned in parallel, with the combustion cylinder in the center. The pistons were rigidly attached to each other, and their main functions (combustion and pumping) occurred at the right of the pistons. The combustion

would drive the piston assembly to the left, and a set of springs reversed the motion back to the right, thus initiating the pumping phase. Figure 4-1 shows a schematic of this previous prototype.

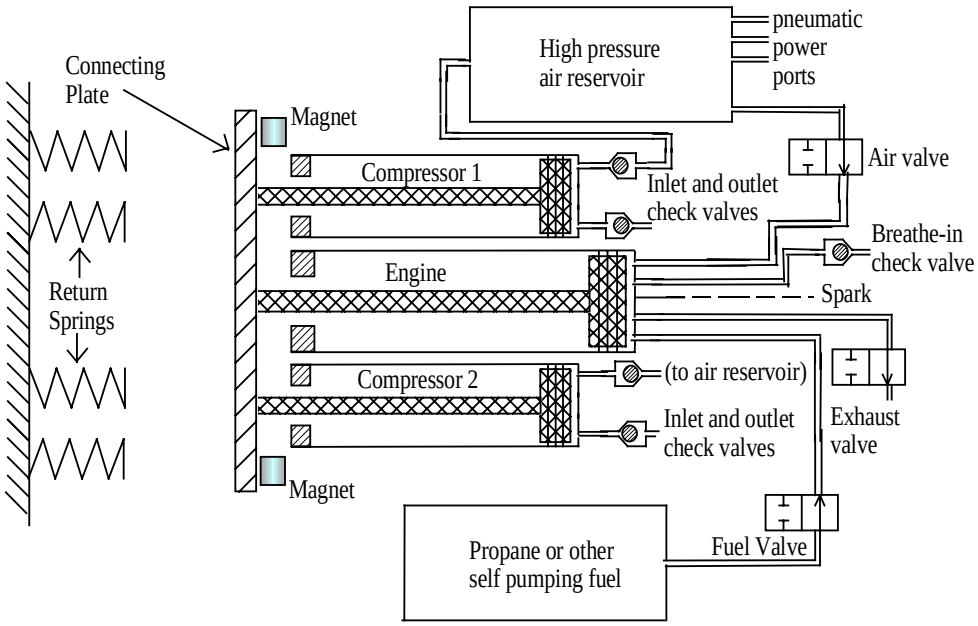

Figure 4-1: Schematic of Old Version of FPC.

The most appealing aspect of this configuration was that combustion and pumping occurred on separate strokes, so the inertial loading during combustion was not resisted by the compressed air. While this prototype provided some useful and insightful data, it also showed some limitations. These were mostly due to energy losses associated with collisions with the springs, the non-ideality of the springs in storing and returning energy, and the high friction in the cylinders. The rigid linking of the pistons also provided a very slight misalignment, which accounted for even greater friction. Additionally, the exhaust valve, breathe-in check valve, and inlet and outlet check valves were offering severe flow

restrictions, which suggested the use of a smaller cylinder bore, or alternatively, larger valves.

Figure 4-2 shows a schematic of the new version of the FPC. This prototype highlights combustion and pumping within the same stroke. The device consists of two cylinders in-line and opposing one another. Both cylinders have a combustion side (back of the piston) and a pumping side (rod side of the piston).

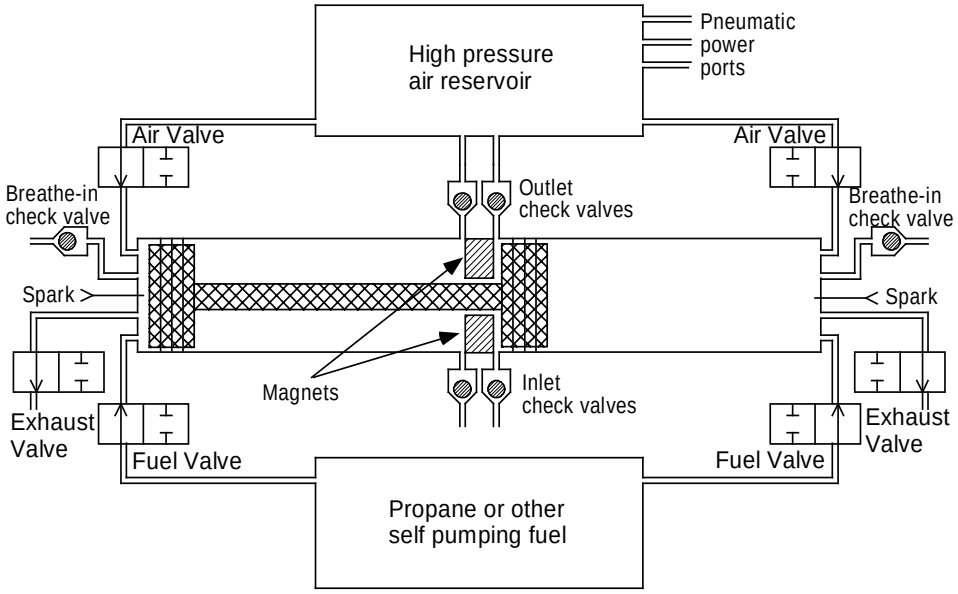

Figure 4-2: Schematic of New Version of FPC.

The device is completely symmetrical, so its starting position can be on either side. Assuming the piston's initial position is at the left, the piston is held in place by the magnets while injecting a mixture of pressurized air and propane into the combustion chamber. Once the proper amount of mixture has entered the chamber, the air and propane valves close and a sparkplug initiates combustion. The piston will then travel to the right while serving four functions: (1) pump fresh air into the air reservoir; (2)

exhaust the diluted combustion products from previous combustion out of the right cylinder's combustion chamber; (3) breathe in fresh air into the right cylinder's pumping chamber; and (4) breathe in fresh air into the combustion chamber after the pressure has dropped below atmospheric, thus cooling down and diluting the combustion products. At the end of the stroke the piston will be held in place by the magnets on the right side, and the cycle can occur on the opposite side in the same fashion (from right to left). The work required to break the magnetic holding force after combustion is retrieved at the end of pumping. The force-distance profile of the magnets also allows dominantly inertial loading presented to the combustion pressure after a very short distance after break-away has occurred.

Design

Figure 4-3 shows a picture of the new FPC prototype. Most of the hardware was inherited from the first prototype (valves, magnets, sensors, spark plugs). The cylinders were replaced with two 4-inch stroke, ¾-inch bore BIMBA® standard air cylinders, and ported appropriately. Figure 4-4 shows a close-up of the new cylinder configuration, with the piston fully retracted (and the opposite piston disconnected).

By examining Figure 4-3, it should be noted that the hardware implementation of this prototype mainly differs from the generalized schematic (Figure 4-2) in that the piston rods are connected to each other through a moving mass, which is needed for inertial loading purposes. Another important difference to note is that the moving mass carries the magnets (2 on each side), which snap onto the ferrous plates at the end of each stroke. Figure 4-4 shows the magnets pressed against the ferrous plate.

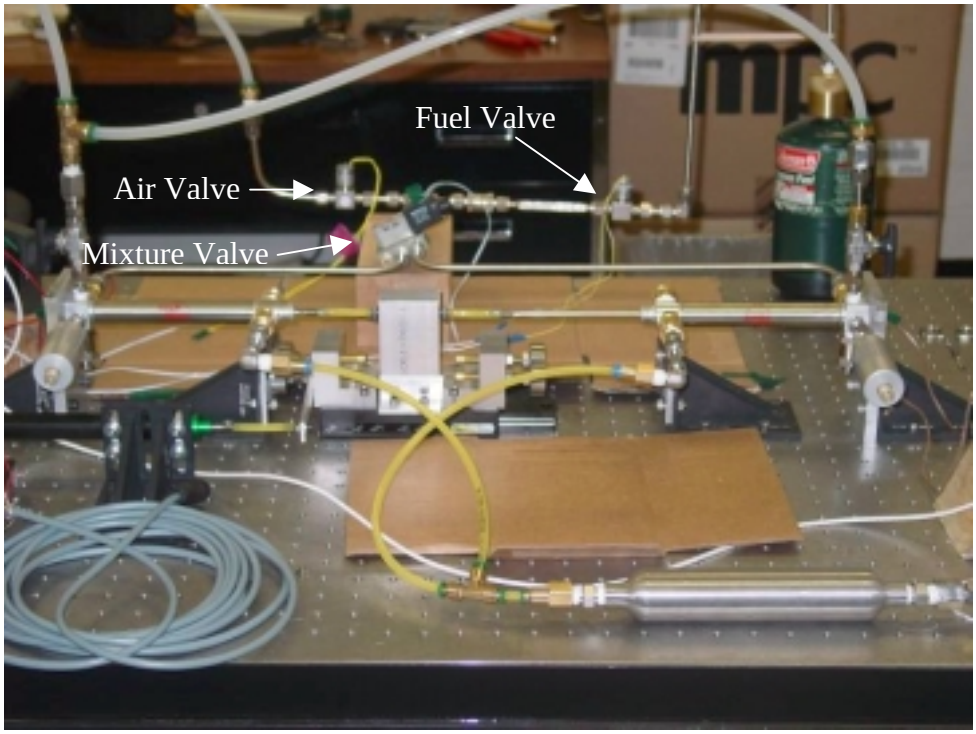

Figure 4-3: Picture of New FPC

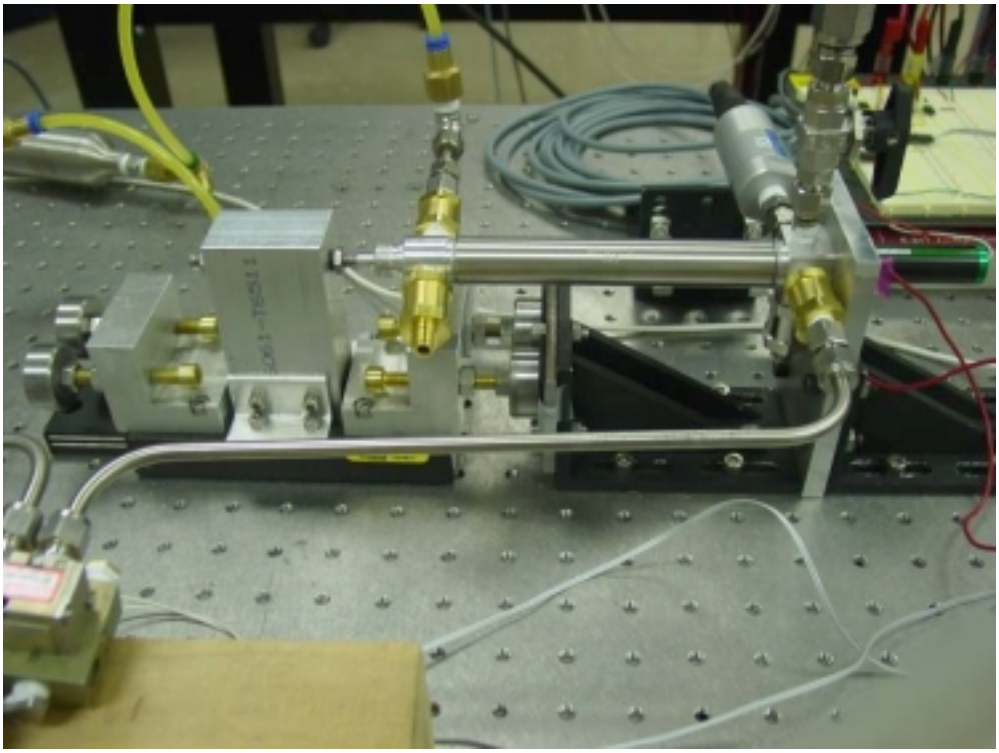

Figure 4-4: Close-up Picture of Cylinder

This new configuration addresses some of the limitations found in the previous version of the FPC. The cylinder rods were connected to the moving mass with small pieces of plastic tubing in order to avoid a purely rigid connection, which would yield friction due to misalignments. Added to that, the cylinders chosen are much smoother than the previous ones, so the frictional losses in this system are reduced. The lack of return springs makes the system quieter and a bit more energy efficient. Also, with these cylinders' bore, flow restrictions through valves are no longer contributing noticeable energetic losses.

Since the main objective of this paper is to show the total efficiency of the system from stored chemical energy of propane to stored pneumatic potential energy of compressed air, it is imperative to be as precise as is reasonably possible with all measurements. The most difficult, yet one of the most important measurements to determine is the mass of propane used for combustion. Knowing this mass and the energy density of propane, the total amount of initial energy can be determined and compared to the potential energy of compressed air in the reservoir. This potential energy is equal to $(P_s - P_{atm})V_s$, where P_s and V_s are the pressure and volume in the reservoir, and P_{atm} is atmospheric pressure.

Measuring the Mass of Propane

As shown in Figure 4-3, the air/fuel mixture enters the chamber by controlled opening and closing of the air, fuel and mixture valves. The air and fuel valves are timed such that a stoichiometric mixture exists within a common mixing line at the exit of both valves. This mixture is then admitted to one of the two combustion chambers via a three-way

mixture valve. The air and fuel valves are Parker® Series-9 valves, and operate as two-way on/off valves. The nominal response time of these valves is 12 ms, while their commanded opening times for this application will range between 8-12 ms for propane and 50-80 ms for air. A mass flow meter could not be used to determine the mass of propane flowing because these are small pulses, and not steady flows. Also, since the propane valve operates at opening times close to the valve response time, the small pulse flow dynamics would not be similar to the steady flow dynamics. The mass was instead calculated by injecting propane into an inverted graduated cylinder on a beaker with water, and observing the water displacement in the cylinder for various durations of the commanded opening pulse sent to the fuel valve. This was done for 8, 9, and 10 ms pulses, and each one was performed several times to obtain an average. The standard deviation of measured displaced water for each pulse duration was very close to the readability of the scale. The same was done for the air, in order to find stoichiometric values based on air and fuel valve opening times. It should be noted that this match of opening times yields accurate stoichiometric mixtures only if flowing into atmospheric pressure.

For precise data acquisition purposes, the engine was run only in single fire shots. Before each fire, the exhaust port and mixture valve was opened, and the fuel and air valves opened for specific durations previously determined to yield a stoichiometric mixture. This was done several times such that the entire mixing line would contain a precise air-fuel ratio. The exhaust port was then closed and some of the stoichiometric air/fuel mixture remaining in the mixture line was pushed into the combustion chamber, by opening the mixture valve, until reaching the desired injection pressure. This

pressurized mixture can be taken as an ideal gas, so the mass in the chamber can be calculated as $m = \frac{PV}{RT}$, where P and V are the pressure and volume in the chamber, T is the temperature of the mixture (approx. room temperature), and R is the gas constant of the stoichiometric propane/air mixture. Then, with knowledge of a stoichiometric mass ratio, the mass of propane subject to combustion can be determined.

Adjusting Mixture while Pumping

Ideally, every firing should be strong enough for the piston to just barely make it to the other side. If combustion is stronger than it needs to be, the piston will carry extra energy that will not be used for pumping, but dissipated in colliding with the other side. This is quite wasteful and brings down the total efficiency of the system. Conversely, if the combustion is weak and the piston carries less kinetic energy than needed to pump a full stroke, it will not make it to the other side, and some energy would need to be re-invested (by utilizing the air injection valve and energy stored in the reservoir) to push the piston to the other side (note that the area of the rod side being less that the piston side will allow this to occur when both sides are ultimately presented with the reservoir pressure). Precisely controlling the strength of the combustion for continuous operation would require more sophisticated equipment and is beyond the scope of this paper. However, full compression of the air reservoir is achieved here with discrete increases of valve opening times as needed. It should be noted that due to the low resolution of the valves at these extremely low mass flows, the combustion pressure increase between any two valve-opening times is relatively large. Figure 4-5 shows the average amounts of

propane mass and combustion pressures yielded by all three sets of valve timings used for this experiment.

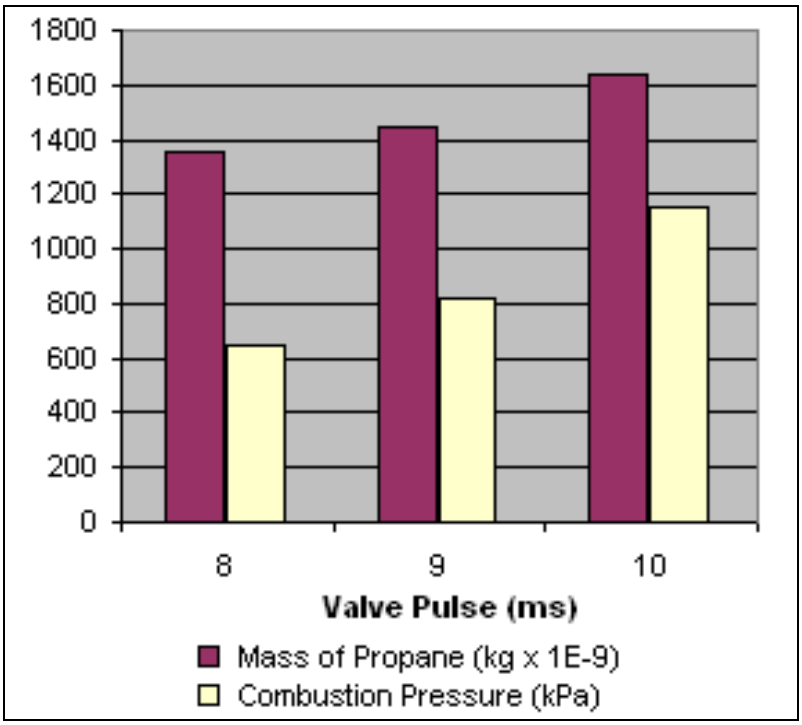

Figure 4-5: Fuel Masses and Combustion Pressures

For data gathering, the FPC is fired first with the lowest set of valve opening times. After a certain number of firings, the pressure in the air reservoir will reach a certain threshold, at which point the combustion pressure will not be adequate for the free piston to complete the stroke, and the injection is re-adjusted to the next set of opening times. It should be intuitive that the first few shots after a threshold are the least efficient, while the last few shots before a threshold are the most efficient.

Experimental Results and Evaluation

Experimentation consisted of a series of single fire shots. Combustion took place in a 6.4 mL volume, with a moving mass of 1.82 kg. Three different opening times of the fuel valve were used for combustion (8, 9, and 10 ms), depending on the combustion pressure desired. The data shown in Figures 4-6 through 4-13 are taken from two single shots of the device. The first set (Figures 4-6 through 4-9) show a less than ideal shot and the second set (Figures 4-10 through 4-13) show a more ideal shot. This variation is a result of the lack of adequate valve opening resolution resulting from the hardware used with this experimental setup. Figures 4-6, 4-7, 4-8, and 4-9 show combustion pressure, air reservoir pressure, position of the piston and velocity of the piston, respectively. These were taken from a typical firing at a low pumping pressure and exhibit the inadequacy of resolution of the air and fuel valves – note the collision with the opposing side apparent from the sharp decrease in velocity shown in Figure 4-9. The spark occurs at 0.4 seconds. Figure 4-6 also shows the injection pressure in the combustion chamber before ignition.

Despite the inefficient operation shown for Figures 4-6, 4-7, 4-8 and 4-9, it should be noted that these plots still exhibit the main features of the PFC outlined in [10], such as the inertial loading (nearly adiabatic expansion in Figure 4-6) and the breathe-in mechanism (combustion pressure decreases to atmospheric pressure before the end of the stroke). Also, the frequency for continuous operation can be maximized by reducing the time between signals. With basic knowledge of the injection, combustion and expansion timings, the duration of each stroke can be reduced to just under 0.4 seconds. This yields a total operational frequency of 2.5 strokes per second.

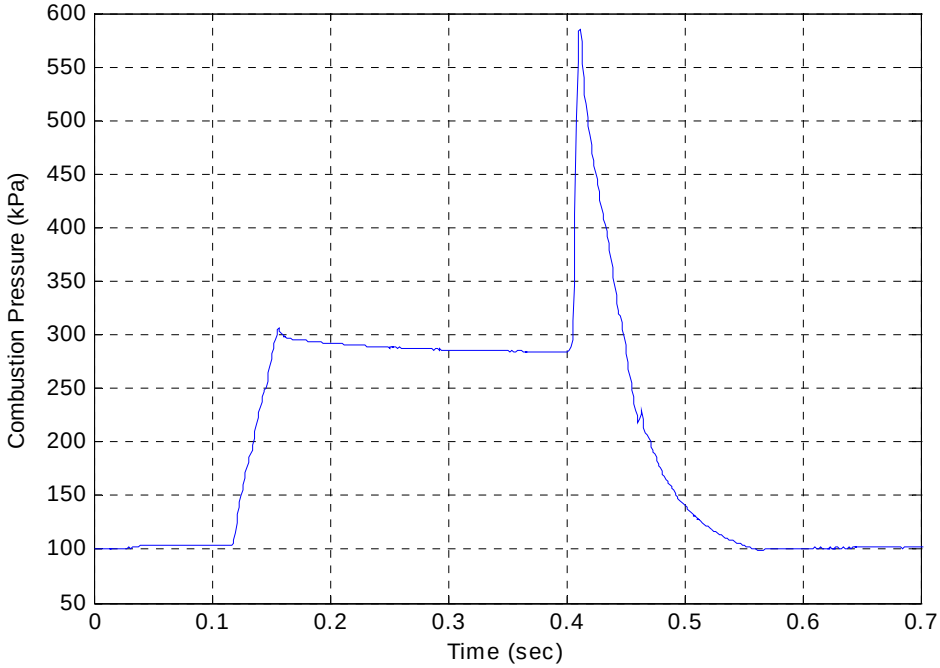

Figure 4-6: Pressure in the Combustion Chamber.

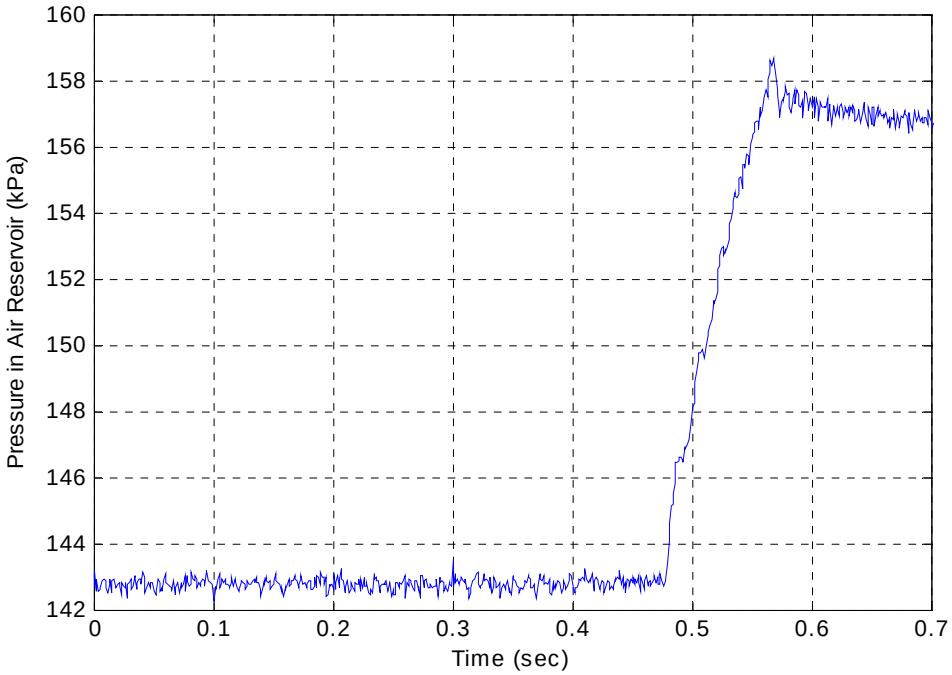

Figure 4-7: Pressure in the Air Reservoir.

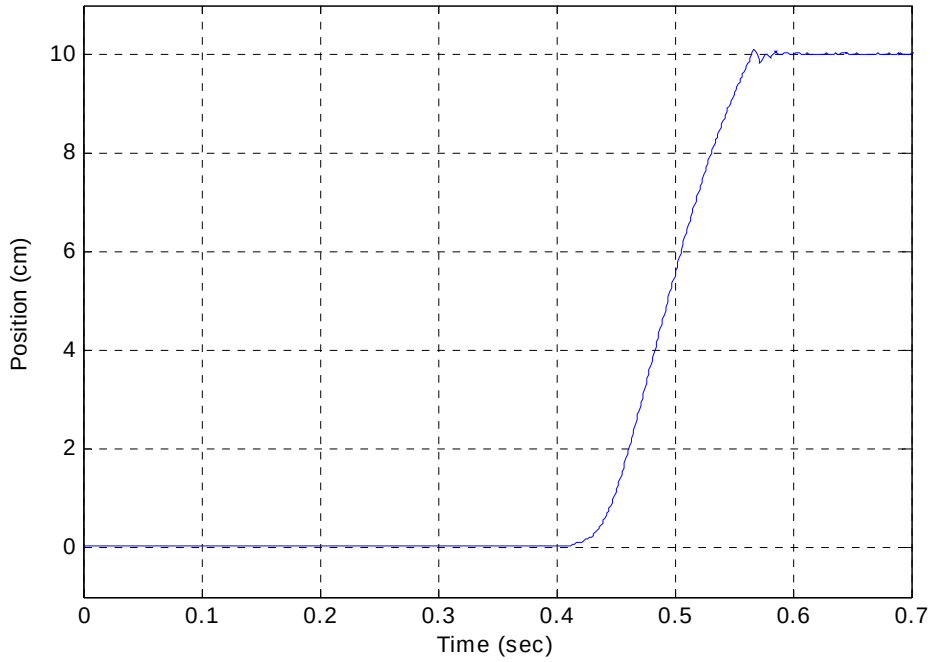

Figure 4-8: Position of the Free Piston.

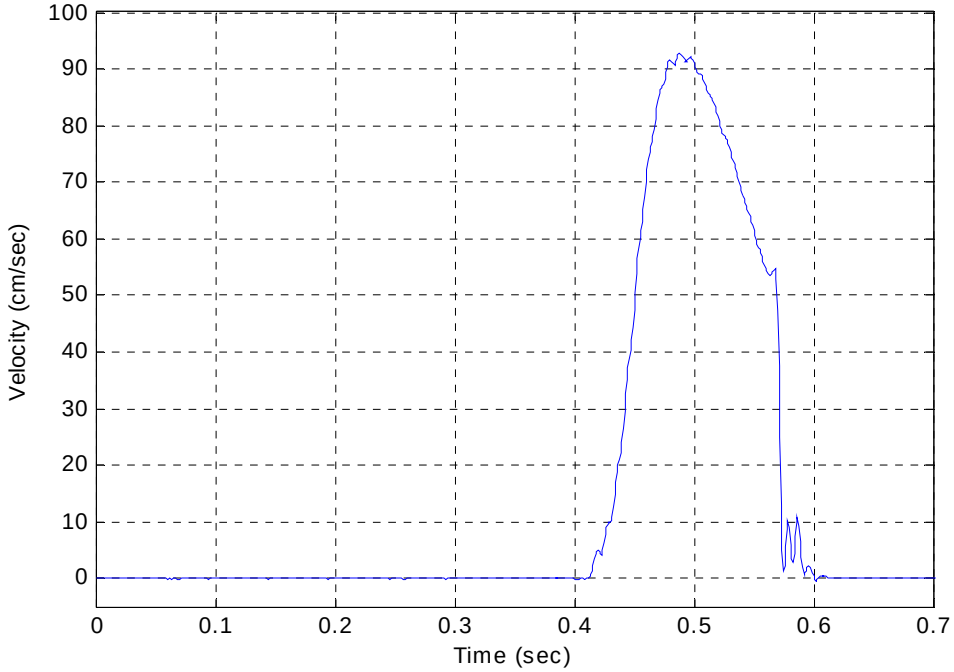

Figure 4-9: Velocity of the Free Piston.

Through single fire shots, the air reservoir was successfully compressed from atmospheric pressure up to 310 kPa. It took 52 strokes to achieve this pressure, which can be achieved in 20 seconds of continuous operation (based on the previously described operational frequency). This compression pressure is limited by the ratio of stroke volume (engine displacement) over dead volume in the rod (compressing) side of the chosen cylinders. This dead volume was quite large (about 4.1 mL), and is a nonideality (as noted in [2]) that should be reduced in future design considerations. This nonideality presents the main drawback in this version of the FPC.

The total energetic merit of this system is represented by the efficiency of conversion from chemically stored energy in propane to pneumatic potential energy of compressed air. As shown analytically in [2], this efficiency also increases for larger combustion pressures. Experimentally, this efficiency was calculated for a single fire shot in which the piston just barely made it to the other side – the ideal case which could conceivably be achieved for every stroke given adequate valve resolution. Figures 4-10, 4-11, 4-12, and 4-13 show the respective pressures, displacement and velocity for this particular shot. By looking at the position and velocity in Figures 4-12 and 4-13, it can be observed that the piston "barely made it" to the other side, with a little help from the magnetic force. This shot used 1.42×10^{-6} kg of propane and resulted in an increase of the pressure in the air reservoir (a volume of 1.866×10^{-4} m^3) from 222.75 kPa to 235 kPa, yielding a pneumatic potential energy increase of 2.29 Joules. The total efficiency of this shot is calculated as,

$$\eta_{total} = \frac{0.002286\,\text{kJ}}{\frac{46350\,\text{kJ}}{\text{kg fuel}} \times 1.42 * 10^{-6}\,\text{kg fuel}} \times 100 = 3.47\% \quad (1)$$

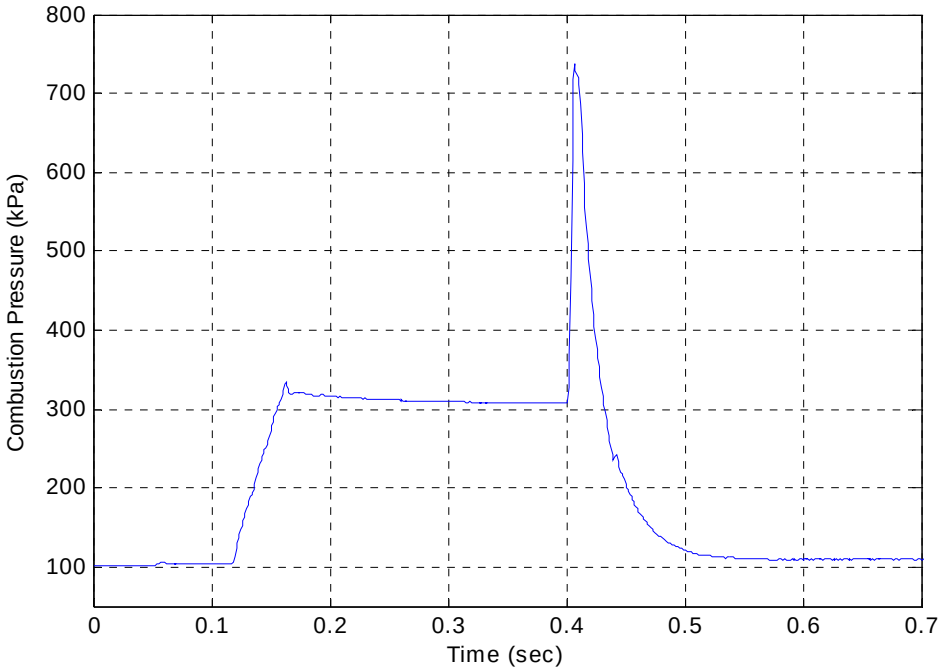

Figure 4-10: Pressure in the Combustion Chamber.

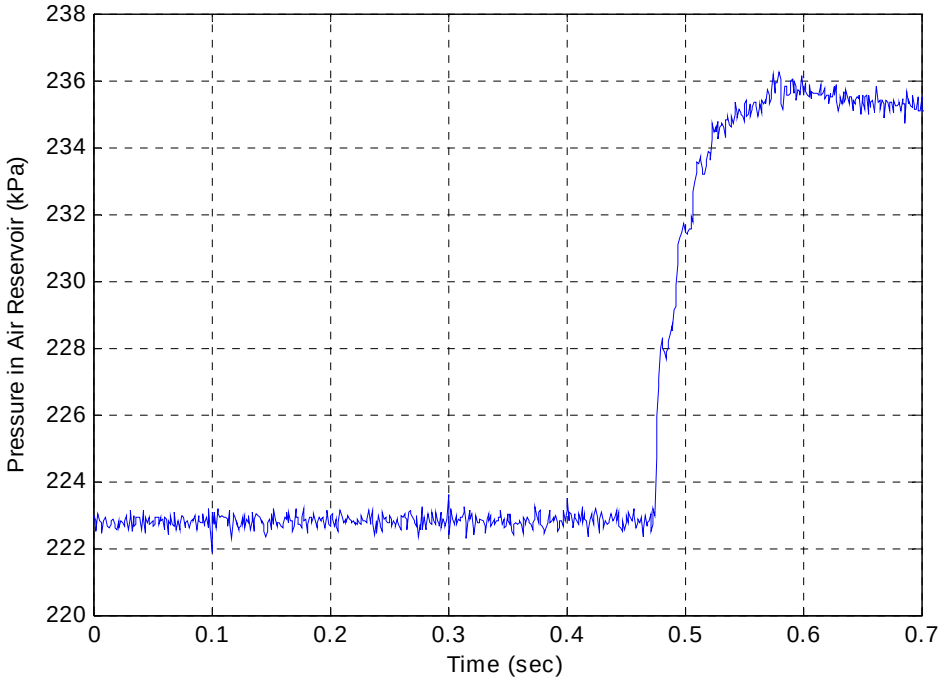

Figure 4-11: Pressure in the Air Reservoir.

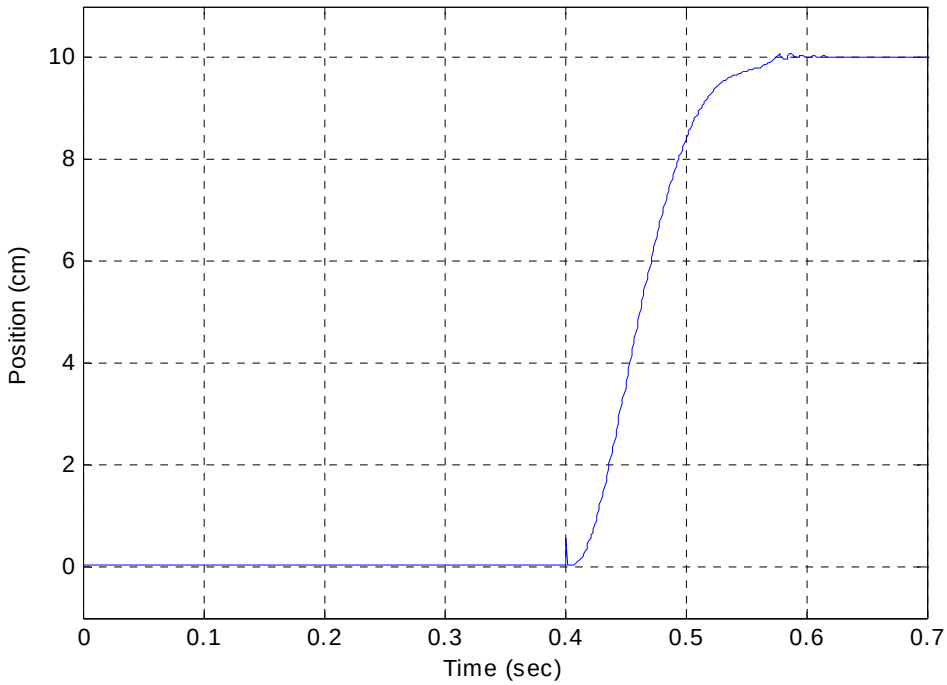

Figure 4-12: Position of the Free Piston

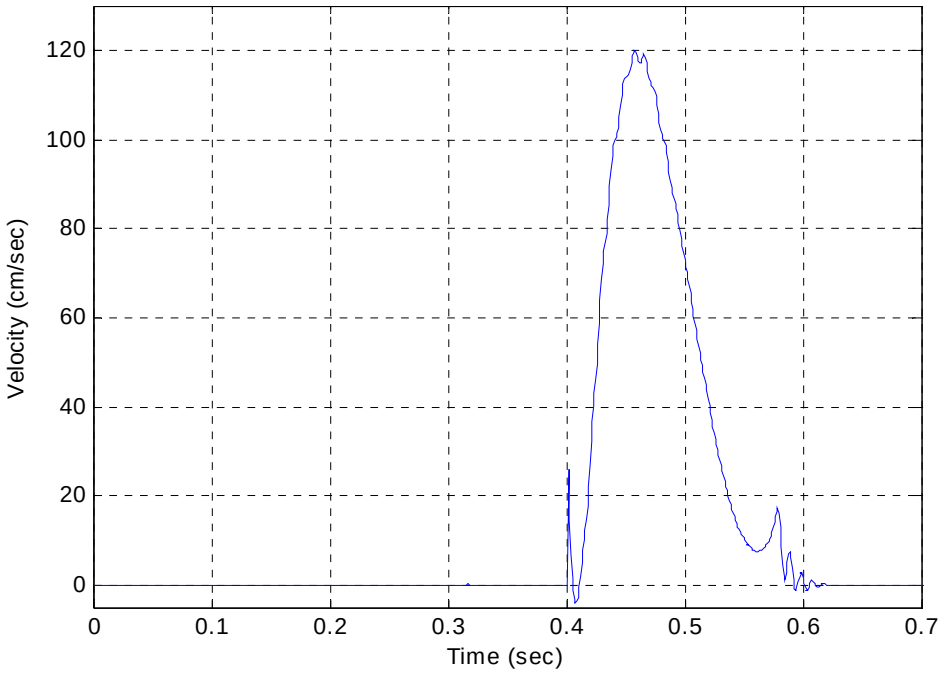

Figure 4-13: Velocity of the Free Piston.

Based on a simple thermodynamic analysis presented in [2], the total efficiency of the system with these parameters is calculated to be 7.62%. However, this calculation assumes zero dead volume in the compressing side of the cylinder, no heat losses in the combustor side and high heat losses in the compressor side. The issue of excess dead volume in the compressor side present in this experimental prototype would be difficult to fully address with standard pneumatic equipment (such as those used here), and would require custom made parts in order to reduce the minimum rod-side volume. As also shown in [2], the efficiency of the device increases with increased combustion pressure (up to 20% efficiency). With these points in mind, the experimental efficiency met reasonable expectations, while leaving room for improvement in future designs.

Conclusions

The design of a new version of a Free Piston Compressor was presented. This device is a small-scale internal combustion engine capable of pumping air into a high-pressure air reservoir, with satisfactory efficiency. The proposed technology is intended to be coupled with a pneumatic untethered robotic system, and aims to provide an order of magnitude greater energetic merit than state of the art power supply and actuation systems (electrical batteries coupled with DC motors).

The experimental prototype FPC exhibited predicted desirable design features such as: reliable and consistent firing, inertial loading and nearly adiabatic expansion of combustion gases, combustion pressures that decrease to atmospheric pressure before the end of the stroke thereby employing the breathe-in mechanism for cooling and low noise, and a predicted frequency of continuous operation of 2.5 strokes per second. It was

shown that further design work regarding the resolution of the air and fuel valves is needed to secure decent efficiencies across different reservoir pressures, and further work regarding the dead volume in the rod-side of the piston is needed to increase efficiency.

A measured efficiency of 3.47% was achieved in converting stored chemical energy into stored pneumatic potential energy with a datum at atmospheric pressure: $(P_s - P_{atm})V_s$. In comparing this power supply system with state-of-the-art rechargeable batteries, an energy density of 180 kJ/kg for NiMH batteries and a conversion efficiency of 50% for an electromagnetic motor and mated gearhead would yield 90 kJ of delivered controlled mechanical work per kilogram of source energetic material. For the FPC under consideration, an energy density of 46350 kJ/kg for propane, a measured conversion efficiency of 3.47% from stored chemical to pneumatic energy, a 75% efficiency associated with the computed mass reinvestment from the air reservoir for the next combustion event (see [2]), and an assumed conversion efficiency of 30% from stored pneumatic energy to delivered controlled mechanical work of an associated pneumatic actuator, would yield 365 kJ of controlled work per kilogram of source energetic material. This increase, coupled with the equally important high power density of pneumatic actuators over electromagnetic motors (approximately 450 W/kg versus 50 W/kg), should contribute to a power supply and actuation system more appropriate for untethered human scale and power comparable robots and actuated devices. It is expected that design changes to the next generation of this device will result in further improvements.

References

[1] Goldfarb, M., Barth, E. J., Gogola, M. A., Wehrmeyer, J. A., "Design and Energetic Characterization of a Liquid-Propellant-Powered Actuator for Self-Powered Robots". *IEEE/ASME Transactions on Mechatronics*, vol. 8, no. 2, pp. 254-262, June 2003.

[2] Barth, E. J., and Riofrio, J., "Dynamic Characteristics of a Free Piston Compressor," *2004 ASME International Mechanical Engineering Congress and Exposition (IMECE)*, IMECE2004-59594, November 13-19, 2004, Anaheim, CA.

[3] Pescara, R. P., "Motor Compressor Apparatus," U.S. Patent No. 1,657,641, Jan. 31, 1928.

[4] Klotsch, P., "Ford Free-Piston Engine Development," *SAE Technical Paper Series*, 590045, vol. 67, pp. 373-378, 1959.

[5] Underwood, A. F., "The GMR 4-4 'Hyprex' Engine: A Concept of the Free-Piston Engine for Automotive Use," *SAE Technical Paper Series*, 570032, vol. 65, pp. 377-391, 1957.

[6] Aichlmayr, H. T., Kittelson, D. B., and Zachariah, M. R., "Miniature free-piston homogenous charge compression ignition engine-compressor concept – Part I: performance estimation and design considerations unique to small dimensions," *Chemical Engineering Science*, 57, pp. 4161-4171, 2002.

[7] Aichlmayr, H. T., Kittelson, D. B., and Zachariah, M. R., "Miniature free-piston homogenous charge compression ignition engine-compressor concept – Part II: modeling HCCI combustion in small scales with detailed homogeneous gas phase chemical kinetics," *Chemical Engineering Science*, 57, pp. 4173-4186, 2002.

[8] Beachley, N. H. and Fronczak, F. J., "Design of a Free-Piston Engine-Pump," *SAE Technical Paper Series*, 921740, pp. 1-8, 1992.

[9] McGee, T. G., Raade, J. W., and Kazerooni, H., "Monopropellant-Driven Free Piston Hydraulic Pump for Mobile Robotic Systems," *ASME Journal of Dynamic Systems, Measurement, and Control*, vol. 126, pp. 75-81, March 2004.

[10] Riofrio, J., and Barth, E. J., "Design of a Free Piston Pneumatic Compressor as a Mobile robot Power Supply," *Proceedings of the 2005 IEEE International Conference on Robotics and Automation (ICRA)*, pp. 236-241, Barcelona, Spain, April 2005.

[11] Black, William Z., and James G. Hartley, *Thermodynamics, Third Edition*, New York: Harper Collins, 1996.

CHAPTER IV

MANUSCRIPT 3

ADDENDUM

Pneumatic Stored Energy

The revised thermodynamic efficiency presented in the Addendum of Manuscript 1 (Chapter II) showed a more adequate representation of the pneumatic stored energy in the air reservoir:

$$E_{stored} = \frac{P_s V_f}{1-\gamma}\left[\left(\frac{P_s}{P_{atm}}\right)^{\frac{1-\gamma}{\gamma}} - 1\right] \tag{2}$$

In calculating the stored energy resulted from one stroke, a change in pressure of 12.25 kPa was measured in the 1.866×10^{-4} m^3 air reservoir. Applying Equation (2), this energy is computed as 2.48 Joules.

Mass of Propane used for Combustion

While presenting a effective way to ensuring a stoichiometric air/fuel mixture, this manuscript overestimated the total mass of fuel used for combustion, since the fuel injection was assumed an isothermal process instead of an adiabatic process. To account for this adiabatic compression, we can consider the following relationship:

$$P_{atm} V_{line}^{\gamma_{mix}} = P_{inj} V_{e0}^{\gamma_{mix}} \tag{3}$$

where P_{atm} is the atmospheric pressure, V_{line} is the partial volume of the mixture before entering the combustion chamber, P_{inj} is the injection pressure, V_{e0} is the dead volume in the combustion chamber, and γ_{mix} is the ratio of specific heats of the air/fuel mixture. Additionally, by conservation of mass, and assuming an ideal gas, we have:

$$m_{inj} = \frac{P_{atm} V_{line}}{R_{mix} T_{amb}} = \frac{P_{inj} V_{e0}}{R_{mix} T_{inj}} \tag{4}$$

where m_{inj} and R_{mix} are the mass and average gas constant of the fuel mixture, respectively, and T_{amb} is the ambient temperature and T_{inj} is the injection temperature, previously unaccounted for. Combining Equations (3) and (4), the injected mass of fuel can be calculated as:

$$m_{inj} = \frac{P_{atm}}{R_{mix} T_{amb}} \left(\frac{P_{inj}}{P_{atm}} \right)^{\frac{1}{\gamma_{mix}}} \tag{5}$$

The mass of propane used for efficiency calculations, then, is 9.93×10^{-7} kg. The efficiency of conversion from chemically stored energy in propane to pneumatic potential energy of compressed air can be re-calculated as:

$$\eta_{total} = \frac{0.00248\,\text{kJ}}{\frac{46350\,\text{kJ}}{\text{kg fuel}} \times 1.05 * 10^{-6}\ \text{kg fuel}} \times 100 = 5.10\% \tag{6}$$

A more detailed energetic evaluation, including the efficiency obtained from air mass re-investment, is presented in Manuscript 4 (Chapter V).

CHAPTER V

MANUSCRIPT 4

A FREE PISTON PNEUMATIC COMPRESSOR AS A MOBILE ROBOT POWER SUPPLY: DESIGN, CHARACTERIZATION AND EXPERIMENTAL OPERATION

José A. Riofrio and Eric J. Barth

Department of Mechanical Engineering

Vanderbilt University

Nashville, TN 37235

(Submitted to the *International Journal of Fluid Power*)

Abstract

The design and dynamic characterization of a free piston compressor (FPC) is presented in this paper. The FPC is a proposed device that utilizes combustion of a hydrocarbon fuel to compress air into a high-pressure supply tank, thus serving as a portable pneumatic power supply. The device is configured such that the transduction from thermal energy to stored energy, in the form of compressed gas, is efficient relative to other small-scale portable power supply systems. This efficiency is achieved by matching the dynamic load of the compressor to the ideal adiabatic expansion of the hot gas combustion products. It is shown that a load that is dominantly inertial provides a nearly ideally matched load for achieving high thermodynamic efficiency in a heat engine. The device proposed exploits this fact by converting thermal energy first into kinetic energy of the free piston, and then compressing air during a separate compressor phase. The proposed technology is intended to provide a compact pneumatic power supply source appropriate for human-scale robots. An analytical model of the proposed device is developed, and an FPC prototype is designed and built and its yielded experimental results are compared with theoretical.

Introduction

The need for an effective portable power supply for human-scale robots has increasingly become a matter of interest in robotics research. Current prototypes of humanoid robots, such as the Honda P3, Honda ASIMO and the Sony QRIO, show significant limitations in the capacity of their power sources in between charges (the operation time of the humanoid-size Honda P3, for instance, is only 25 minutes). This

limitation becomes a strong motivation for the development and implementation of a more adequate source of power. Moreover, the power density of the actuators coupled to the power source needs to be maximized such that, on a systems level evaluation, the combined power supply and actuation system is both energy and power dense. Put simply, state-of-the-art batteries are too heavy for the amount of energy they store, and electric motors are too heavy for the mechanical power they can deliver, in order to present a viable combined power supply and actuation system that capable of delivering human-scale mechanical work in a human-scale self contained robot package, for a useful duration of time. The motivation details are discussed more thoroughly in [7].

The total energetic merit of an untethered power supply and actuation system is a combined measure of 1) the source energy density of the energetic substance being carried, 2) the efficiency of conversion to controlled mechanical work, 3) the energy converter mass, and 4) the power density of the actuators. With regard to a battery powered electric motor actuated system, the efficiency of conversion from stored electrochemical energy to shaft work after a gear head can be high (~50%) with very little converter mass (e.g. PWM amplifiers); however, the energy density of batteries is relatively low (about 180 kJ/kg for NiMH batteries), and the power density of electrical motors is not very high (on the order of 50 W/kg), rendering the overall system heavy in relation to the mechanical work that it can output. With regard to the hydrocarbon-pneumatic power supply and actuation approach presented here relative to the battery/motor system, the converter mass is high and the total conversion efficiency is shown to be low. However, the energy density of hydrocarbon fuels, where the oxidizer is obtained from the environment and is therefore free of its associated mass penalty, is in

the neighborhood of 45 MJ/kg, which is more than 200 times greater than the energy density of state of the art electrical batteries. This implies that even with poor conversion efficiency (poor but within the same order of magnitude), the available energy to the actuator per unit mass of the energy source is still at least one order of magnitude greater than the battery/motor system. Additionally, linear pneumatic actuators have roughly one order of magnitude greater power density than state of the art electrical motors. Therefore, the combined factors of a high-energy density fuel, the efficiency of the device, the compactness and low weight of the device, and the use of the device to drive lightweight linear pneumatic actuators (lightweight as compared with power comparable electric motors) is projected to provide at least an order of magnitude greater total system energy density (power supply and actuation) than state of the art power supply (batteries) and actuators (electric motors) appropriate for human-scale power output.

The FPC presented in this paper serves the function of converting chemically stored energy of a hydrocarbon into pneumatic potential energy of compressed air. More specifically, it extracts the energy by producing combustion of a stoichiometric mixture of propane and air, and the combustion-driven free piston acts as an air pump to produce the compressed air.

The idea of using a free piston combustion-based device as a pump has been around since the original free-piston patent by Pescara in 1928 [11]. Junkers developed a free piston compressor that became widely used by German submarines through World War 2 [10]. The automotive industry conducted a large amount of research in the 1950's. Ford Motor Company considered the use of a free piston device as a gasifier in 1954 [8]. General Motors presented the "Hyprex" engine in 1957 [14]. Such endeavors were aimed

at an automotive scale engine and were largely unsuccessful. In more recent times, the free piston engine concept has been considered for small-scale power generation. Aichlmayr, et. al. [1, 2] have considered the use of a free piston device as an electrical power source on the 10 W scale meant to compete with batteries. Beachley and Fronczak [5], among others, have considered the design of a free-piston hydraulic pump. McGee, et. al. have considered the use of a monopropellant-based catalytic reaction as an alternative to combustion, as applied to a free piston hydraulic pump [9].

Even though free piston devices have been studied in the past, none of these previous designs explicitly featured what is perhaps the main advantage of a free piston, which is its capability to offer a purely inertial load. The main focus of this work is to exploit the fact that a free piston can present a purely inertial load to the combustion, and as a result, desirable operational characteristics can be obtained, such as high efficiency, low noise, and low temperature operation. Additionally, this work aims to demonstrate that a free piston compressor stands as a strong candidate for a portable power supply system for untethered human-scale pneumatic robots.

An outline of this paper is as follows. Section 2 describes the proposed device and its operation, and outlines its main features. Section 3 presents parts of the model and a simulation of the generalized system, and its yielded theoretical predictions. Section 4 presents the design and implementation of a bench-top laboratory prototype FPC, and its main design features. Section 5 shows all relevant experimental data along with their respective analysis and evaluation, and compares experimentally obtained data with theoretical predictions. Finally, section 6 presents the main conclusions and a discussion of the FPC’s capability to compete with state-of-the-art power supply technology.

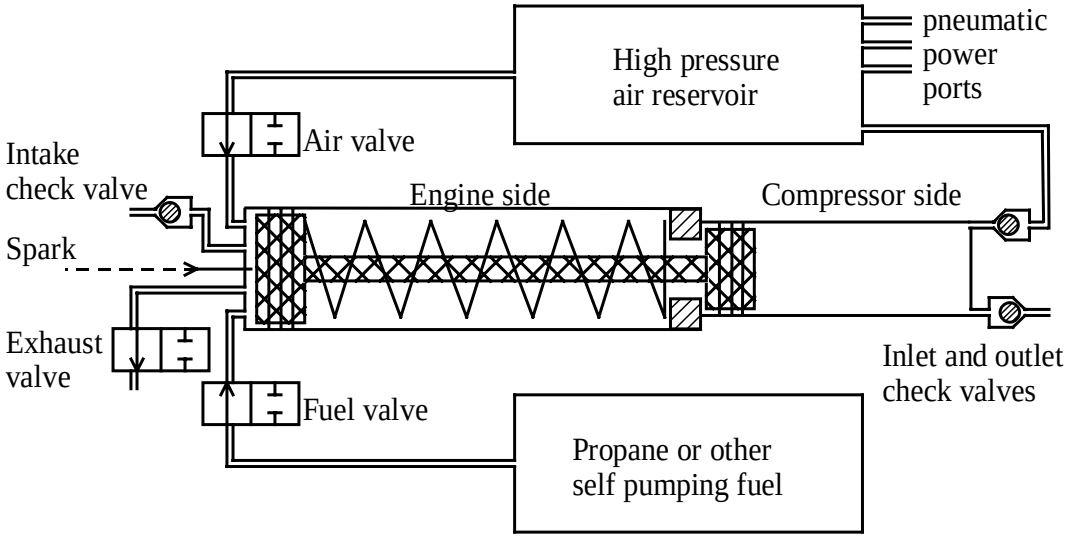

Figure 5-1: Schematic of the free piston compressor system

The Free Piston Compressor

A generalized schematic of the free piston compressor system is shown in Figure 5-1. In the position shown, the device operates by first opening the air and fuel valves to allow the proper mixture and amount of air and fuel into the combustion chamber of the engine side. Once the proper air/fuel mixture is inside, the valves close and a spark initiates the combustion. Upon combustion, the free piston moves to the right as the combustion gases expand, converting the energy of combustion into kinetic energy of the free piston. The compressor side of the device is configured such that the piston sees a negligible compressive force for a distance greater than required for the combustion gasses to both expand down to atmospheric pressure, and allow the intake of fresh cool air to cool the exhaust products through the intake check valve. After this point the kinetic energy of the free piston is converted into the work required to compress and then pump the gasses in the compressor chamber into the high-pressure reservoir. The cycle is completed when

the light return spring moves the piston to the left pushing out the diluted exhaust products of the engine side, and refilling the compressor side with air drawn in through an inlet check valve.

Besides advantages regarding efficiency related to inertial loading, the free piston compressor offers on-demand start and stop (since there is no compression stroke in the engine side), cool operation (given that the combustion products are greatly diluted with air after expanding down below atmospheric pressure), quiet operation (given that there is no exhaust of high-pressure gasses), and simplicity. These characteristics are achieved due to the following main features of the FPC:

Inertial Loading – The free piston is not rigidly attached to a crankshaft or any timing linkage alike, so it offers purely inertial loading to the expanding combustion gasses. This allows the free piston to store as kinetic energy the work done by the ideal adiabatic expansion of the combustion gasses. The combustion gasses are allowed to expand until they reach atmospheric pressure, all while still contributing to the inertial loading. This full expansion contributes to a higher efficiency than if full expansion were not allowed as is the case with most small-scale IC engines (Figure 5-2). Typical IC engines (large-scale or small-scale) are required to provide a high immediate output power profile in their design specifications, so they are concerned only with extracting the higher-power portion of the combustion curve, while wastefully exhausting the rest. The FPC, on the other hand, is independent from the main device's (e.g. robot) output power, since its function is only to store potential energy, and therefore it can extract the lower-power portion of the P-V curve as well. As an additional consequence, the FPC has a quiet exhaust, since no high-pressure gasses will be exhausted into the atmosphere.

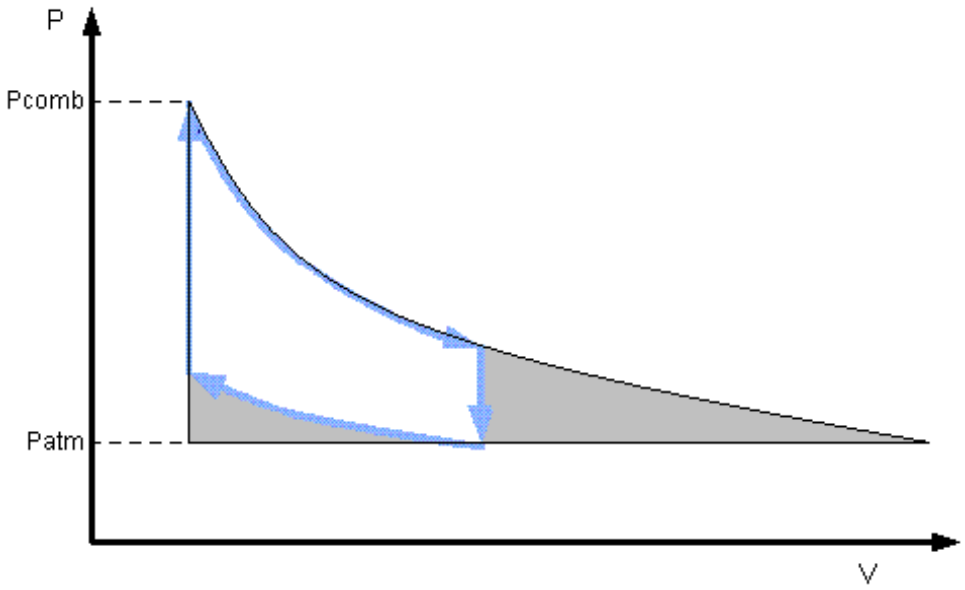

Figure 5-2: P-V diagram of FPC cycle superimposed on a P-V diagram of the Otto cycle. The shaded region to the right represents the additional work extracted in the FPC cycle that is not extracted in the Otto cycle.

Breathe-in Mechanism – When the combustion gasses reach atmospheric pressure, the free piston will still be traveling (with maximum kinetic energy), and thus will induce a drop of pressure in the combustion chamber as the motion continues. This pressure drop will cause an intake check valve to open and allow fresh atmospheric air to enter the chamber. This fresh air will both cool down and dilute the combustion products. Therefore, the breathe-in mechanism ensures a low temperature operation of the device, as well as reduced concentration of emission products.

Start on Demand – Since the intake valves and spark plug are electrically actuated, and since high-pressure injection of air and fuel eliminate the need for a conventional intake and compression stroke, the FPC does not require the implementation of a starter. This allows the engine to start on demand, without the need for a separate starting cycle. This feature highlights the compatibility between the FPC and a pneumatic power supply for a

robotic system, since they can be tied together by implementing a simple control loop to maintain a particular pressure in the supply reservoir. The FPC would receive a signal and start operating as soon as the actuation pressure supply drops, and likewise turn off once reaching the desired pressure.

Theoretical Predictions

Both the thermodynamic and dynamic characteristics of the system were modeled prior to hardware design. From a thermodynamic analysis, the energetic characteristics of the FPC are modeled separately by the engine side (combustion) and the pump side (compression and pumping).

Engine Side

The engine side converts the energy of combustion into kinetic energy of the free piston, while the compressor side then converts this kinetic energy into stored compressed gas in the high-pressure reservoir. Presenting a purely inertial load during the expansion of the combustion products allows the right loading characteristics such that the high-pressure combustion products are allowed to fully expand down to atmospheric pressure. When this is the case, and assuming an adiabatic process in the combustion chamber immediately following combustion, the work done on the inertial load will be equal to the following,

$$W_e = \frac{P_{e0}V_{e0}^{\gamma_e}}{1-\gamma_e}\left(V_{ef}^{1-\gamma_e} - V_{e0}^{1-\gamma_e}\right) - P_{atm}\left(V_{ef} - V_{e0}\right) \quad (1)$$

where P_{e0} is the initial combustion pressure, V_{e0} and V_{ef} are the initial and final volume of the combustion chamber respectively, γ_e is the ratio of specific heats of the combustion gases (products of combustion), and P_{atm} is the atmospheric pressure. Assuming losses associated with friction are negligible, the kinetic energy of the piston will be equal to the work done W_e, when reaching the position associated with the final volume V_{ef}. It is shown in [4] that the efficiency of conversion from stored chemical energy of the fuel to kinetic energy of the free piston is given by,

$$\eta_{KE} = \frac{W_e}{m_{e0}e} = \left(\frac{R_e T_{AFT}}{e}\right)\left(\frac{\gamma_e P_{e0}^{1/\gamma_e} P_{atm}^{(\gamma_e-1)/\gamma_e} - P_{e0} + (1-\gamma_e)P_{atm}}{(1-\gamma_e)P_{e0}}\right) \tag{2}$$

where m_{e0} is the mass of the fuel/air mixture used for combustion, R_e is the average gas constant of the combustion products, T_{AFT} is the adiabatic flame temperature of combustion, and e is the mass specific energy of the fuel/air mixture computed as the following for the air supported combustion of propane:

$$e = \frac{46350\,\text{kJ}}{\text{kg fuel}} \times \frac{1\,\text{kg fuel}}{16.63\,\text{kg fuel/air mixture}} = 2{,}787{,}000\ \frac{\text{J}}{\text{kg fuel/air mixture}} \tag{3}$$

Compressor Side and Reservoir

The compressor side of the FPC holds two separate processes: firstly, the adiabatic (or polytropic) compression of air, and secondly, the constant pressure process of pumping the air into the high-pressure reservoir. As shown in [4], the work associated with the adiabatic compression process and the constant pressure pumping process are given by the following,

$$W_{c1} = \frac{P_{atm}V_{c0}^{\gamma}}{1-\gamma}\left(V_{ci}^{1-\gamma} - V_{c0}^{1-\gamma}\right) - P_{atm}\left(V_{ci} - V_{c0}\right) \tag{4a}$$

$$W_{c2} = (P_s - P_{atm})(V_{cf} - V_{ci}) \tag{4b}$$

where γ is the ratio of specific heats of air, and V_{c0} and V_{ci} are the initial volume of the compression chamber where compression begins, and the intermediary volume where pumping begins, respectively. V_{cf} is the final volume of the compressor side (i.e. the dead volume of the cylinder not able to be pumped out), and is approximated as zero. At the intermediary volume V_{ci}, the air is at a temperature T_{ci} and is being pumped at the constant pressure P_s, which is the pressure in the air reservoir. Once the air is in the reservoir, and assuming that the reservoir is large, at constant pressure, and that the residence time of the air is large, this air will cool to the ambient temperature, T_{amb}, and undertake its final partial volume, V_f. At this point, the compressed air will take its final form as stored pneumatic potential energy, which, if considered to be its capacity to perform adiabatic work (i.e. in a pneumatic actuator), is given by,

$$E_{stored} = \frac{P_s V_f}{1-\gamma}\left[\left(\frac{P_s}{P_{atm}}\right)^{\frac{1-\gamma}{\gamma}} - 1\right] \tag{5}$$

Since the mass of air is the same at V_{c0}, V_{ci} and V_f, and noting that the pressure and temperature at V_{c0} are P_{atm} and T_{amb}, respectively, we can use ideal gas law expressions to derive the following relationship:

$$V_f = \left(\frac{P_{atm}}{P_s}\right) V_{co} \tag{6}$$

Finally, the efficiency of converting the kinetic energy of the free piston into stored pneumatic potential energy of compressed air is given by,

$$\eta_{PE} = \frac{E_{stored}}{W_e} \tag{7}$$

Mass Investment

To complete the cycle, the mass of air utilized from the reservoir to support the combustion process must be taken into account. Since the energy stored is proportional to the mass in the reservoir, the investment of air mass needed for the combustion, as shown in [4], can be expressed as the following efficiency:

$$\eta_{invest} = \frac{m_c - \frac{15.63}{16.63} m_{e0}}{m_c} = 1 - \frac{15.63}{16.63} \frac{P_{e0} V_{e0} R T_{amb}}{P_{atm} V_{c0} R_e T_{AFT}} \tag{8}$$

where the functionally constrained volume ratio of initial combustion chamber volume to initial compressor chamber volume, V_{e0}/V_{c0}, is shown in [4] to be:

$$\frac{V_{e0}}{V_{c0}} = \frac{\frac{\gamma P_{atm}}{(1-\gamma)}\left[1 - \left(\frac{P_{atm}}{P_s}\right)^{\frac{1-\gamma}{\gamma}}\right]}{\frac{P_{e0}}{(1-\gamma_e)}\left[\gamma_e\left(\frac{P_{atm}}{P_{e0}}\right)^{\frac{\gamma_e - 1}{\gamma_e}} - 1 + (1-\gamma_e)\left(\frac{P_{atm}}{P_{e0}}\right)\right]} \tag{9}$$

System Efficiency

The overall efficiency of the system can be found by multiplying the individual efficiencies regarding the conversion of energy released in combustion to kinetic energy of the free piston, η_{KE}, the conversion of kinetic energy to energy stored in the reservoir at ambient temperature, η_{PE}, and the efficiency related to the required investment of reservoir air to the combustion event, η_{invest}. By multiplying Equations (2), (7) and (8),

and substituting Equations (5), (6) and (9), the overall system efficiency is found in closed-form as follows:

$$\eta_{sys} = \left(\frac{1}{e}\right)\left(\frac{1}{1-\gamma}\right)\left[\left(\frac{P_s}{P_{atm}}\right)^{\frac{1-\gamma}{\gamma}} - 1\right]\left[\frac{\left(\frac{1}{1-\gamma_e}\right)\left[\left(\frac{P_{atm}}{P_{e0}}\right)^{\frac{\gamma_e - 1}{\gamma_e}} - 1 + (1-\gamma_e)\left(\frac{P_{atm}}{P_{e0}}\right)\right]}{\gamma\left(\frac{P_{atm}}{1-\gamma}\right)\left[1 - \left(\frac{P_{atm}}{P_s}\right)^{\frac{1-\gamma}{\gamma}}\right]} - \frac{15.63}{16.63} R_{air} T_{amb}\right] \tag{10}$$

Figure 5-3 shows the overall system efficiency as a function of the initial combustion pressure for various reservoir pressure values.

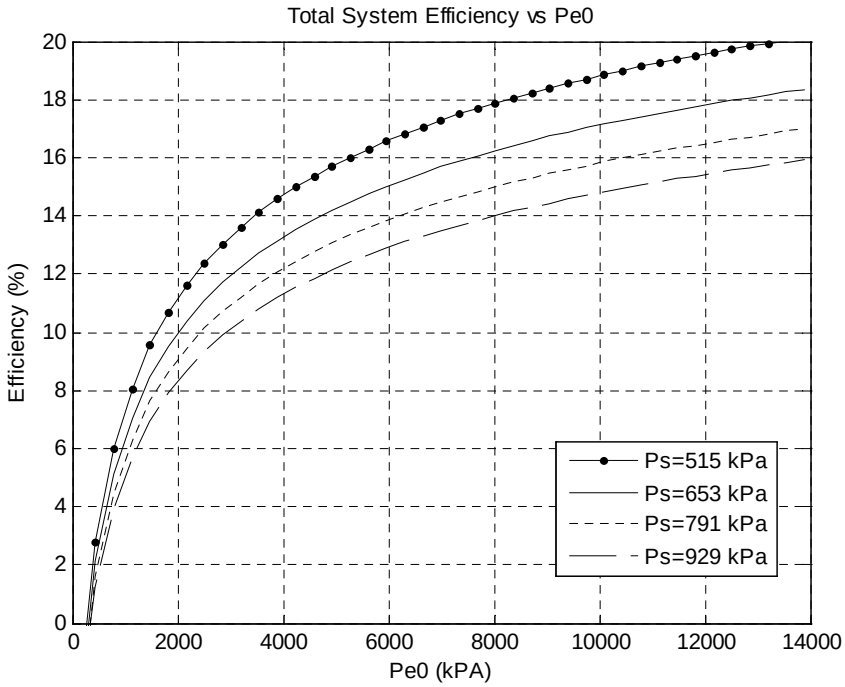

Figure 5-3: The overall system efficiency as a function of the initial combustion pressure (for various values of Ps).

As pointed out earlier, the overall efficiency of the FPC is small relative to a battery powered electric motor actuated system. However, it can be seen from Figure 5-3 that this efficiency, while smaller than that in the electrical domain, is adequate enough to

provide at least an order of magnitude greater total system energy density by exploiting the high energy density of a hydrocarbon fuel.

While a thermodynamic model was developed to model the total system efficiency, a dynamic model was likewise obtained in order to characterize the time-based behavior of the system.

Dynamic Model of the Engine Side

Immediately following combustion, the pressure and temperature dynamics in the combustion side are determined by the following power balance:

$$\dot{U}_e = \dot{H}_e + \dot{Q}_e - \dot{W}_e \tag{11}$$

where $\dot{U}_e$ is the rate of internal energy stored in the control volume comprising the combustion chamber, $\dot{H}_e$ is the rate of enthalpy crossing the CV boundary, $\dot{Q}_e$ is the heat flux rate into or out the CV, and $\dot{W}_e$ is the work rate. Assuming an ideal gas, the rate of internal energy storage is given by the following two relationships,

$$\dot{U}_e = \dot{m}_e c_{ve} T_e + m_e c_{ve} \dot{T}_e = \frac{1}{\gamma_e - 1}(\dot{P}_e V_e + P_e \dot{V}_e) \tag{12}$$

where $\dot{m}_e$ is the mass flow rate of gas entering (positive values) or exiting (negative values) the combustion chamber, c_{ve} and γ_e are the constant-volume heat capacity and ratio of specific heats, respectively, of the gas in the combustion chamber, and P_e, V_e and T_e are the pressure, volume, and temperature, respectively, of the combustion chamber. The values of c_{ve} and γ_e must in general be found from the appropriately weighted

average of the temperature dependent values of c_p of the species contained within the chamber. The enthalpy rate of energy entering or exiting the control volume is given by,

$$\dot{H}_e = \dot{m}_e c_{p,in/out} T_{in/out} \tag{13}$$

where $c_{p,in/out}$ is the constant-pressure heat capacity of the gas entering or exiting the combustion chamber, and $T_{in/out}$ is the temperature of the mass entering or exiting the chamber. If it is assumed that the engine side is adiabatic, then $\dot{Q}_e = 0$. The work rate is given as:

$$\dot{W}_e = P_e \dot{V}_e \tag{14}$$

The operation of the "engine side" of the device can be considered in three phases: the work phase (described below), and the intake and exhaust phases (described thoroughly in [4]).

During the work phase, no mass flow occurs and Equations (1-6) reduce to the following relationships regarding the pressure and temperature dynamics inside the combustion chamber:

$$\dot{P}_e = \frac{-\gamma_e P_e \dot{V}_e}{V_e} \tag{15}$$

$$\dot{T}_e = \frac{-P_e \dot{V}_e}{m_{e0} c_{ve}} \tag{16}$$

The work phase persists while $P_e > P_{atm} - P_{cvd}$ where P_{cvd} represents the minimum pressure difference necessary to open the intake check valve.

The dynamics in the engine side and the compressor side are related to each other through the movement of the free piston. Neglecting viscous and Coulomb friction, the dynamics of motion of the free piston are given by,

$$M\ddot{x} = (P_e - P_{atm})A_e - (P_c - P_{atm})A_c - F_s \tag{17}$$

where M is the mass of the free piston, A_e and A_c are the areas on the piston on the engine and compressor side respectively, x is the displacement of the piston assembly as denoted in Figure 5-1, and F_s is the return spring force. The volumes of the combustion chamber and compressor chamber, and their associated derivatives, are given by the following:

$$V_e = A_e x \tag{18}$$

$$V_c = A_c (l_c - x) \tag{19}$$

where l_c is the length of the compressor chamber when $x = 0$.

A dynamic simulation of the system was performed using Simulink. The following parameters were used for the simulation: mass of free piston M = 250 g, area of engine side $A_e = 5.07\,\text{cm}^2 =$ 5.07 (a diameter of 1 in.), area of compressor side $A_c = 2.85\,\text{cm}^2$ (a diameter of 0.75 in.), initial combustion pressure $P_{e0} = 3548\,\text{kPa}$ (500 psig), a constant-force spring with $F_s = 0.09\,\text{N}$, a check valve cracking pressure $P_{cvd} = 2.3\,\text{kPa}$ (1/3 psi), and a reservoir pressure $P_s = 653\,\text{kPa}$ (80 psig). The portion of the simulation relating the work phase in the combustion chamber with the inertial dynamics of the free piston is sufficient to model the post-combustion pressure profile (Figure 5-4). This profile shows that the combustion gasses are allowed to adiabatically

expand all the way down to atmospheric pressure, whereupon the intake check valve opens allowing the mixture to dilute with cool air. This full expansion is essential for the inertial loading characteristic of the FPC, and as it can be seen, it occurs within a very short duration of time, indicating a rapid transduction from stored chemical to kinetic energy. This rapid transduction helps mitigate the effect of heat loss through the combustion chamber wall and also enhances efficiency.

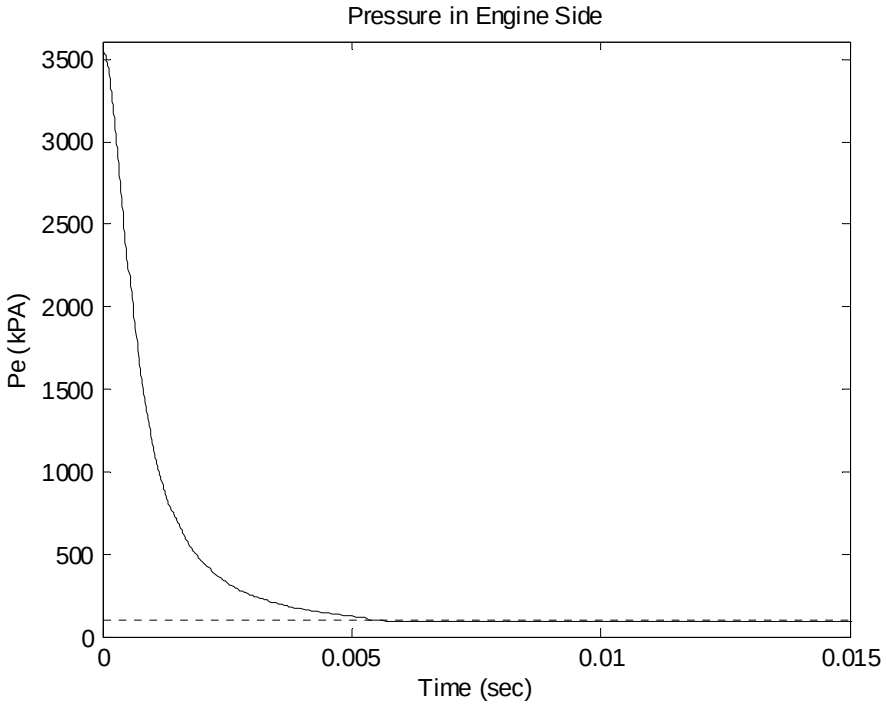

Figure 5-4: Pressure drop in engine side right after combustion.

Design and Implementation

A bench-top prototype of the FPC was built using off-the-shelf pneumatic equipment. This prototype is slightly different than the generalized schematic shown in Figure 5-1, and the main differences are results of evaluating design choices from an intermediary

prototype (not shown). The prototype design evolution is presented in detail in [12] and [13]. Figure 5-5 shows a schematic of the current version of the FPC. This device consists of two cylinders in-line and opposing one another. Both cylinders have a combustion side (back of the piston) and a pumping side (rod side of the piston).

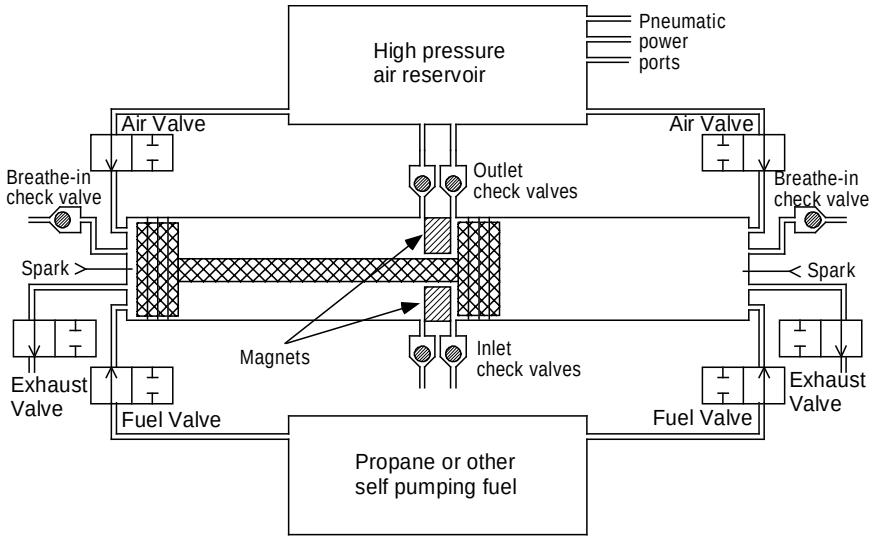

Figure 5-5: Schematic of hardware version of FPC.

The device is completely symmetrical, so its starting position can be on either side. The piston is held in place by two magnets while injecting a mixture of pressurized air and propane into the combustion chamber. Once the proper amount of mixture has entered the chamber, the air and propane valves close and a sparkplug initiates combustion. The piston will then travel to the other side while serving four functions: (1) pump fresh air into the air reservoir; (2) exhaust the diluted combustion products from previous combustion out of the opposing cylinder's combustion chamber; (3) breathe in fresh air into the opposing cylinder's pumping chamber; and (4) breathe in fresh air into

the combustion chamber after the pressure has dropped below atmospheric, thus cooling down and diluting the combustion products. At the end of the stroke the piston will be held in place by the opposing magnets, and the cycle can occur on the opposite side in the same fashion. The work required to break away the magnetic holding force after combustion is retrieved at the end of pumping. The force-distance profile of the magnets also allows dominantly inertial loading presented to the combustion pressure after a very short distance after break-away has occurred.

Figure 5-6 shows a picture of the current FPC prototype, and Figure 5-7 shows a close up of one of the cylinders. The setup of the FPC consists of two 4-inch stroke, ¾-inch bore BIMBA® standard air cylinders, ported appropriately for all necessary flow. The two piston rods are connected to a moving mass with small pieces of plastic tubing in order to avoid a purely rigid connection, which would yield increased friction due to misalignments. The moving mass carries two neodymium-iron-boron magnets on each side, which serve the purpose of holding the free piston in its starting position in order to overcome the injection pressure before combustion (section 4.1). These magnets snap onto ferrous plates at the end of each stroke, as can be observed in Figures 6 and 7. As stated earlier, the work invested in breaking away this magnetic force right after combustion will be regained at the end of the stroke, when the magnets from the opposite side pull the moving mass into place. Note that this pulling magnetic force will aid the free piston to make it to the other side and snap into place for a new injection phase. For all fluid flow purposes, standard check valves, 2-way on/off valves and 4-way valves were used where needed. The fuel in use is a bottle of COLEMAN® propane, available at

most convenience stores at low cost. Finally, the spark plugs are NGK ME-8, normally used for model aircraft.

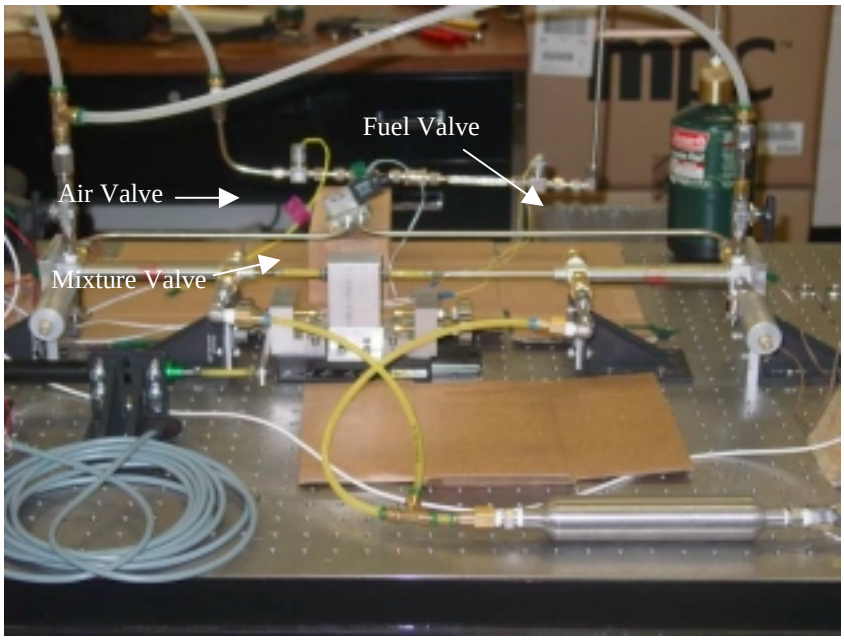

Figure 5-6: Picture of FPC Prototype.

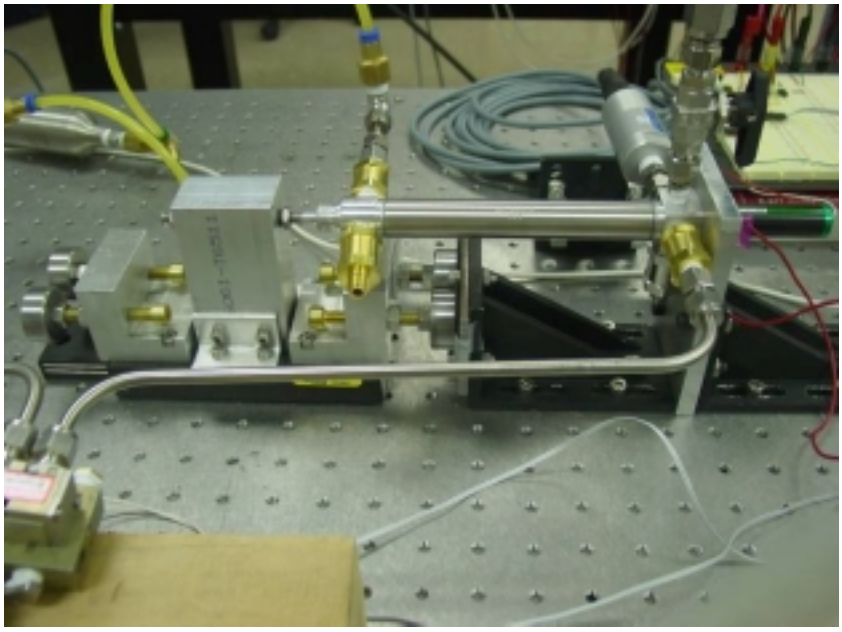

Figure 5-7: Close-up Picture of Cylinder

Injection Pressure

In order to obtain desirable combustion characteristics, it is mentioned in [4] that the injection pressure of the air/fuel mixture needs to be adequate enough to achieve the target initial combustion pressure. This minimum injection pressure requirement is given by,

$$P_{inj} = \left(\frac{R_{reac} T_{inj}}{R_e T_{AFT}} \right) P_{e0} \tag{20}$$

where R_{reac} and R_e are the average gas constants of the reactants and combustion products, respectively; T_{inj} and T_{AFT} are the temperature immediately preceding combustion and adiabatic flame temperature, respectively; and P_{e0} is the initial combustion pressure needed such that the FPC extracts enough work to pump all the air drawn into the compressor cylinders into the high-pressure reservoir. In order to obtain the appropriate injection pressure that corresponds to such an initial combustion pressure, the free piston needs to be locked in its initial position during injection. A sufficiently stiff spring could serve this purpose, but would offer so much resistance upon the combustion stroke that the desired inertial loading would be spoiled. To overcome this, the four neodymium-iron-boron magnets were installed to hold the free piston in its starting position before combustion. The magnetic gap is adjustable by the turn of a screw, such that the bonding magnetic force can be set just slightly higher than the force exerted on the free piston by the injection pressure. Additionally, this magnetic force acts over such a small portion of the total stroke length that its effect against the inertial loading is negligible once the motion of the piston begins. This implementation of

magnets replaces what in a conventional IC engine would be both the intake and compression strokes.

Mixture Quality

Additionally to injection pressure, proper combustion requires good air/fuel mixture quality. Ideally, this mixture should match the stoichiometric mass ratio for combustion, namely 15.67 for air and propane. For complete combustion, it is also imperative that the mixture is uniform. This type of mixing is not instantaneous, and occurs by diffusion and any flow mixing present. By injecting the air and propane into the chamber through separate ports, it would take an unacceptable amount of time for the two substances to uniformly mix, thus affecting the cycle rate of the system and making it less reliable. As a solution, the air and propane were first injected into a common flow stream, which enforced a turbulent enough flow such that the mixture was sufficiently uniform upon reaching the combustion chamber.

Since one of the main objectives of this paper is to show the total efficiency of the system from stored chemical energy of propane to stored pneumatic potential energy of compressed air, it is imperative to be as precise as is reasonably possible with all measurements. The most difficult, yet one of the most important measurements to determine, is the mass of propane used for combustion. Knowing this mass and the energy density of propane, the total amount of initial energy can be determined and compared to the potential energy of compressed air in the reservoir.

Measuring the Mass of Propane

As shown in Figure 5-6, the air/fuel mixture enters the chamber by controlled opening and closing of the air, fuel and mixture valves. The air and fuel valves are timed such that a stoichiometric mixture exists within a common mixing line at the exit of both valves. This mixture is then admitted to one of the two combustion chambers via a three-way mixture valve. The air and fuel valves are Parker® Series-9 valves, and operate as two-way on/off valves. The nominal response time of these valves is 12 ms, while their commanded opening times for this application will range between 8-12 ms for propane and 50-80 ms for air. A mass flow meter could not be used to determine the mass of propane flowing because these are small pulses, and not steady flows. Also, since the propane valve operates at opening times close to the valve response time, the small pulse flow dynamics would not be similar to the steady flow dynamics. The mass was instead calculated by injecting propane into an inverted graduated cylinder of a beaker with water, and observing the water displacement in the cylinder for various durations of the commanded opening pulse sent to the fuel valve. This was done for 8, 9, and 10 ms pulses, and each one was performed several times to obtain an average. The standard deviation of measured displaced water for each pulse duration was very close to the readability of the scale. The same was done for the air, in order to find stoichiometric values based on air and fuel valve opening times. It should be noted that this match of opening times yields accurate stoichiometric mixtures only if flowing into atmospheric pressure. A method to obey this restriction during operation is discussed below.

For precise data acquisition purposes, the engine was run only in single fire shots. Before each fire, the exhaust port and mixture valve was opened, and the fuel and air

valves opened for specific durations previously determined to yield a stoichiometric mixture. This was done several times such that the entire mixing line would contain a precise air-fuel ratio. The exhaust port was then closed and some of the stoichiometric air/fuel mixture remaining in the mixture line was pushed into the combustion chamber, by opening the mixture valve, until reaching the desired injection pressure. It was ensured that the mixing line was long enough such that only a portion of the line was required for injection, and thus maintaining a proper mixture. The fuel injection process can be considered an adiabatic compression; thus, we can consider the following relationship:

$$P_{atm}V_{line}^{\gamma_{mix}} = P_{inj}V_{e0}^{\gamma_{mix}} \tag{21}$$

where V_{line} is the partial volume of the mixture before entering the combustion chamber, and γ_{mix} is the ratio of specific heats of the air/fuel mixture.

Additionally, by conservation of mass, and assuming an ideal gas, we have:

$$m_{e0} = \frac{P_{atm}V_{line}}{R_{mix}T_{amb}} = \frac{P_{inj}V_{e0}}{R_{mix}T_{inj}} \tag{22}$$

where m_{e0} and R_{mix} are the mass and average gas constant of the fuel mixture, respectively, and T_{inj} is the injection temperature (immediately preceding combustion). Combining Equations (21) and (22), the injected mass of fuel can be calculated as:

$$m_{e0} = \frac{P_{atm}}{R_{mix}T_{room}}\left(\frac{P_{inj}}{P_{atm}}\right)^{\frac{1}{\gamma_{mix}}} \tag{23}$$

Adjusting Mixture while Pumping

Ideally, every firing should be strong enough for the piston to just barely make it to the other side. If combustion is stronger than it needs to be, the piston will carry extra

energy that will not be used for pumping, but dissipated in colliding with the opposite side. This is quite wasteful and brings down the total efficiency of the system. Conversely, if the combustion is weak and the piston carries less kinetic energy than needed to pump a full stroke, it will not make it to the other side, and some energy would need to be re-invested (by utilizing the air injection valve and energy stored in the reservoir) to push the piston to the other side (note that the area of the rod side being less that the piston side will allow this to occur when both sides are ultimately presented with the reservoir pressure). Precisely controlling the strength of the combustion for continuous operation would require more sophisticated equipment and is beyond the scope of this paper. However, full compression of the air reservoir is achieved here with discrete increases of valve opening times as needed. It should be noted that due to the low resolution of the valves at these extremely low mass flows, the combustion pressure increase between any two valve-opening times is relatively large. Figure 5-8 shows the average amounts of propane mass and combustion pressures yielded by all three sets of valve timings used for this experiment.

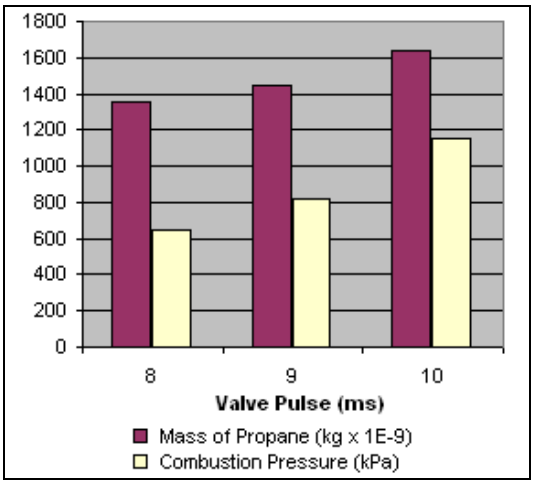

Figure 5-8: Fuel Masses and Combustion Pressures

For data gathering, the FPC is fired first with the lowest set of valve opening times. After a certain number of firings, the pressure in the air reservoir will reach a certain threshold, at which point the combustion pressure will not be adequate for the free piston to complete the stroke, and the injection is re-adjusted to the next set of opening pulse-times. It should be intuitive that the first few shots after a threshold are the least efficient, while the last few shots before a threshold are the most efficient.

Experimental Results and Evaluation

Experimentation consisted of a series of single fire shots. Combustion took place in a 6.4 mL volume, with a moving mass of 1.82 kg. Three different opening times of the fuel valve were used for combustion (8, 9, and 10 ms), depending on the combustion pressure desired. The data shown in Figures 5-9 through 5-17 are taken from two single shots of the device. The first set (Figures 5-9 through 5-13) show a less than ideal shot and the second set (Figures 5-14 through 5-17) show a more ideal shot. This variation is a result of the lack of adequate valve opening resolution resulting from the hardware used with this experimental setup. Figures 5-9, 5-10, 5-11, and 5-12 show combustion pressure, air reservoir pressure, position of the piston and velocity of the piston, respectively. These were taken from a typical firing at a low pumping pressure and exhibit the inadequacy of resolution of the air and fuel valves – note the collision with the opposing side apparent from the sharp decrease in velocity shown in Figure 5-12. The spark occurs at 0.4 seconds. Figure 5-9 also shows the injection pressure in the combustion chamber before ignition.

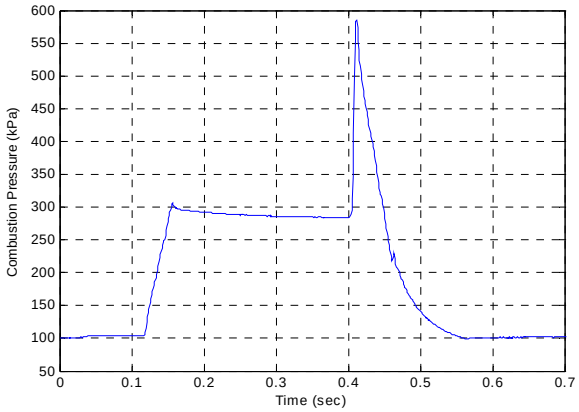

Figure 5-9: Pressure in the combustion chamber. Fuel injection occurs between 0.1 and 0.2 second; spark ignites at 0.4 seconds.

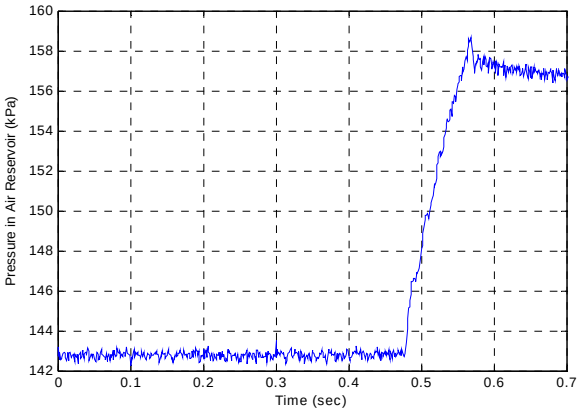

Figure 5-10: Pressure in the Air Reservoir.

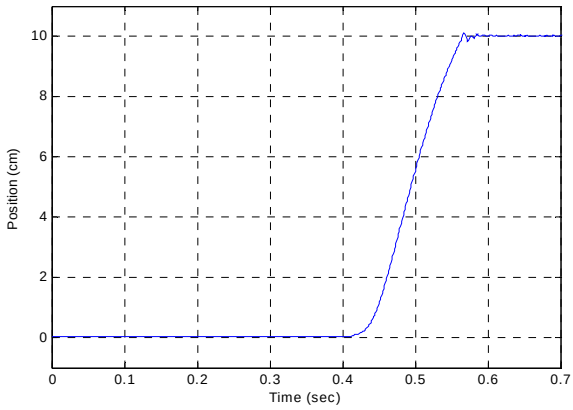

Figure 5-11: Position of the Free Piston. Sharp corner at the top indicates abrupt collision of piston with magnets (loss of energy).

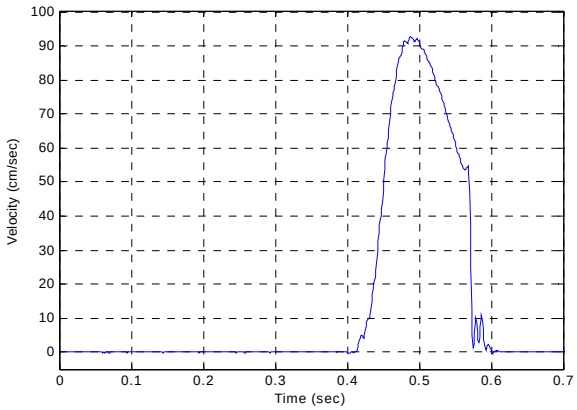

Figure 5-12: Velocity of the Free Piston. Vertical line at the right indicates wasted kinetic energy.

Despite the inefficient operation shown for Figures 5-9, 5-10, 5-11 and 5-12, it should be noted that these plots still exhibit the main features of the FPC, such as the inertial loading (full expansion of combustion gasses in Figure 5-9) and the breathe-in mechanism (combustion pressure decreases to atmospheric pressure before the end of the stroke). Also, the frequency for continuous operation can be maximized by reducing the time between signals. With basic knowledge of the injection, combustion and expansion timings, the duration of each stroke can be reduced to just under 0.4 seconds. This yields a total operational frequency of 2.5 strokes per second.

An evaluation of the experimentally obtained P-V curve, shown in Figure 5-13, compares the experimental prototype device with the theoretically adiabatic behavior of $PV^{\gamma_e} = \text{constant}$. It can be seen that the experimentally obtained curve becomes flat at atmospheric pressure as hoped and indicates that the device is capable of both fully expanding the combustion products as well as being able to intake cool air from the environment to dilute the exhaust products. In light of the comparison of the experimentally obtained P-V curve as compared with the adiabatic P-V curve, heat loss

appears to be non-negligible but manageable. It should be noted that the curve shown is from the device firing the first time when the device is cold and when heat losses would be at a maximum. Heat losses can be further reduced by choosing a different material for the combustion chamber walls (currently aluminum) and increasing the combustion dead volume (which would increase the ratio of volume to surface area).

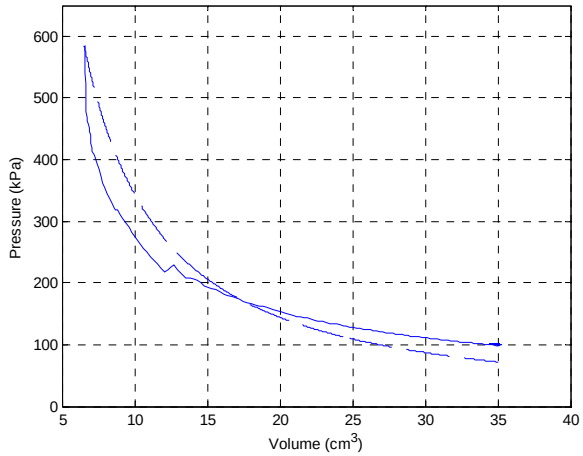

Figure 5-13: P-V curve in the combustion chamber. The solid line shows the experimentally measured P-V curve, and the dashed line shows the ideal adiabatic P-V curve.

Through single fire shots, the 187-mL air reservoir was successfully compressed from atmospheric pressure up to 310 kPa. It took 52 strokes to reach this pressure, which can be achieved in 20 seconds of continuous operation (based on the previously described operational frequency). This compression pressure is limited by the ratio of stroke volume (engine displacement) over dead volume in the rod (compressing) side of the chosen cylinders. This dead volume was quite large (about 4.1 mL), and is a nonideality (as noted in [4]) that should be reduced in future design considerations. This nonideality presents the main drawback in this version of the FPC.

The total energetic merit of this system is represented by the efficiency of conversion from chemically stored energy in propane to pneumatic potential energy of compressed air. As shown analytically in [4], and outlined in Figure 5-3, this efficiency also increases for larger combustion pressures. Experimentally, this efficiency was calculated for a single fire shot in which the piston just barely made it to the other side – the ideal case which could conceivably be achieved for every stroke given adequate valve resolution. Figures 5-14, 5-15, 5-16, and 5-17 show the respective pressures, displacement and velocity for this particular shot. By looking at the position and velocity in Figures 5-16 and 5-17, it can be observed that the piston "barely made it" to the other side, with a little help from the magnetic force.

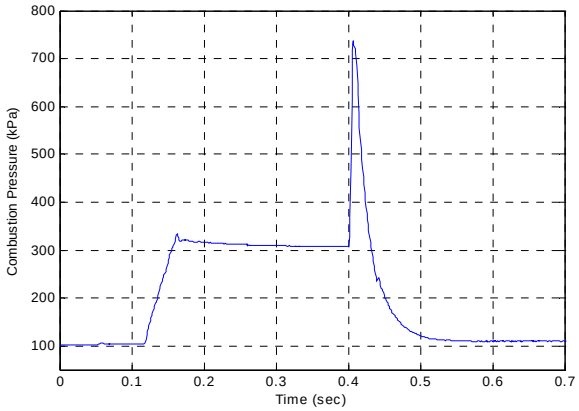

Figure 5-14: Pressure in the Combustion Chamber for efficient firing.

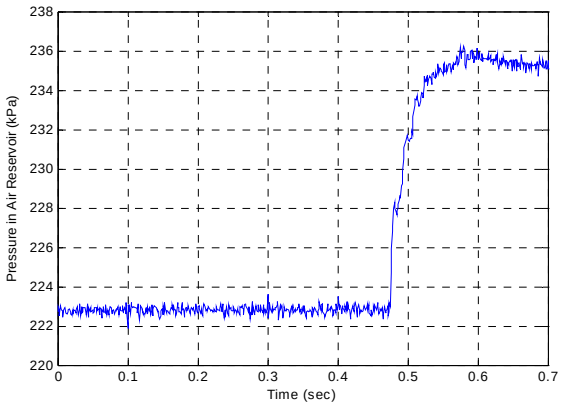

Figure 5-15: Pressure in the Air Reservoir

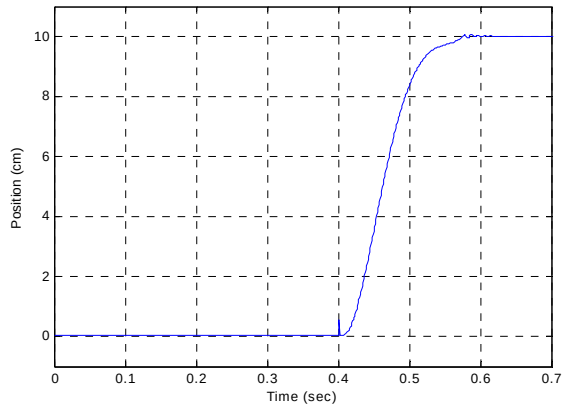

Figure 5-16: Position of the Free Piston. Smooth curve at the top indicates that piston 'barely made it' to the other side

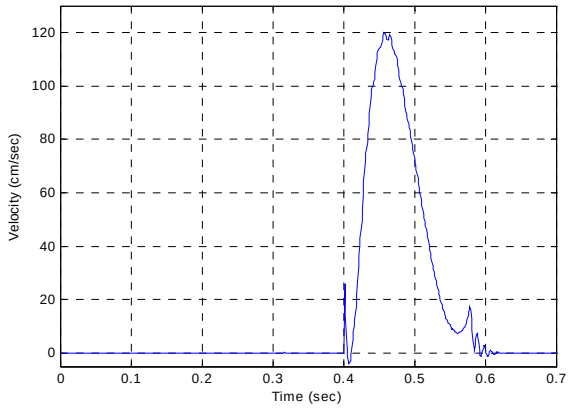

Figure 5-17: Velocity of the Free Piston. Spike at the bottom left shows the piston snapping into the magnets, hence an efficient firing.

This shot used 1.05×10^{-6} kg of propane and resulted in an increase of the pressure in the air reservoir (a volume of 1.866×10^{-4} m^3) from 222.75 kPa to 235 kPa. Using equation (5), the pneumatic potential energy increase is calculated as 2.48 Joules. The total efficiency of conversion from chemically stored energy of the fuel to stored pneumatic energy of the compressed air, is calculated as,

$$\eta_{total} = \frac{0.00248337\,\text{kJ}}{\frac{46350\,\text{kJ}}{\text{kg fuel}}\times 1.05*10^{-6}\,\text{kg fuel}}\times 100 = 5.10\% \tag{24}$$

Additionally, to calculate the overall system efficiency, we need to take into account the efficiency associated with the air re-investment; that is, the air from the reservoir that is utilized for the subsequent combustion cycle. Using Equation (8), this efficiency can be calculated as,

$$\eta_{invest} = \frac{2.69\times10^{-5} - 1.645*10^{-5}}{2.69\times10^{-5}}\times 100 = 39\% \tag{25}$$

Hence, the overall system efficiency of this shot becomes,

$$\eta_{sys} = \eta_{total}\eta_{invest} = 1.99\%$$

Based on a simple thermodynamic analysis presented in [4], the total theoretical efficiency of the system with these parameters is calculated to be 5.19%. However, this calculation assumes zero dead volume in the compressing side of the cylinder, no heat losses in the combustor side and high heat losses in the compressor side. The issues of excess dead volume in the compressor side and combustor heat losses present in this experimental prototype would be difficult to fully address with standard pneumatic equipment (such as those used here), and would require custom made parts in order to reduce the minimum rod-side volume, increase the combustor volume (without

sacrificing stroke length), and use a better insulating material for the combustor walls. As also shown in [4], the efficiency of the device increases with increased combustion pressure (up to 20% efficiency). With these points in mind, the experimental efficiency obtained experimentally met reasonable expectations, while leaving room for improvement in future designs.

Conclusions

The design, characterization and experimental operation a Free Piston Compressor (FPC) were presented. The FPC is a small-scale internal combustion engine capable of pumping air into a high-pressure air reservoir, and is intended to serve as a pneumatic power supply system. The proposed technology is intended to be coupled with an untethered pneumatic robotic system, and aims to provide an order of magnitude greater energetic merit than state of the art power supply and actuation systems (electrical batteries coupled with DC motors).

Experimental results demonstrate that the device is capable of fully expanding the combustion products down to atmospheric pressure as designed and demonstrate the merits of presenting a purely inertial load in a combustion process. Such dynamic loading serves to increase efficiency, allows the device to operate with low noise due to not having a high pressure exhaust “pop”, and allows the combustion products to be diluted with cool external air to contribute toward a low operating temperature compared to more conventional internal combustion engines. Experimental results also demonstrate that the device is capable of start on demand, making it well suited to a pressure regulation control loop in a portable pneumatic power supply system. Finally, it was shown that

further design work regarding the resolution of the air and fuel valves is needed to secure decent efficiencies across different reservoir pressures, and further work regarding the dead volumes in both sides of the piston is needed to increase efficiency.

A measured efficiency of 5.10% was achieved in converting stored chemical energy of propane into stored pneumatic potential energy. In comparing this power supply system with state of the art rechargeable batteries, an energy density of 180 kJ/kg for NiMH batteries and a conversion efficiency of 50% for an electromagnetic motor and mated gearhead would yield 90 kJ of delivered controlled mechanical work per kilogram of source energetic material. For the FPC under consideration, an energy density of 46350 kJ/kg for propane, a measured conversion efficiency of 5.10% from stored chemical to pneumatic energy, a 39% efficiency associated with the computed mass reinvestment from the air reservoir for the next combustion event, and an assumed conversion efficiency of 30% from stored pneumatic energy to delivered controlled mechanical work of an associated pneumatic actuator, would yield 277 kJ of controlled work per kilogram of source energetic material. This increase, coupled with the equally important high power density of pneumatic actuators over electromagnetic motors (approximately 450 W/kg versus 50 W/kg), should contribute to a power supply and actuation system more appropriate for untethered human scale and power comparable robots and actuated devices. Table 5-1 below shows an energetic comparison between conventional rechargeable batteries and the FPC system. It should be noted that the theoretical conversion efficiency (5.2%) corresponds only to the specific parameters from the experimental data (combustion pressure and pressure in the air reservoir, namely),

and can significantly increase as shown in Figure 5-3. It is also expected that design changes to the next generation of this device will result in further improvements.

Table 5-1: Energetic Comparison Between FPC system, at the particular experimental values of combustion and air reservoir pressures used, and state of the art rechargeable batteries.

System	Source Energy Density (kJ/kg)	Conversion Efficiency	Actuation Efficiency (Stored to Delivered Mechanical Work)	Controlled Delivered Mechanical Work (kJ/kg)
Batteries	180	100% (PWM)	50% (Gearhead & Friction)	**90**
FPC (Theory)	46350	5.20%	30% (Pneumatic Actuator)	**725 (8 times batteries)**
FPC (Experimental)	46350	2.0%	30% (Pneumatic Actuator)	**277 (3 times batteries)**

References

[1] Aichlmayr, H. T., Kittelson, D. B., and Zachariah, M. R., "Miniature free-piston homogenous charge compression ignition engine-compressor concept – Part I: performance estimation and design considerations unique to small dimensions," *Chemical Engineering Science*, 57, pp. 4161-4171, 2002.

[2] Aichlmayr, H. T., Kittelson, D. B., and Zachariah, M. R., "Miniature free-piston homogenous charge compression ignition engine-compressor concept – Part II: modeling HCCI combustion in small scales with detailed homogeneous gas phase chemical kinetics," *Chemical Engineering Science*, 57, pp. 4173-4186, 2002.

[3] Barth, E. J., "Method and System for a Compact Efficient Free Piston Compressor". Regular U.S. patent application 11/120,128, filed May 2005.

[4] Barth, E. J., and Riofrio, J., "Dynamic Characteristics of a Free Piston Compressor," *2004 ASME International Mechanical Engineering Congress and Exposition (IMECE)*, IMECE2004-59594, November 13-19, 2004, Anaheim, CA.

[5] Beachley, N. H. and Fronczak, F. J., "Design of a Free-Piston Engine-Pump," *SAE Technical Paper Series*, 921740, pp. 1-8, 1992.

[6] Black, William Z., and James G. Hartley, *Thermodynamics, Third Edition*, New York: Harper Collins, 1996.

[7] Goldfarb, M., Barth, E. J., Gogola, M. A., Wehrmeyer, J. A., "Design and Energetic Characterization of a Liquid-Propellant-Powered Actuator for Self-Powered Robots". *IEEE/ASME Transactions on Mechatronics*, vol. 8, no. 2, pp. 254-262, June 2003.

[8] Klotsch, P., "Ford Free-Piston Engine Development," *SAE Technical Paper Series*, 590045, vol. 67, pp. 373-378, 1959.

[9] McGee, T. G., Raade, J. W., and Kazerooni, H., "Monopropellant-Driven Free Piston Hydraulic Pump for Mobile Robotic Systems," *ASME Journal of Dynamic Systems, Measurement, and Control*, vol. 126, pp. 75-81, March 2004.

[10] Nakahara M., Free Piston Kikai-Kouzou to Rekisi, Shinko-Techno Gihou, Vol.13, No.25 & 26 (2001).

[11] Pescara, R. P., "Motor Compressor Apparatus," U.S. Patent No. 1,657,641, Jan. 31, 1928.

[12] Riofrio, J. A., and Barth, E. J., "Design of a Free Piston Pneumatic Compressor as a Mobile robot Power Supply," *Proceedings of the 2005 IEEE International*

Conference on Robotics and Automation (ICRA), pp. 236-241, Barcelona, Spain, April 2005.

[13] Riofrio, J. A., and Barth, E. J., "Experimental Operation and Characterization of a Free Piston Compressor," Submitted to the *2005 ASME International Mechanical Engineering Congress and Exposition (IMECE).*

[14] Underwood, A. F., "The GMR 4-4 'Hyprex' Engine: A Concept of the Free-Piston Engine for Automotive Use," *SAE Technical Paper Series*, 570032, vol. 65, pp. 377-391, 1957.

APPENDIX A

SIMULINK DIAGRAMS

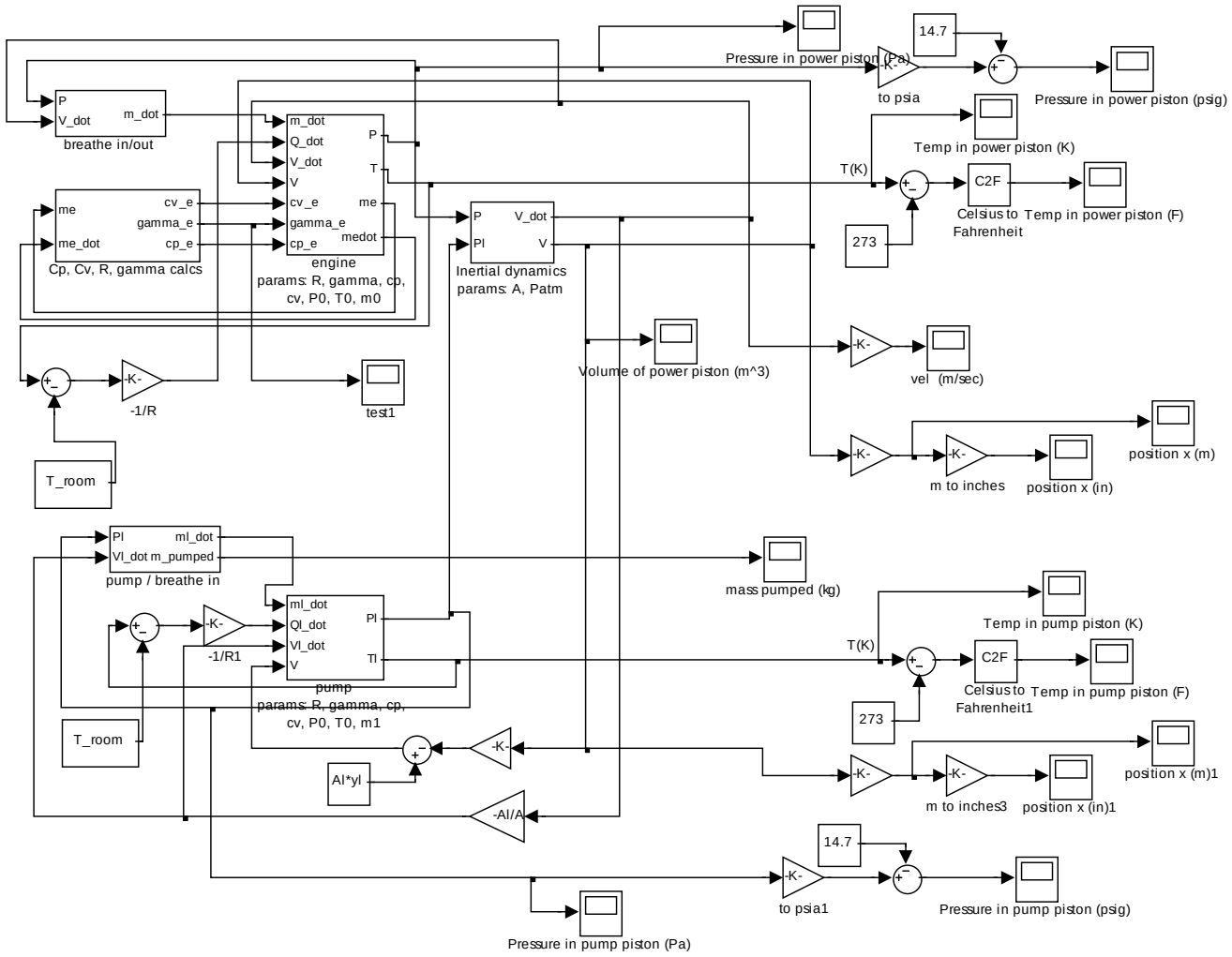

Figure A-1: Block diagram of FPC simulation used in Manuscript 1.

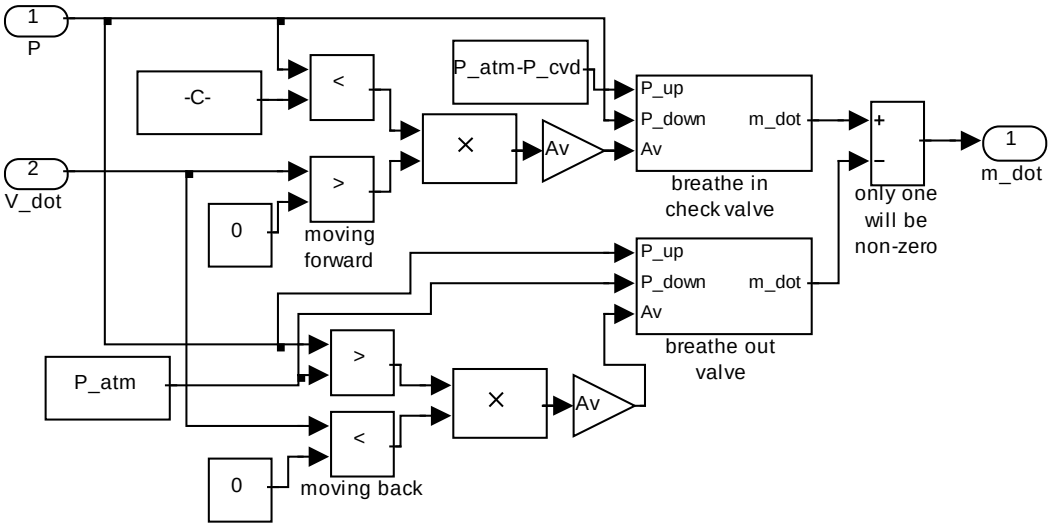

Figure A-2: Contents of sub-block "Breathe in/out." (Manuscript 1)

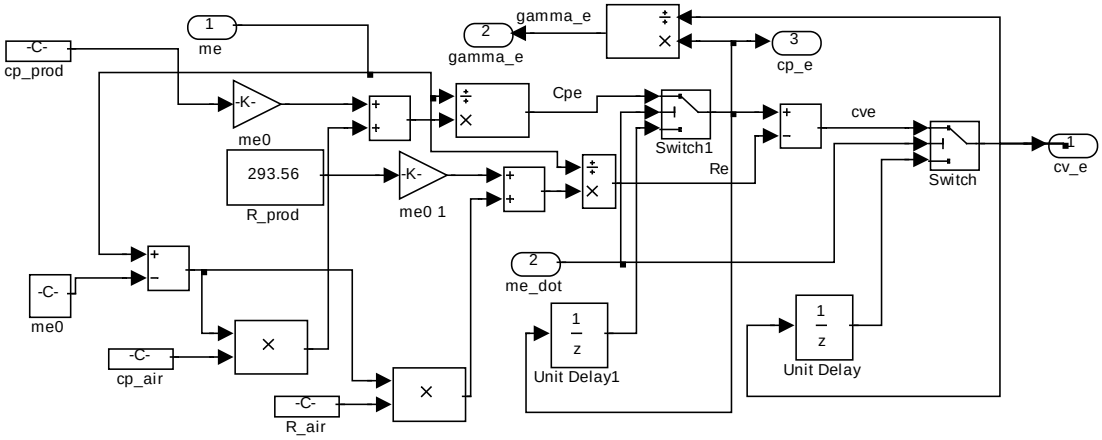

Figure A-3: Contents of sub-block "Cp, Cv, R, Gamma Calculations." (Manuscript 1)

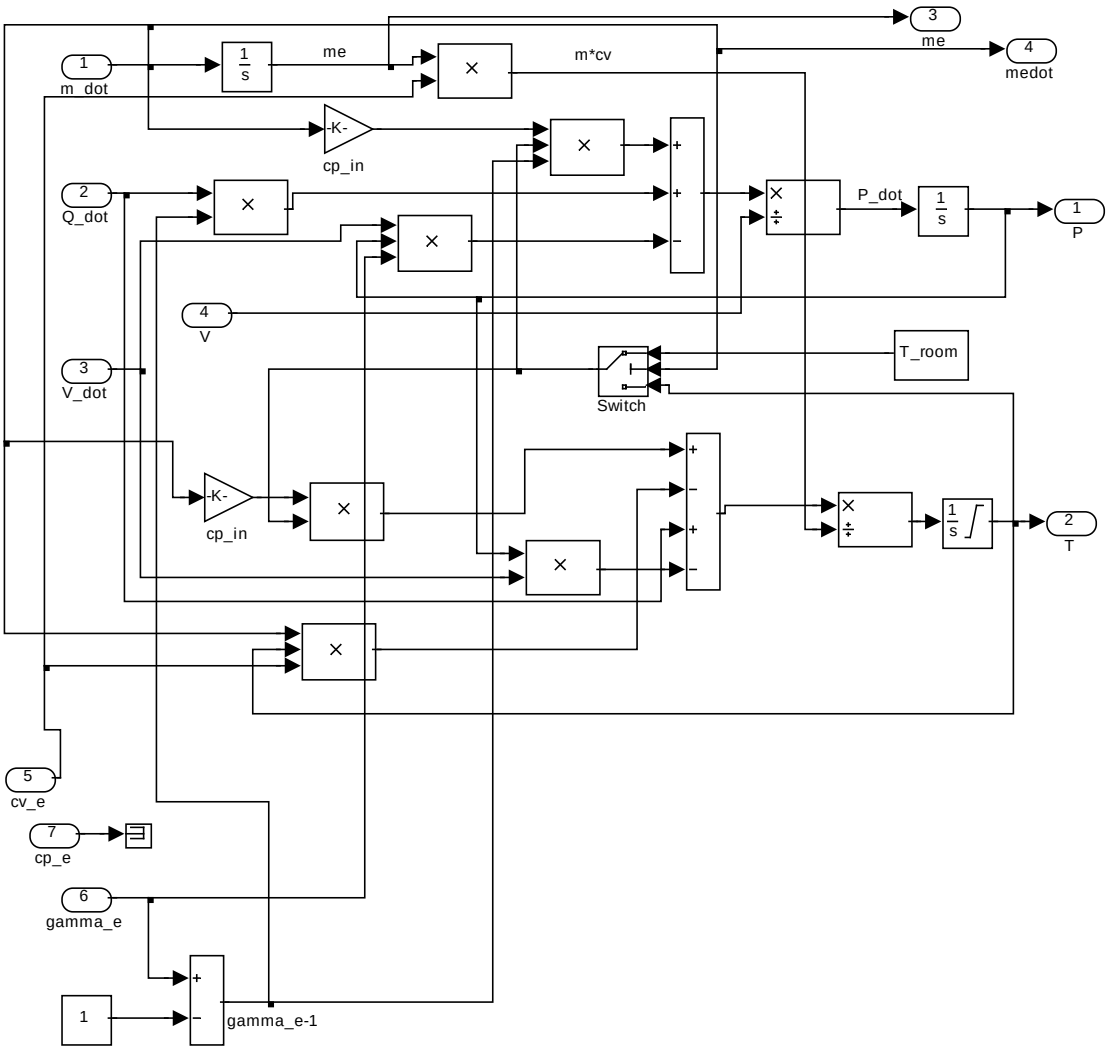

Figure A-4: Contents of sub-block "Engine Parameters." (Manuscript 1)

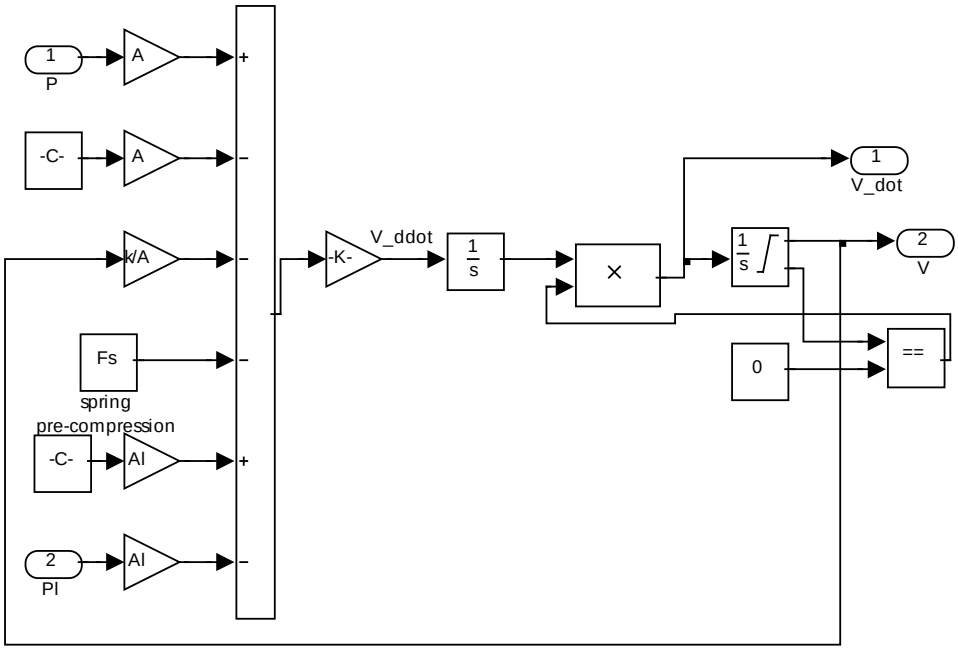

Figure A-5: Contents of sub-block "Inertial Dynamics Parameters." (Manuscript 1)

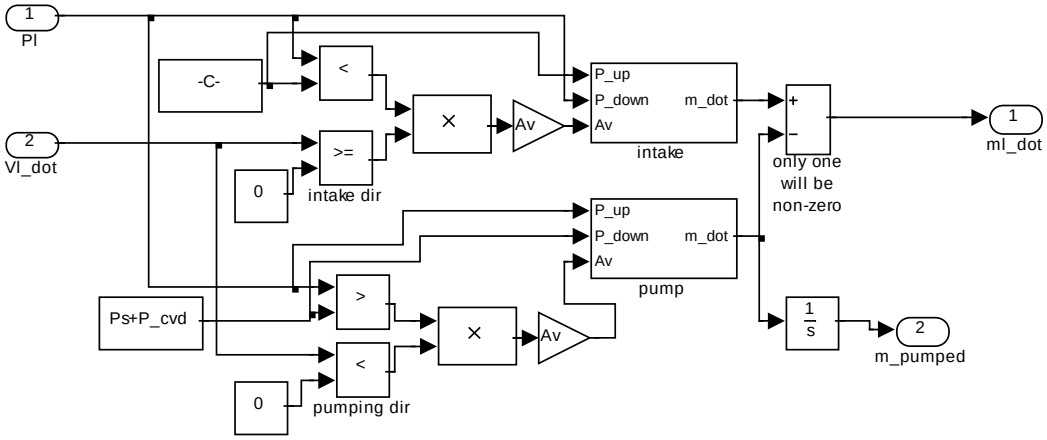

Figure A-6: Contents of sub-block "Pump / Breathe in." (Manuscript 1)

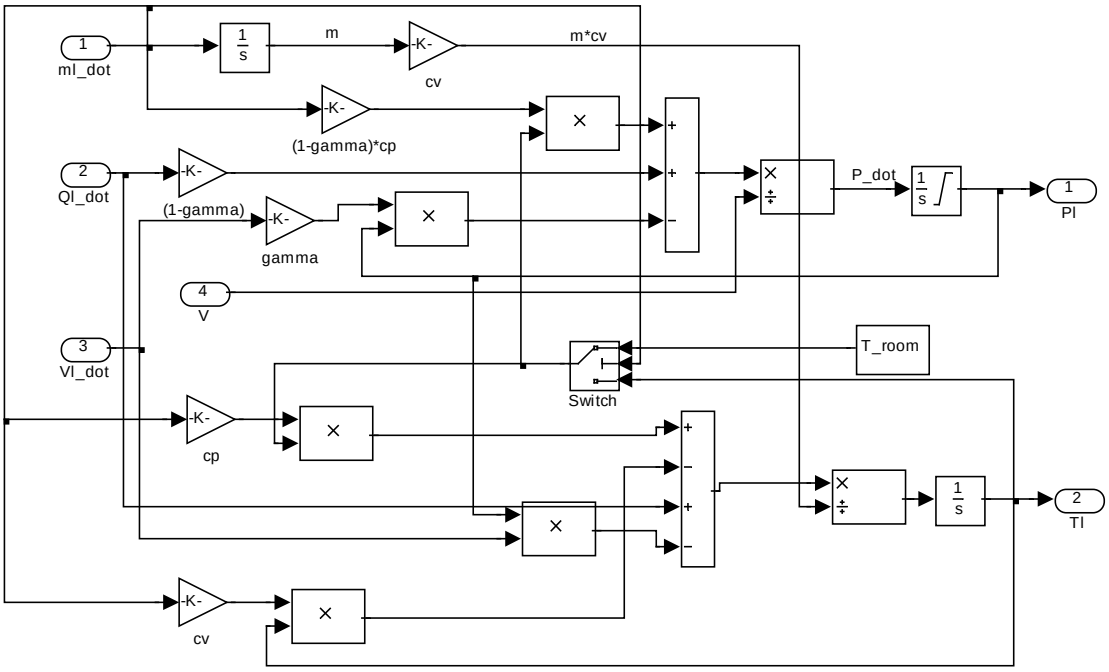

Figure A-7: Contents of sub-block "Pump Parameters." (Manuscript 1)

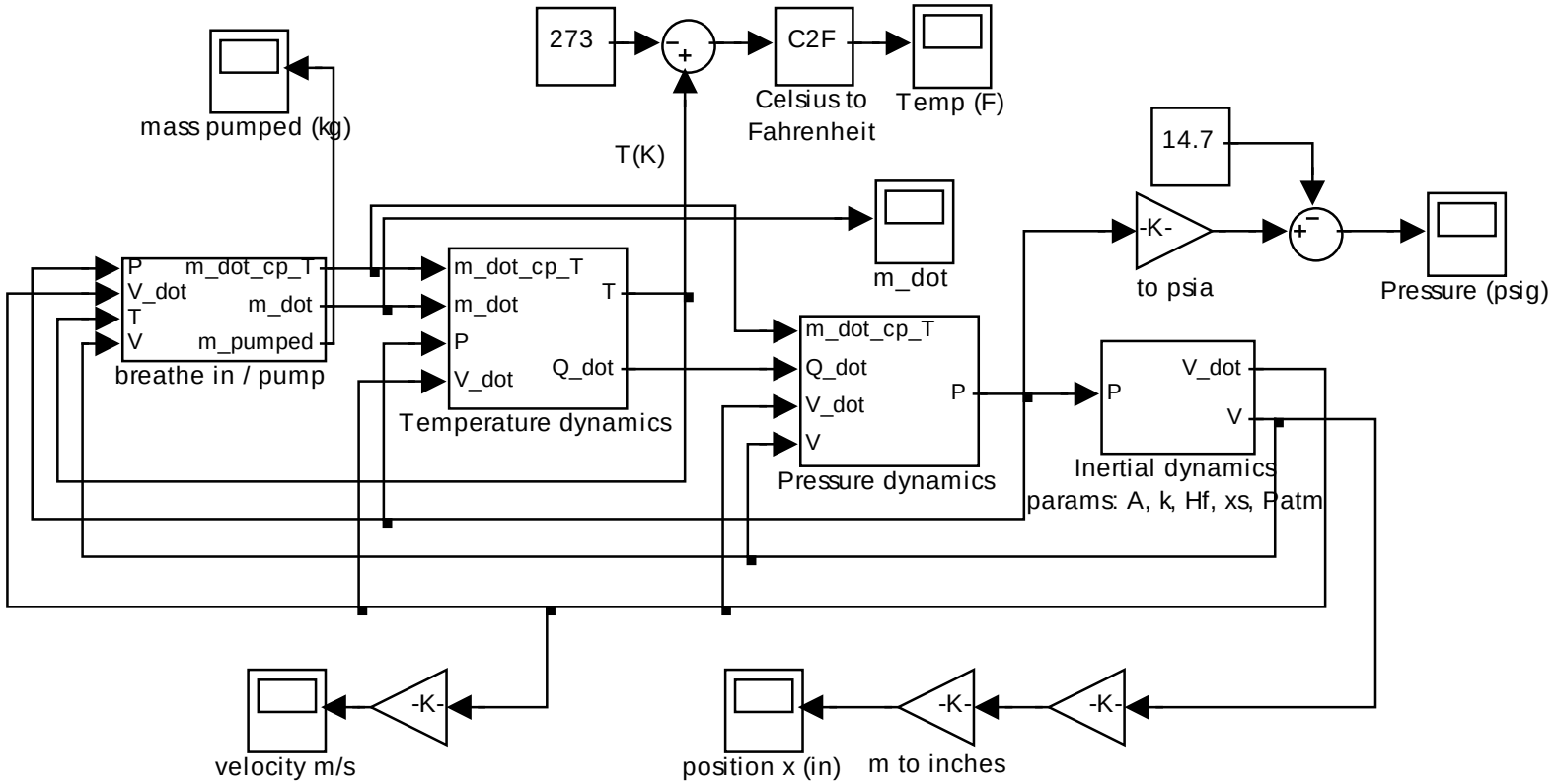

Figure A-8: Block diagram of 'Pump-On-Return' simulation used in Manuscript 2.

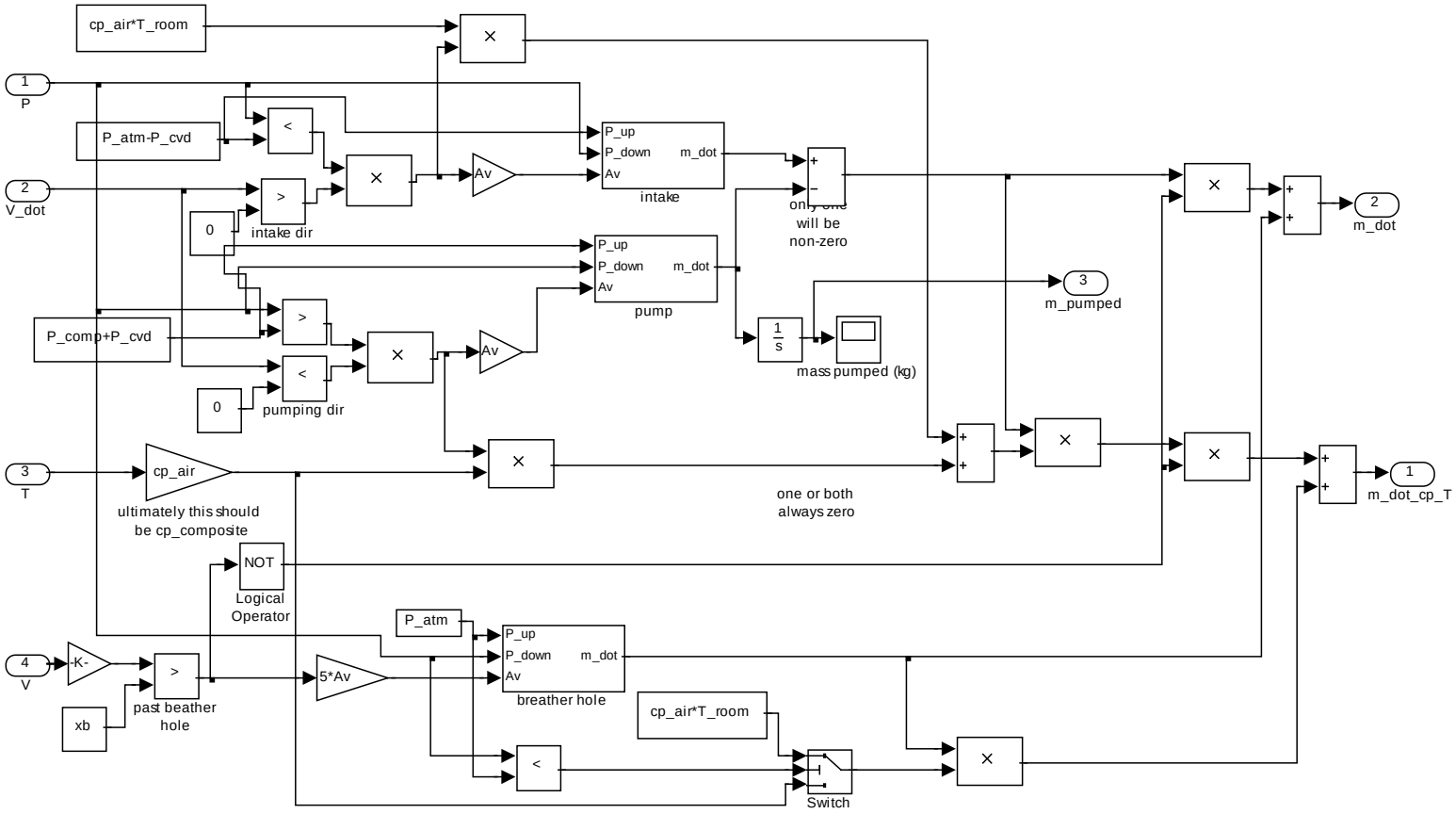

Figure A-9: Contents of sub-block "Breathe in / Pump." (Manuscript 2)

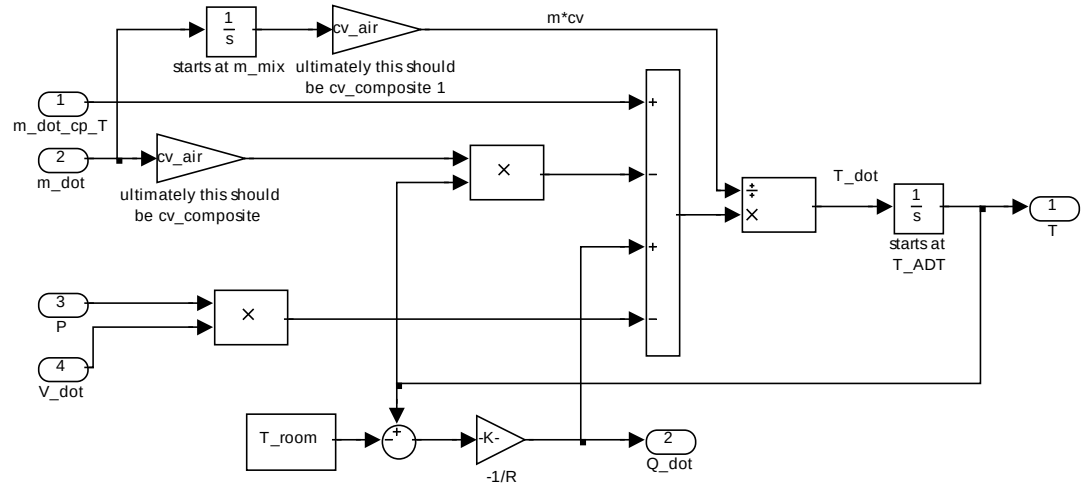

Figure A-10: Contents of sub-block "Temperature Dynamics." (Manuscript 2)

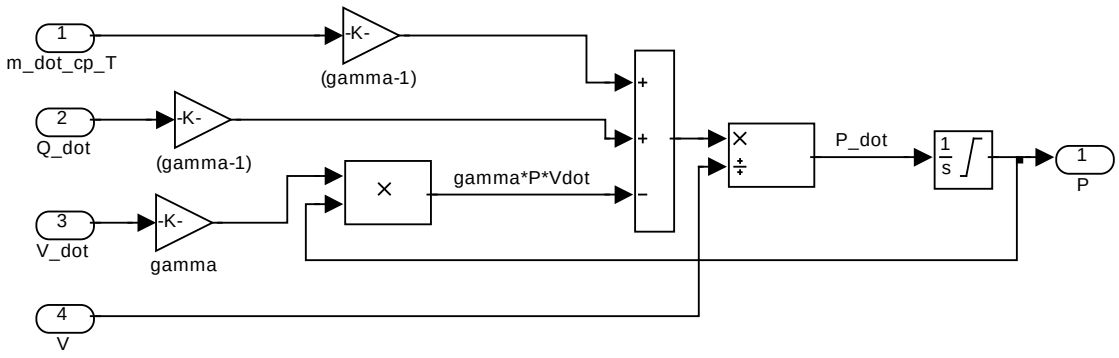

Figure A-11: Contents of sub-block "Pressure Dynamics." (Manuscript 2)

.

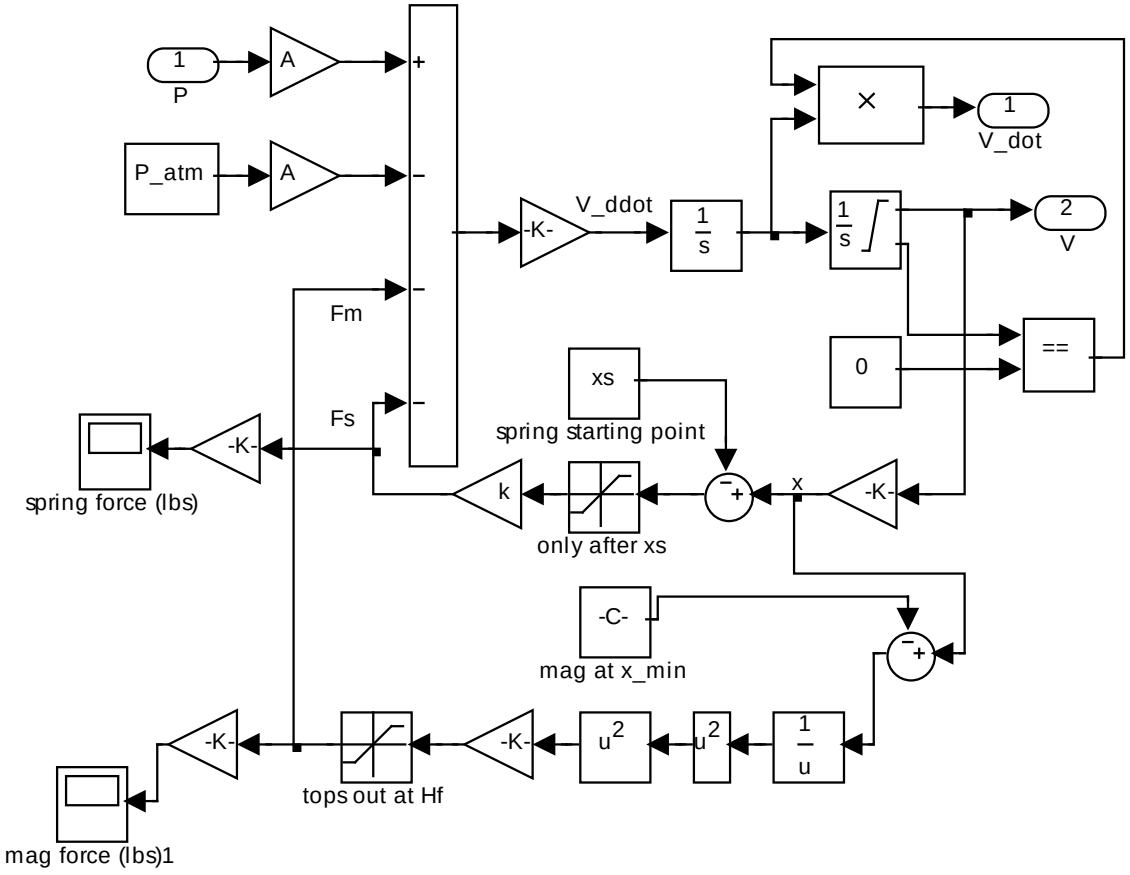

Figure A-12: Contents of sub-block "Inertial Dynamics Parameters." (Manuscript 2)

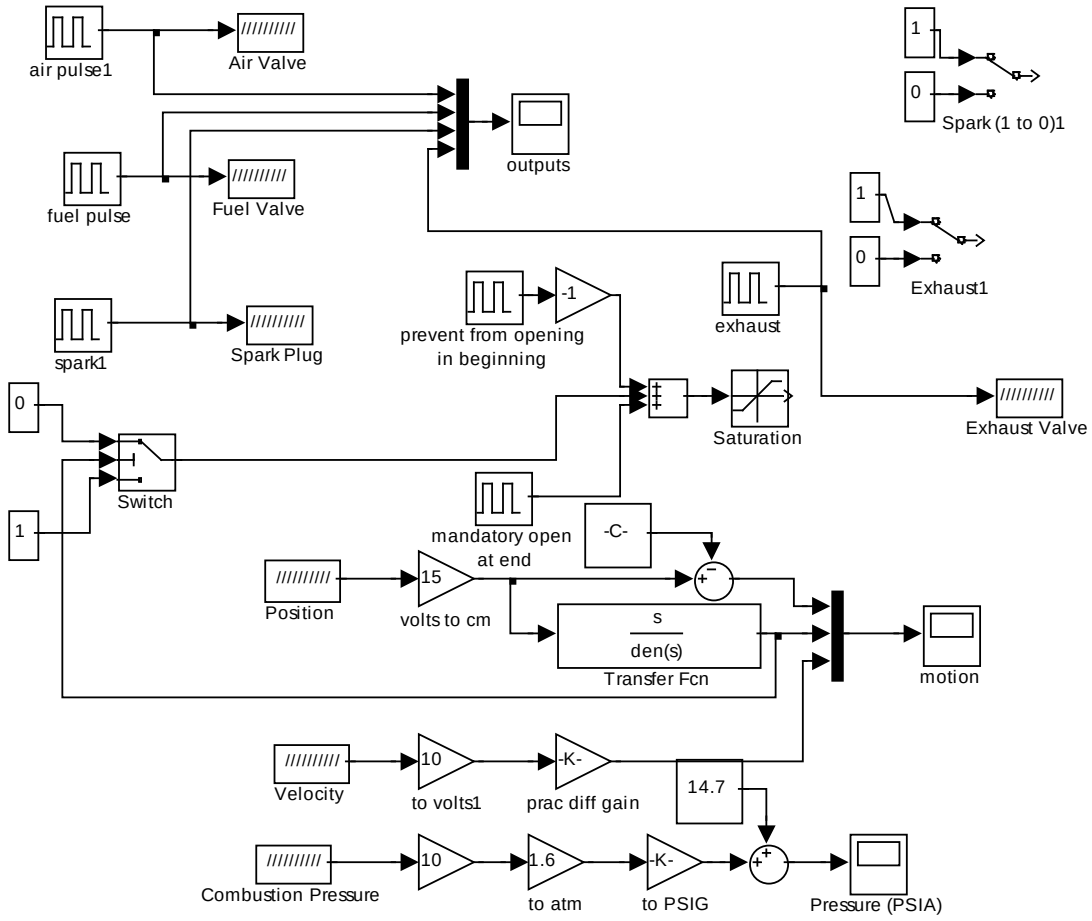

Figure A-13: Block diagram of Real Time Workshop implementation for Manuscript 2.

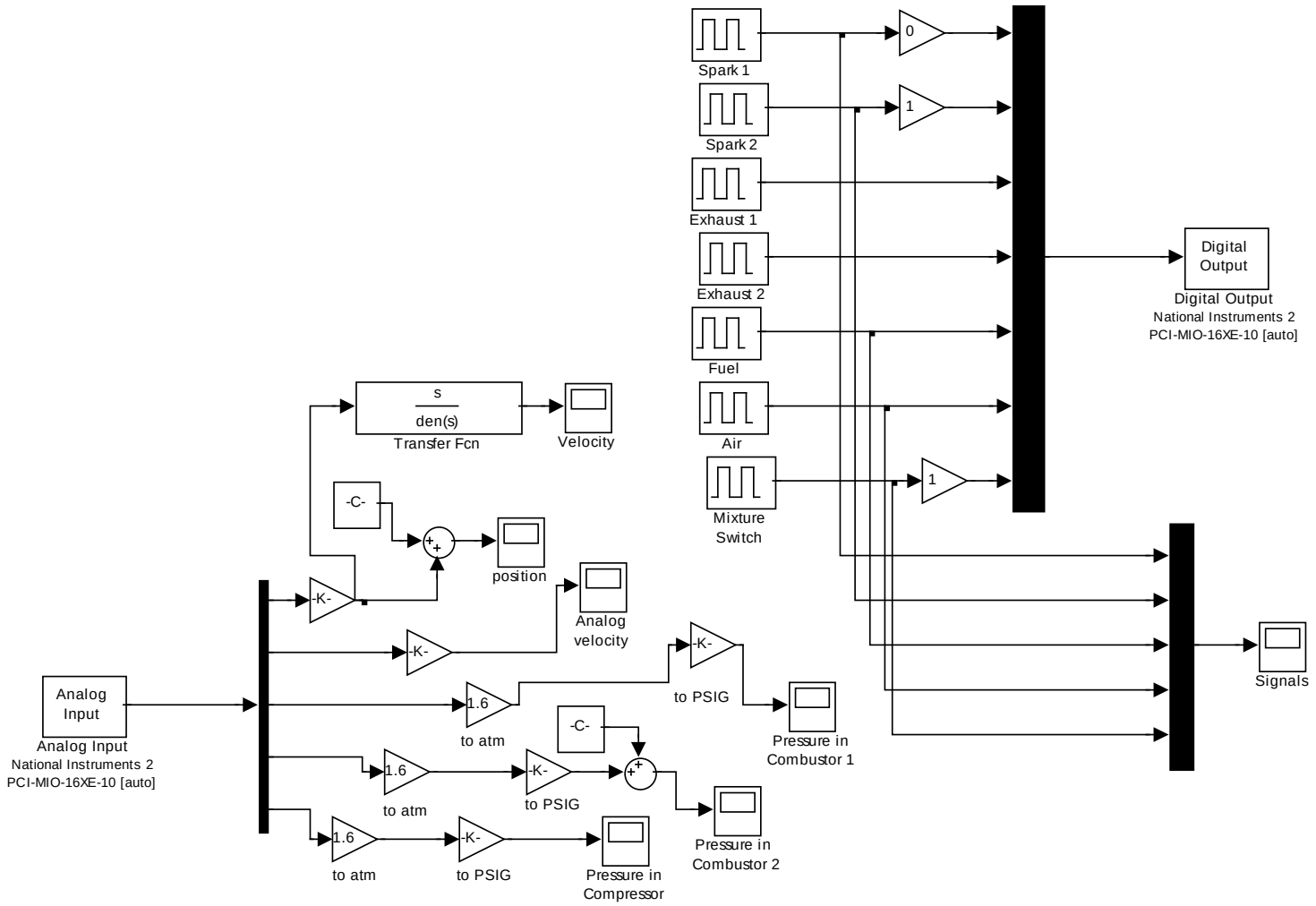

Figure A-14: Block diagram of Real Time Workshop implementation for Manuscript 3.

APPENDIX B

MATLAB CODE

Matlab function used to evaluate SIMULINK diagram shown in Figure A-1 (used to generate simulation data for Manuscript 1):

```
%% full_device_init
%% Eric J. Barth
%% 5/03/04

%% general/device
%M=5/2.2; % mass of pistons, linkages, bearings (kg)
M=1.8175; % mass of pistons, linkages, bearings (kg)
cv_air=716.5; % in (m^2)/(sec^2.K), Van Wylen and Sonntag
R_air=287.1; % Van Wylen and Sonntag
cp_air=1003.5; % Van Wylen and Sonntag
cp_in=cp_air;
gamma=1.4; % Van Wylen and Sonntag
T_room=22+273;

R_reactants=282.1794;  % R_univ/MW_ave_reactants
R_prod=293.56;  % R_univ/MW_ave_products
gamma_prod=1.2682; % obtained from temperature dependent equations for
mid temp
spec_energy_propane=46300; % in kJ/(kg propane) (lower heating value)
spec_energy_mix=2787.13; % in kJ/(kg mix)
%l= 5 * 2.54/100;  % length (in to m)
%Av=(3/1000)^2; % valve area
Av=1e-6; % valve coefficient (linear mass flow approx)
H_cond_e=0; % 1/R linear heat transfer conductance ENGINE SIDE
H_cond_c=0.0; % 1/R linear heat transfer conductance COMPRESSOR SIDE

%% pistons
A=pi*( 0.75/2*2.54/100)^2; % Area of power piston (in to m^2)  ENGINE
Al=pi*( 0.75/2*2.54/100)^2; % Area of power piston (in to m^2)
COMPRESSOR
%A=pi*( 1.5 /100)^2; % Area of power piston (in to m^2)  ENGINE
%Al=pi*( 1.25 /100)^2; % Area of power piston (in to m^2) COMPRESSOR
%P_init=(500+14.7)*101325/14.7; % initial combustion pressure at
x=x_deadvol (Pa)
P_init=585000; %(Pa)
V_dot0=0;
T_ADT=1977+273; % temperature of combustion (K)
P_inj=R_reactants*T_room/R_prod/T_ADT *P_init;
k=0 /12/2.54*100*4.46; % spring constant (lbs/ft to N/m)
%Fs=0.01*2*4.46; % spring pre-compression (lbs to N) (or constant force
spring if k=0)
Fs=0;

%% pump piston (loads)
P_atm=14.7*101325/14.7; % atmosphereic pressure (Pa)
P_cvd=1/3*101325/14.7; % check valve (both) pressure drop (Pa)

%% Shortcut Values
g=gamma_prod; R=R_prod; P0=P_init; e=spec_energy_mix*1000;
%Ps=(80+14.7)*101325/14.7; %Reservior pressure
Ps=228000;
g_a=1.4; % air in compresor side
```

```
g_a2=1.01; % for nearly isothermal conditions in the compressor (_alt
calculations)

% auto analysis
x_dead=2/1000; % 1 mm -> (m)
V0=A*x_dead;  % this is Ve0 -> use formula to find required Vc0
Ve0overVc=( P_atm* ((g_a/(1-g_a))*(1-(P_atm/Ps)^((1-g_a)/g_a))  ) ) / (
P0*( g/(1-g)*(P_atm/P0)^((g-1)/g) - 1/(1-g) + (P_atm/P0) ) );
Vc0=V0/Ve0overVc; % this will utilize all the ke and just barely run
into stop
yl=(A*Vc0+Al*V0)/(Al*A);  %% see simulation
l=x_dead+Vc0/Al;
Vmax=A/l;
disp('**********************************')
disp('Device Specs:')
disp(['Length (in) = ' num2str(l/2.54*100)]);
disp(['Engine Diameter (in) = ' num2str(sqrt(A/pi)*2/2.54*100)]);
disp(['Compressor Diameter (in) = ' num2str(sqrt(Al/pi)*2/2.54*100)]);

%m_mix=P_inj*V0/R_reactants/(22+273); % mass of gasses in power piston
(propane + air) (kg)
m_mix=P_init*V0/R_prod/T_ADT; % mass of gasses in power piston (propane
+ air) (kg)
m_air=m_mix*15.63/16.63;
m_c0=P_atm*Vc0/R_air/T_room;

sim('full_device_const2');

disp(['Injection pressure (psig) = ' num2str(P_inj*14.7/101325-14.7)]);
disp(['Combustion pressure (psig) = ' num2str(P_init*14.7/101325-
14.7)]);
disp(['x_dead (in) = ' num2str(x_dead/2.54*100)]);
disp(' ');

disp('Simulation Results:')
T_final_F=min(T_power_piston_F(:,2));

v_max=max(v(:,2));
KE=0.5*M*v_max^2;
KE_eff=KE/(spec_energy_mix*1000*m_mix)*100;
disp(['T_final = ' num2str(T_final_F) ' deg F']);
disp(['KE Efficiency (U to KE) = ' num2str(KE_eff) ' %']);

m_c=max(m_pumped(:,2));
E_stored=(Ps-P_atm)/Ps*(m_c-15.63/16.63*m_mix)*R_air*T_room;
sys_eff_sim=(E_stored)/(spec_energy_mix*1000*m_mix)*100;
disp(['Total System Efficiency  = ' num2str(sys_eff_sim) ' %']);

%%%% PLOTS
close all

plot(P_power_piston(:,1),P_power_piston(:,2)/1000,'k',[0 1.5e-
2],[101.325 101.325],'k:');
xlabel('Time (sec)');
ylabel('Pe (kPA)');
title('Pressure in Engine Side');
axis([0 1.5e-2 0 3600])
```

```
figure
plot(T_power_piston(:,1),T_power_piston(:,2),'k',[0 0.015],[295
295],'k:');
xlabel('Time (sec)');
ylabel('Te (K)');
title('Temperature in Engine Side');
axis([0 0.015 200 2400])

figure
plot(P_pump_piston(:,1),P_pump_piston(:,2)/1000,'k',[0 0.15],[101.325
101.325],'k:');
xlabel('Time (sec)');
ylabel('Pc (kPA)');
title('Pressure in Compressor Side');
axis([0 0.15 0 750])

figure
plot(T_pump_piston(:,1),T_pump_piston(:,2),'k',[0 0.15],[295
295],'k:');
xlabel('Time (sec)');
ylabel('Tc (K)');
title('Temperature in Compressor Side');
axis([0 0.15 250 550])

figure
plot(m_pumped(:,1),m_pumped(:,2)*1000,'k');
xlabel('Time (sec)');
ylabel('mc (g)');
title('Mass Pumped into Reservoir');
axis([0 0.02 -0.005 3e-2])


%% expansion ratio
ind=find(P_power_piston(:,2)<=101325);
Vf=V_power_piston(ind(1),2);

%% work done (theory vs. integrated sim)
work=(P_init*V0^1.2682)/(1-1.2682)*(Vf^(1-1.2682)-V0^(1-1.2682)) -
P_atm*(Vf-V0);

%%%%%%%%%%%%%%%%%%%%%%%%%%%%%%%%%%%%%%%%%%%%%%%%%%%%%%%%%%%%
%%%%%%%%%%%%%%%%%%%%%%%%%%%%%%%%%%%%%%%%%%%%%%%%%%%%%%%%%%%%
%%%%%%%%%%%%%%%%%%%%%%%%%%%%%%%%%%%%%%%%%%%%%%%%%%%%%%%%%%%%
disp(' ');
disp('Thermodynamic Analysis:')

%% KE eff
eff_e=R*T_ADT*( ( g*P0^(1/g)*P_atm^((g-1)/g) - P0)/(1-g) +
P_atm)/(e*P0);
disp(['KE Efficiency (formula) = ' num2str(eff_e*100) ' %']);

%disp(['Expansion ratio (Vf/V0) = ' num2str(Vf/V0)]);

if 0,
%% PLOT ke efficiency versus Pe0;
Pmax=(2000+14.7)*101325/14.7;
```

```
P=P_atm:(Pmax-P_atm)/40:Pmax;
P0_plot=P;
eff_ke_plot=R*T_ADT*( ( g*P.^(1/g)*P_atm^((g-1)/g) - P)/(1-g) +
P_atm)./(e.*P);
close all
%plot(P*14.7/101325-14.7,100*eff_ke_plot,'k');
%xlabel('Pe0 (psig)');
plot(P/1000,100*eff_ke_plot,'k');
xlabel('Pe0 (kPA)');
ylabel('Efficiency (%)');
title('Engine KE Efficiency vs Pe0');
axis([0 14000 0 50]);
grid
end

% Compressor efficiency
eff_comp=(1-g_a)/g_a*( (P_atm/Ps)^((1-g_a)/g_a) - (P_atm/Ps)^(1/g_a) )/
( 1-(P_atm/Ps)^((1-g_a)/g_a) );
eff_comp_alt=(1-g_a2)/g_a2*( (P_atm/Ps)^((1-g_a2)/g_a2) -
(P_atm/Ps)^(1/g_a2) )/ ( 1-(P_atm/Ps)^((1-g_a2)/g_a2) );
disp(['Compressor Efficiency (formula) = ' num2str(eff_comp*100) '
%']);
%disp(['Total Device Efficiency (formula) = ' num2str(eff_tot*100) '
%']);

%% reservoir heat loss efficiency
eff_res= P_atm^((g_a-1)/g_a)*Ps^((1-g_a)/g_a);
eff_res_alt= P_atm^((g_a2-1)/g_a2)*Ps^((1-g_a2)/g_a2);
disp(['Reservoir Heat Loss Efficiency (formula) = '
num2str(eff_res*100) ' %']);
disp(['Compressor and Heat loss Combined Efficiency (formula) = '
num2str(eff_comp*eff_res*100) ' %']);
disp(['Compressor (alt) and Heat loss Combined Efficiency (formula) = '
num2str(eff_comp_alt*eff_res_alt*100) ' %']);

if 0,
%% PLOT combined compressor and reservoir efficiency with and without
heat loss in compressor vs. Ps
figure
Pmax=(200+14.7)*101325/14.7;
Psp=P_atm+1:(Pmax-P_atm)/40:Pmax;
eff_comp_plot=(1-g_a)/g_a*( (P_atm./Psp).^((1-g_a)/g_a) -
(P_atm./Psp).^(1/g_a) ) ./ ( 1-(P_atm./Psp).^((1-g_a)/g_a) );
eff_res_plot= P_atm^((g_a-1)/g_a).*Psp.^((1-g_a)/g_a);
eff_comp_plot_alt=(1-g_a2)/g_a2*( (P_atm./Psp).^((1-g_a2)/g_a2) -
(P_atm./Psp).^(1/g_a2) ) ./ ( 1-(P_atm./Psp).^((1-g_a2)/g_a2) );
eff_res_plot_alt = P_atm^((g_a2-1)/g_a2).*Psp.^((1-g_a2)/g_a2);
%plot(Psp*14.7/101325-14.7,100*eff_comp_plot.*eff_res_plot,'k.-
',Psp*14.7/101325-14.7,100*eff_comp_plot_alt.*eff_res_plot_alt,'k');
%xlabel('Ps (psig)');
plot(Psp/1000,100*eff_comp_plot.*eff_res_plot,'k.-
',Psp/1000,100*eff_comp_plot_alt.*eff_res_plot_alt,'k');
xlabel('Ps (kPA)');
ylabel('Compressor Efficiency (%)');
legend('Without heat loss in compressor ( \gamma=1.4) ','With heat loss
in compressor ( \gamma=1.01)');
title('Compressor Efficiency vs Ps');
```

```
grid
end

%% mass investment efficiency
Ve0overVc=( P_atm* ((g_a/(1-g_a))*(1-(P_atm/Ps)^((1-g_a)/g_a))  ) ) / (
P0*( g/(1-g)*(P_atm/P0)^((g-1)/g) - 1/(1-g) + (P_atm/P0) ) );
eff_invest= 1 -
15.63/16.63*P0/P_atm*Ve0overVc*R_air*T_room/R_prod/T_ADT ;
Ve0overVc_alt=( P_atm* ((g_a2/(1-g_a2))*(1-(P_atm/Ps)^((1-g_a2)/g_a2))
) ) / ( P0*( g/(1-g)*(P_atm/P0)^((g-1)/g) - 1/(1-g) + (P_atm/P0) ) );
eff_invest_alt= 1 -
15.63/16.63*P0/P_atm*Ve0overVc_alt*R_air*T_room/R_prod/T_ADT ;
disp(['Mass investment Efficiency (formula) = ' num2str(eff_invest*100)
' %']);
disp(['Mass investment (alt) Efficiency (formula) = '
num2str(eff_invest_alt*100) ' %']);

if 0,
%% PLOT mass investment (at Ps=80 psig)
Pmax=(2000+14.7)*101325/14.7;
P0p=Ps/2:(Pmax-P_atm)/40:Pmax;
Ve0overVc_plot=( P_atm* ((g_a/(1-g_a))*(1-(P_atm/Ps)^((1-g_a)/g_a))  )
) ./ ( P0p.*( g/(1-g).*(P_atm./P0p).^((g-1)/g) - 1/(1-g) + (P_atm./P0p)
) );
eff_invest_plot= 1 -
15.63/16.63.*P0p/P_atm.*Ve0overVc_plot*R_air*T_room/R_prod/T_ADT ;
Ve0overVc_alt_plot=( P_atm* ((g_a2/(1-g_a2))*(1-(P_atm/Ps)^((1-
g_a2)/g_a2))  ) ) ./ ( P0p.*( g/(1-g).*(P_atm./P0p).^((g-1)/g) - 1/(1-
g) + (P_atm./P0p) ) );
eff_invest_alt_plot= 1 -
15.63/16.63.*P0p/P_atm.*Ve0overVc_alt_plot*R_air*T_room/R_prod/T_ADT ;
figure
%plot(P0p*14.7/101325-14.7,100*eff_invest_plot,'k.-',P0p*14.7/101325-
14.7,100*eff_invest_alt_plot,'k');
%xlabel('Pe0 (psig)');
plot(P0p/1000,100*eff_invest_plot,'k.-
',P0p/1000,100*eff_invest_alt_plot,'k');
xlabel('Pe0 (kPA)');
ylabel('Efficiency (%)');
legend('Without heat loss in compressor ( \gamma=1.4) ','With heat loss
in compressor ( \gamma=1.01)');
title('Mass Investment Efficiency with Ps=80 psig (653 kPa) vs Pe0');
grid
end


%% Total System Efficiency
eff_tot_sys=(1/e)*(1-P_atm/Ps)*( ( ( g/(1-g)*(P_atm/P0)^((g-1)/g) -
1/(1-g) + (P_atm/P0) )/( (g_a/(1-g_a))*(1-(P_atm/Ps)^((1-g_a)/g_a))  )
)*R_prod*T_ADT - 15.63/16.63*R_air*T_room  );

disp(['Total System Efficiency (formula) = ' num2str(eff_tot_sys*100) '
%']);

disp(['Total System Efficiency (individual mult together) = '
num2str(eff_e*eff_comp*eff_res*eff_invest*100) ' %']);
```

```
disp(['Total System Efficiency (individual mult together alt calc) = '
num2str(eff_e*eff_comp_alt*eff_res_alt*eff_invest_alt*100) ' %']);

disp(' ')


if 0,
%% overall efficiency surface plot (Psp,P0p,eff_comp_plot*eff_ke_plot)
figure
Pmax1=(2000+14.7)*101325/14.7;
P0p=P_atm:(Pmax1-P_atm)/40:Pmax1;
Pmax2=(200+14.7)*101325/14.7;
Psp=P_atm:(Pmax2-P_atm)/40:Pmax2;

% in surf terminology x(j)=P0p(j), y(i)=Psp(i), Z(i,j)=eff_sys;
Z=zeros(length(Psp),length(P0p));
for i=1:length(Psp),
    for j=1:length(P0p),
        Z(i,j)=(1/e)*(1-P_atm/Psp(i))*( ( ( g/(1-g)*(P_atm/P0p(j))^((g-
1)/g) - 1/(1-g) + (P_atm/P0p(j)) )/( (g_a/(1-g_a))*(1-
(P_atm/Psp(i))^((1-g_a)/g_a))  ) )*R_prod*T_ADT -
15.63/16.63*R_air*T_room  );
    end
end
mesh(P0p*14.7/101325-14.7,Psp*14.7/101325-14.7,Z);
%colorbar
xlabel('P0');
ylabel('Ps');
zlabel('Total System Efficiency');
end

if 0,
%%% PLOT overall system efficiency at Ps=80 psig
%% shows both cases: heat losses and no heat losses in compressor
%% equations of state cannot show effect of heat losses in engine side
(gamma=1 is isothermal -> heat input as expands!)
%% uses Ps defined above

eff_comp_plot2=(1-g_a)/g_a*( (P_atm/Ps)^((1-g_a)/g_a) -
(P_atm/Ps)^(1/g_a) )/ ( 1-(P_atm/Ps)^((1-g_a)/g_a) );
eff_comp_alt_plot2=(1-g_a2)/g_a2*( (P_atm/Ps)^((1-g_a2)/g_a2) -
(P_atm/Ps)^(1/g_a2) )/ ( 1-(P_atm/Ps)^((1-g_a2)/g_a2) );

eff_res_plot2= P_atm^((g_a-1)/g_a)*Ps^((1-g_a)/g_a);
eff_res_alt_plot2= P_atm^((g_a2-1)/g_a2)*Ps^((1-g_a2)/g_a2);

Pmax=(2000+14.7)*101325/14.7;
P0p=P_atm+1:(Pmax-P_atm)/40:Pmax;
eff_ke_plot2=R*T_ADT*( ( g*P0p.^(1/g)*P_atm^((g-1)/g) - P0p)/(1-g) +
P_atm)./(e.*P0p);
Ve0overVc_plot2=( P_atm* ((g_a/(1-g_a))*(1-(P_atm/Ps)^((1-g_a)/g_a))  )
) ./ ( P0p.*( g/(1-g).*(P_atm./P0p).^((g-1)/g) - 1/(1-g) + (P_atm./P0p)
) );
eff_invest_plot2= 1 -
15.63/16.63.*P0p/P_atm.*Ve0overVc_plot2*R_air*T_room/R_prod/T_ADT ;
```

```
Ve0overVc_alt_plot2=( P_atm* ((g_a2/(1-g_a2))*(1-(P_atm/Ps)^((1-
g_a2)/g_a2))  ) ) ./ ( P0p.*( g/(1-g).*(P_atm./P0p).^((g-1)/g) - 1/(1-
g) + (P_atm./P0p) ) );
eff_invest_alt_plot2= 1 -
15.63/16.63.*P0p/P_atm.*Ve0overVc_alt_plot2*R_air*T_room/R_prod/T_ADT ;
figure
%plot(P0p*14.7/101325-
14.7,100*eff_ke_plot2.*eff_comp_plot2.*eff_res_plot2.*eff_invest_plot2,
'k.-',P0p*14.7/101325-
14.7,100*eff_ke_plot2.*eff_comp_alt_plot2.*eff_res_alt_plot2.*eff_inves
t_alt_plot2,'k');
%xlabel('P0 (psig)');
plot(P0p/1000,100*eff_ke_plot2.*eff_comp_plot2.*eff_res_plot2.*eff_inve
st_plot2,'k.-
',P0p/1000,100*eff_ke_plot2.*eff_comp_alt_plot2.*eff_res_alt_plot2.*eff
_invest_alt_plot2,'k');
xlabel('Pe0 (kPA)');
ylabel('Efficiency (%)');
legend('Without heat loss in compressor ( \gamma=1.4) ','With heat loss
in compressor ( \gamma=1.01)');
title('Total System Efficiency with Ps=80 psig (653 kPa) vs Pe0');
grid
end

% garbage

%% entire efficiency (engine*pump) & compressor efficiency

%num=( ( g*P0^(1/g)*P_atm^((g-1)/g) - P0)/(1-g) + P_atm); % needs
gamma=g
%den1=P_atm/(1-g_a)* ( 1-(P_atm/Ps)^((1-g_a)/g_a) ) + P_atm* (
(P_atm/Ps)^(1/g_a)-1 ); % needs gamma_air=g_a
%den2=(Ps^((g_a-1)/g_a)*P_atm^(1/g_a)-Ps^(-1/g_a)*P_atm^((g_a+1)/g_a));
% needs gamma_air=g_a
%Vc0overV0=num/(den1+den2);
%Vc0=(Vc0overV0)*V0; % compressor area (max vol) - will be a large mult
of V0!!
%eff_comp= (Vc0/V0) * (Ps^((g_a-1)/g_a)*P_atm^(1/g_a)-Ps^(-
1/g_a)*P_atm^((g_a+1)/g_a)) / ( ( g*P0^(1/g)*P_atm^((g-1)/g) - P0)/(1-
g) + P_atm);
%eff_comp1= Vc0overV0 * (Ps^((g_a-1)/g_a)*P_atm^(1/g_a)-Ps^(-
1/g_a)*P_atm^((g_a+1)/g_a)) / ( ( g*P0^(1/g)*P_atm^((g-1)/g) - P0)/(1-
g) + P_atm);
% disp(['Compressor Efficiency (formula1) = ' num2str(eff_comp*100) '
%']);

%eff_tot=(R*T_ADT/e) * (Vc0/V0) * (Ps^((g_a-1)/g_a)*P_atm^(1/g_a)-Ps^(-
1/g_a)*P_atm^((g_a+1)/g_a))/P0;



disp(['Combustion chamber intial volume Ve0 = ' num2str(V0*100^3) '
cm^3']);
disp(['Required compressor volume Vc0 = ' num2str(V0/Ve0overVc*100^3) '
cm^3']);
disp(['Combustion chamber final volume Vef (down to Patm) = '
num2str(((P_init*V0^g/P_atm)^(1/g))*100^3) ' cm^3']);
```

Matlab function used to evaluate SIMULINK diagram shown in Figure A-8 (used to generate simulation data for Manuscript 2):

```
%% Eric J. Barth
%% 8/10/04

%% general/device
M=2/2.2; % mass of pistons, linkages, bearings (kg)
cv_air=717.75; % in (m^2)/(sec^2.K)
R_air=287.1;
cp_air=cv_air+R_air;
gamma=1.4;
cv_mix=656.75; % mix=air+propane stoichiometric
R_mix=262.7;
cp_mix=cv_mix+R_mix;
P_atm=14.7*101000/14.7; % atmosphereic pressure (Pa)
spec_energy_propane=46300; % in kJ/(kg propane) (lower heating value)
spec_energy_mix=2787.13; % in kJ/(kg mix)
l=4*2.54/100;  % length (m)
%Av=(3/1000)^2; % valve area
Av=1e-5; % valve coefficient (linear mass flow approx)
H_cond=0*1; % 1/R linear heat transfer conductance

%% power piston
A=pi*( 1.25 /2*2.54/100)^2; % Area of power piston (in to m^2)
P_init=(650+14.7)*101000/14.7; % initial combustion pressure at
x=x_deadvol (Pa)
Vmax=A*l;
V_dot0=0;
T_ADT=1900+273; % temperature of combustion (K)
P_inj=P_init*(22+273)/T_ADT;
Fs=2*P_inj*A; % hold against injection pressure (or constant force
spring if k=0)
k= 700 /12/2.54*100*4.46; % spring constant (lbs/ft to N/m) - starts at
Vfc
x_dead=0.149*2.54/100; % dead space giving volume of initial combustion
(m)
V0=A*x_dead;
x_mag=1/1000; % magnetic gap (m)
k_mag=Fs*x_mag^2; % required constant to provide Fs at x_mag
Vfc=(P_init*(V0^gamma)/P_atm)^(1/gamma); % volume where combustion
pressure gets down to atmospheric pressure
m_mix=P_inj*(x_dead*A)/R_mix/(22+273); % mass of gasses in power piston
(propane + air) (kg)
m_air=m_mix*15.63/16.63;

%% pump piston (loads)
Al=pi*( 1.25 /2*2.54/100)^2; % Area of pump piston (m^2)
y_dead=0.01*2.54/100; % for dead volume of pump (in to m)
Vl0=Al*y_dead;
Vlmax=Al*l;
Vl_holes=1*Vlmax; % where side holes are on pump piston
P_comp=(80+14.7)*101000/14.7; % compressor tank pressure (Pa)
P_cvd=1/3*101000/14.7; % check valve (both) pressure drop (Pa)
m_gas_pump=(P_atm-P_cvd)*Vl0/287.1/(22+273); % mass of gasses in pump
piston (air) (kg)
```

```
T_room=22+273;
T_pump_init=22+273;

% auto analysis
sim('folded_fpc_mag');
go=0;
while go,
   %disp(x_dead/2.54*100);
   V0=A*x_dead;
   m_mix=P_inj*(x_dead*A)/R_mix/(22+273); % mass of gasses in power
piston (propane + air) (kg)
   m_air=m_mix*15.63/16.63;
   sim('folded_fpc_mag');
   x_max=max(x(:,2));
   if ((l-x_max)<=l/100)*((l-x_max)>l/1000),
      go=0;
   elseif x_max<l,
      x_dead=(1+(l-x_max)/l)*x_dead;
   else
      x_dead=0.5*x_dead;
   end
end

disp(['Injection pressure (psig) = ' num2str(P_inj*14.7/101000-14.7)]);
disp(['x_dead (in) = ' num2str(x_dead/2.54*100)]);
dum=length(m_pumped(:,2));
mp=m_pumped(dum,2);
% pot energy stored in res after all coming to room temp:
energy_in_res=(mp-m_air)*R_air*T_room; % also accounts for mass of air
needed for combustion
T_final_F=min(T_power_piston_F(:,2));

%t_final_index=length(P_power_piston(:,1));
%dum=find(P_pump_piston(:,2)>=(P_comp+P_cvd-0.01*101000/14.7));
%if (isempty(dum)),
%    disp('Piston did not pump');
%else
%    dum=find(P_power_piston(:,2)==P_power_piston(t_final_index,2));
%    t_index=dum(1);
%    x_open=x(t_index,2);
%    T_open=T_power_piston(t_index,2);
%    T_final=(x_open-x_dead)*(T_open)/(l-x_dead)+(l-
x_open)*(22+273)/(l-x_dead);
%    T_final_F=(T_final-273)*9/5-32;
%    dum=find(P_pump_piston(:,2)>=(P_comp+P_cvd-0.01*101000/14.7));
%    t_index2=dum(1);
%    x_start_pump=x(t_index2,2);
%    y_pump=max(x(:,2))-x(t_index2,2);
%    y_pump_in=y_pump*100/2.54;
%    T_high=T_power_piston(1,2);
%    T_low=T_open;
%    eff=(T_high-T_low)/T_high*100;
%    %adiabatic_energy_stored=energy_stored(t_final_index,2);
%
%tot_adia_eff=adiabatic_energy_stored/(spec_energy_mix*1000*m_mix)*100;
%    % isothermal_energy_stored=y_pump*Al*P_comp; % wrong
```

```
%    % tot_iso_eff=isothermal_energy_stored/(13000*1000*m_gas)*100; %
wrong
%    dum=find(x(:,2)<=x_dead);
%    dum2=find(dum>50);
%%    t_cycle=x(dum(dum2(1)),1);
%    % res stored energy after heat loss down to room temp (see p.49)
%    V1=Al*(yl-x_dead);
%    m1=(P_atm-P_cvd)*V1/R_air/T_room;
%    T2=(P_comp+P_cvd)*Al*(yl-x_start_pump)/m1/R_air;
%    V2=Al*(yl-max(x(:,2)));
%    m2=(P_comp+P_cvd)*V2/R_air/T2;
%    V_res=(m1-m2-m_air)*R_air*T_room/P_comp; % also accounts for mass
of air needed for combustion
%    energy_in_res=P_comp*V_res;
res_iso_eff=energy_in_res/(spec_energy_mix*1000*m_mix)*100;
disp(['T_final = ' num2str(T_final_F) ' deg F']);
disp(['Total Efficiency (inside res cool) = ' num2str(res_iso_eff) '
%']);
%    disp(['Specific Work of engine = '
num2str(spec_energy_propane*eff/100) ' kJ/kg']);
disp(['Total Specific Work (once inside res) = '
num2str(spec_energy_propane*res_iso_eff/100) ' kJ/kg']);
dum=find(x(:,2)<=x_dead);
dum2=find(dum>50);
if ~isempty(dum2),
    t_cycle=x(dum(dum2(1)),1);
    disp(['Device cycle time = ' num2str(t_cycle) ' sec']);
    disp(['Device power output (res) = ' num2str(energy_in_res/t_cycle)
' Watts']);
    disp(['Device frequency = ' num2str(1/t_cycle) ' Hz']);
    disp(' ')
end
```

APPENDIX C

ADDITIONAL EXPERIMENTAL DATA FROM MANUSCRIPT 2 ('Pump-on-Return' Version of FPC)

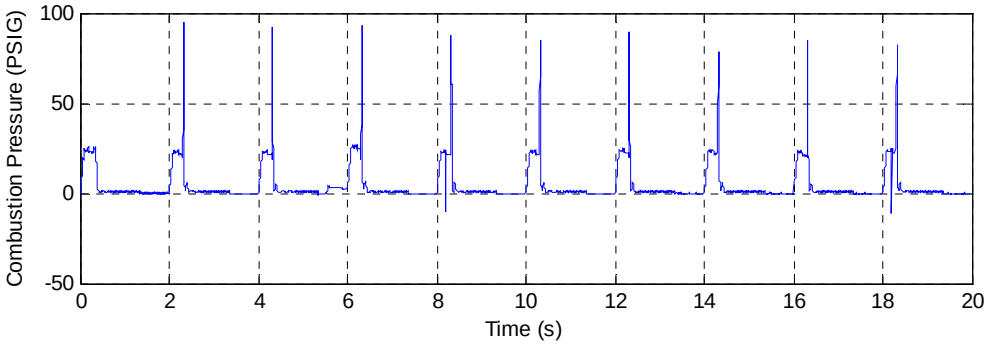

Figure C-1: Combustion Pressure with 95 ms air valve opening time, 13 ms fuel valve opening time, and 50 PSIG air supply. (run090804_v2.mat)

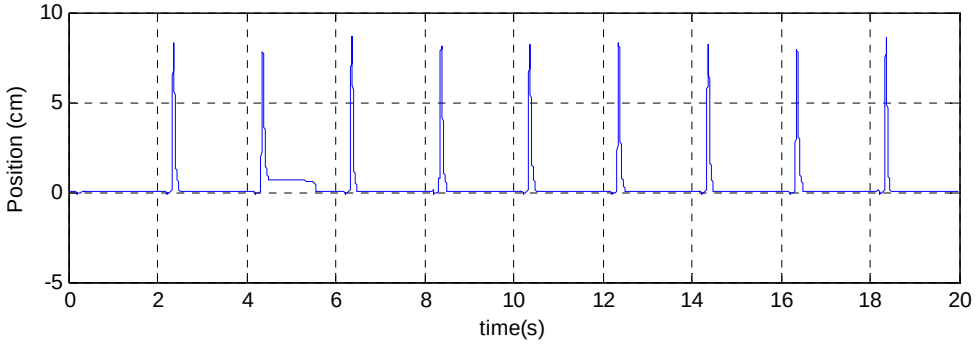

Figure C-2: Position of free piston with 95 ms air valve opening time, 13 ms fuel valve opening time, and 50 PSIG air supply. (run090804_v2.mat)

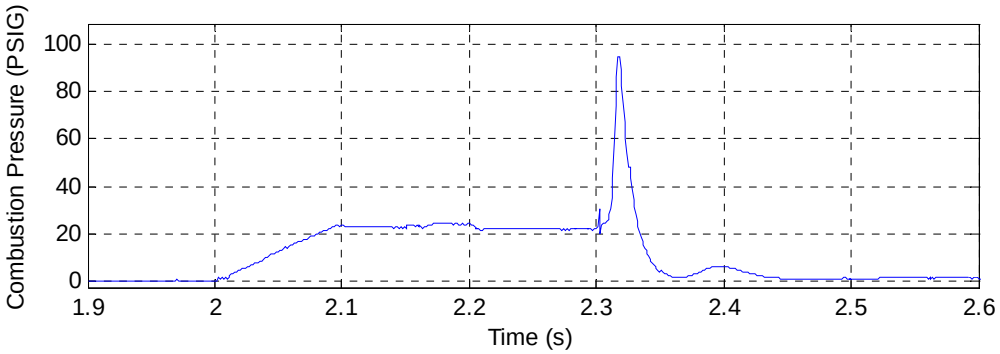

Figure C-3: Up-close view of combustion sample, from Figure C-1. (run090804_v2.mat)

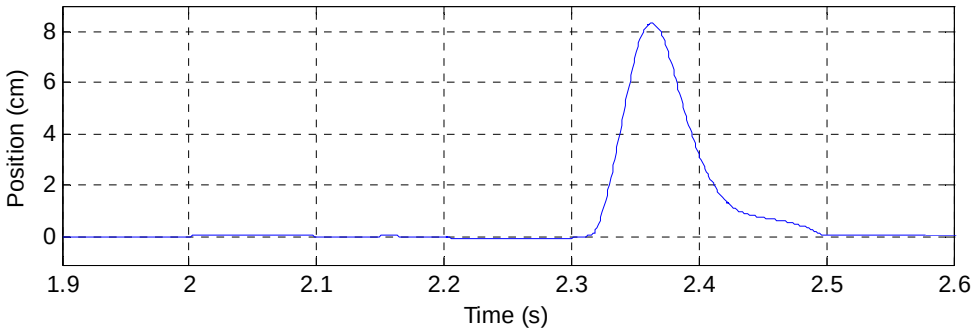

Figure C-4: Up-close view of position profile, from Figure C-2. (run090804_v2.mat)

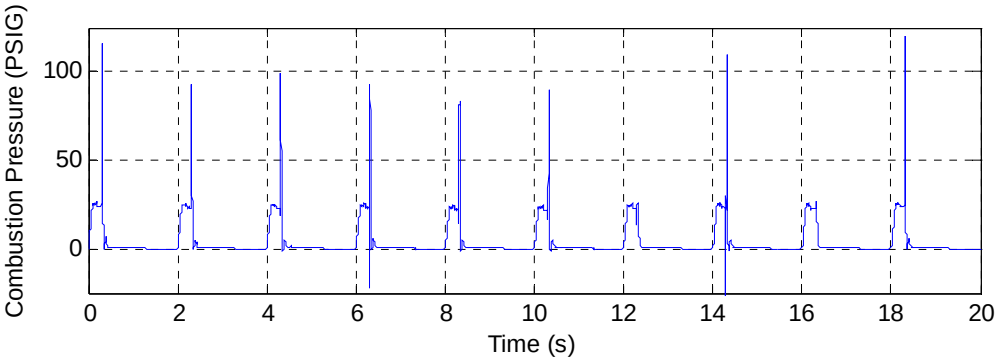

Figure C-5: Combustion Pressure with 100 ms air valve opening time, 13 ms fuel valve opening time, and 50 PSIG air supply. (run090804_v3.mat)

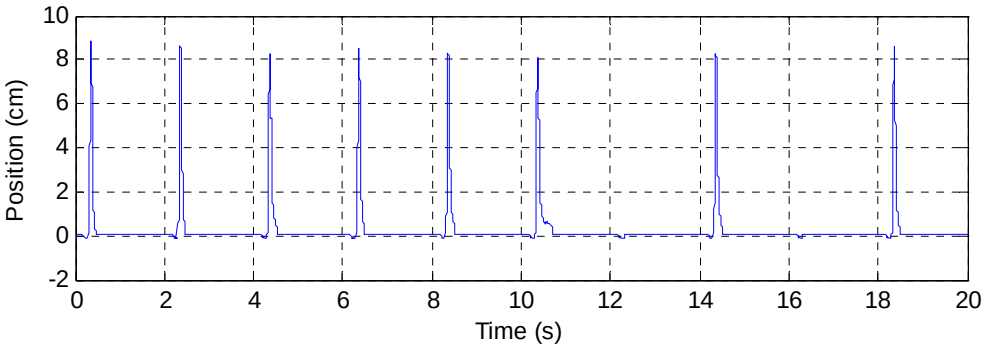

Figure C-6: Position of free piston with 100 ms air valve opening time, 13 ms fuel valve opening time, and 50 PSIG air supply. (run090804_v3.mat)

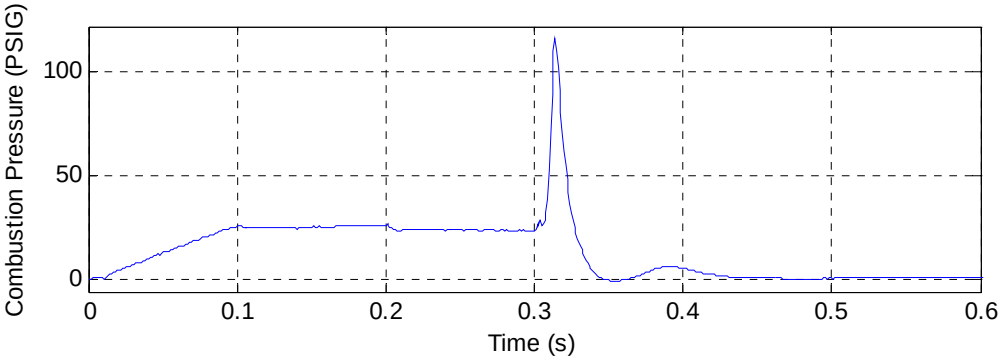

Figure C-7: Up-close view of combustion sample, from Figure C-5. (run090804_v3.mat)

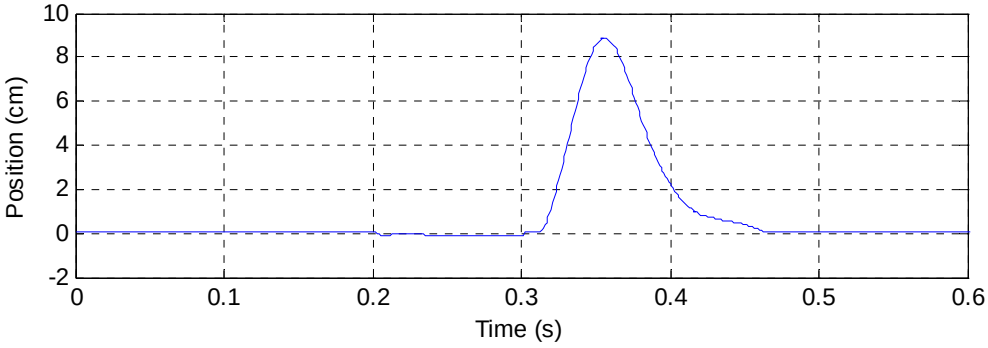

Figure C-8: Up-close view of position profile, from Figure C-6. (run090804_v3.mat)

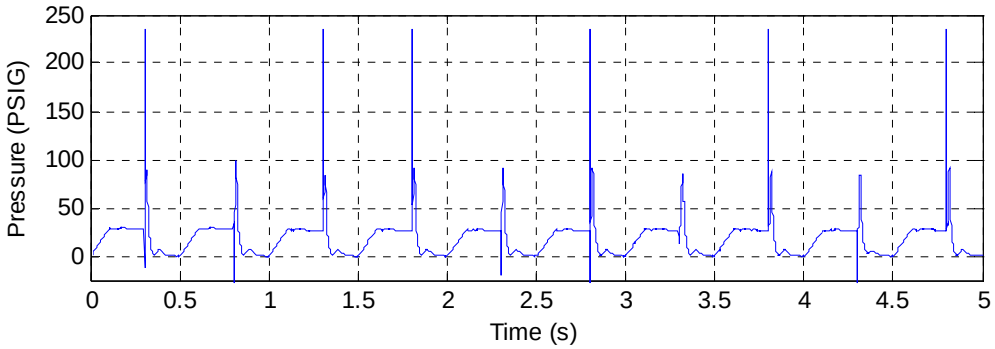

Figure C-9: Combustion Pressure with 110 ms air valve opening time, 14 ms fuel valve opening time, and 50 PSIG air supply. (run091004_v1.mat) (Peaks due to noisy spark)

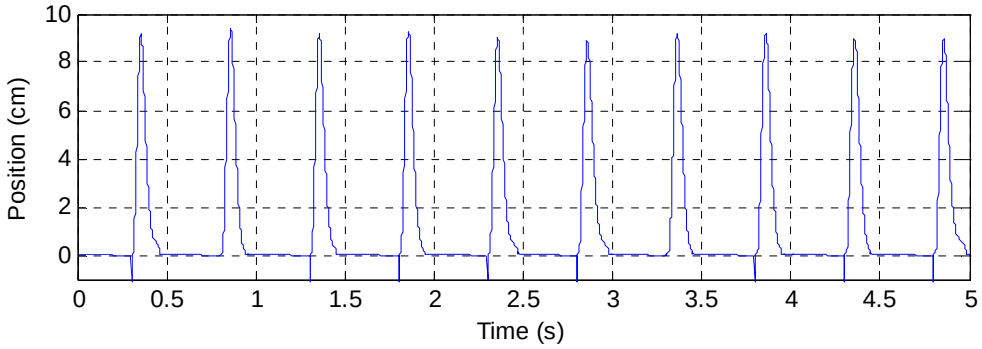

Figure C-10: Position of free piston with 110 ms air valve opening time, 14 ms fuel valve opening time, and 50 PSIG air supply. (run091004_v1.mat)

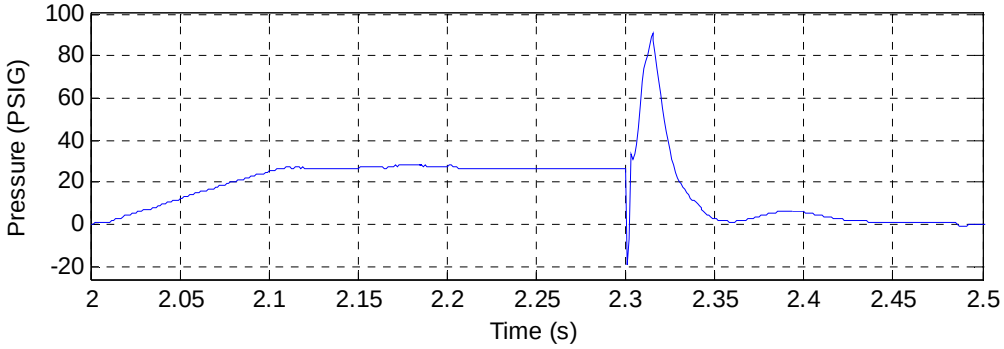

Figure C-11: Up-close view of combustion sample, from Figure C-9. (run091004_v1.mat)

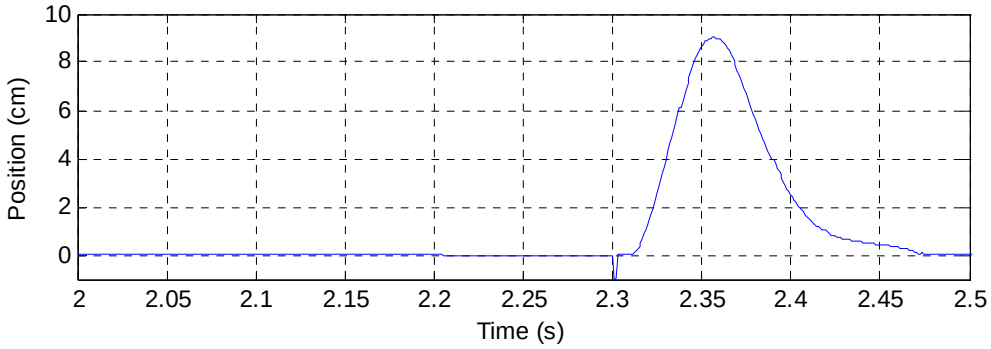

Figure C-12: Up-close view of position profile, from Figure C-10. (run091004_v1.mat)

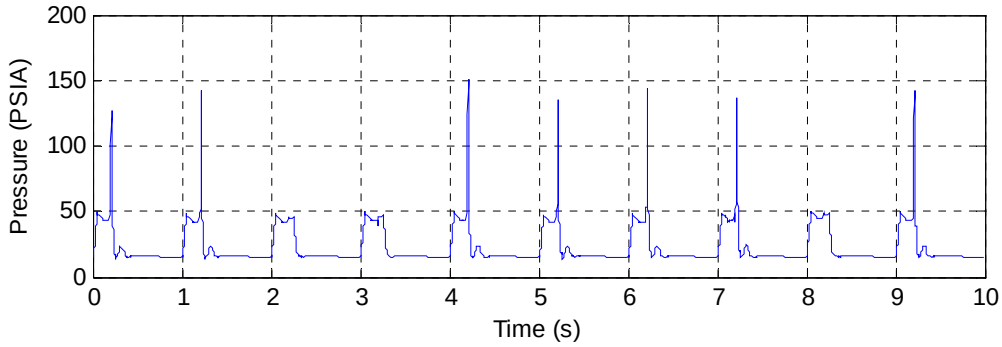

Figure C-13: Combustion Pressure with 50 ms air valve opening time, 11 ms fuel valve opening time, and 78 PSIG air supply. (run111104_v1.mat)

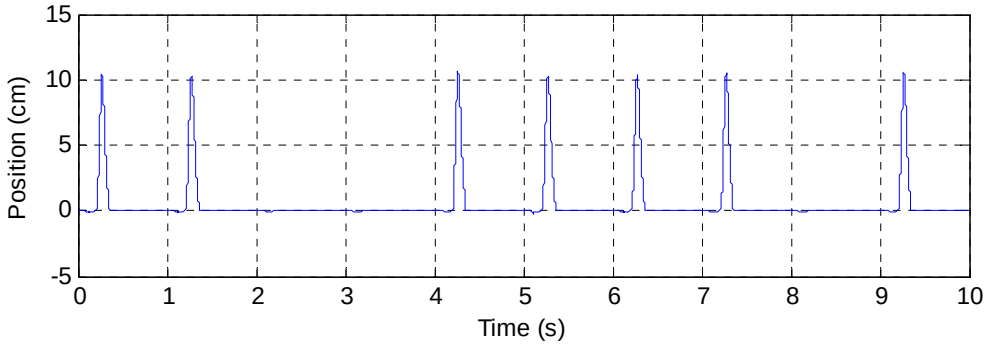

Figure C-14: Position of free piston with 50 ms air valve opening time, 11 ms fuel valve opening time, and 78 PSIG air supply. (run111104_v1.mat)

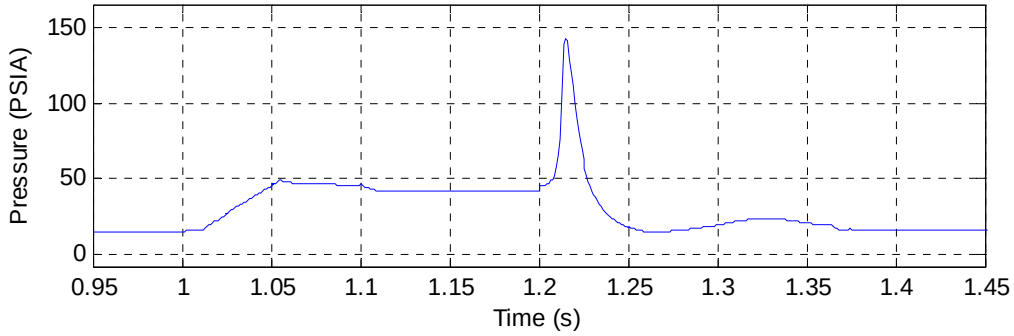

Figure C-15: Up-close view of combustion sample, from Figure C-13. (run111104_v1.mat)

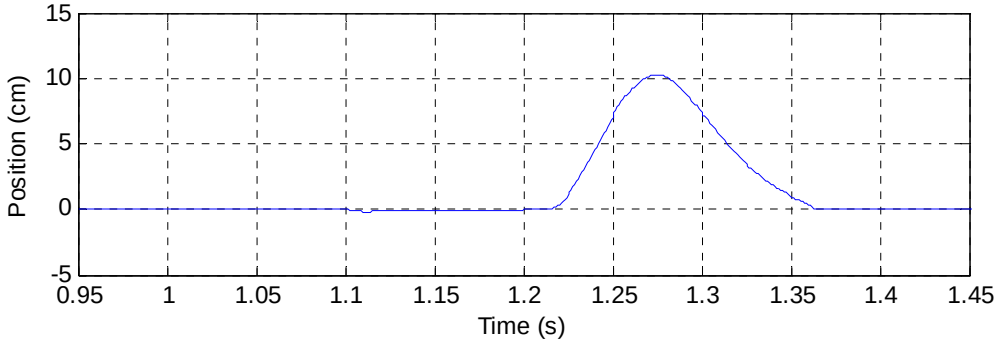

Figure C-16: Up-close view of position profile, from Figure C-10. (run111104_v1.mat)

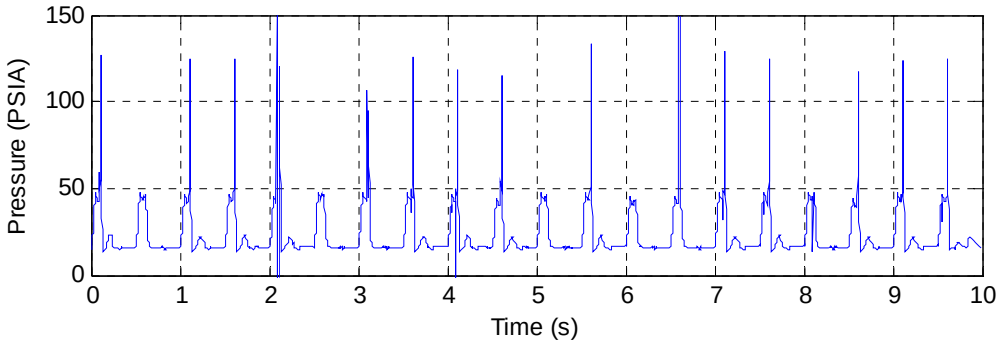

Figure C-17: Combustion Pressure with 45 ms air valve opening time, 9 ms fuel valve opening time, and 78 PSIG air supply. (run111104_v3.mat)

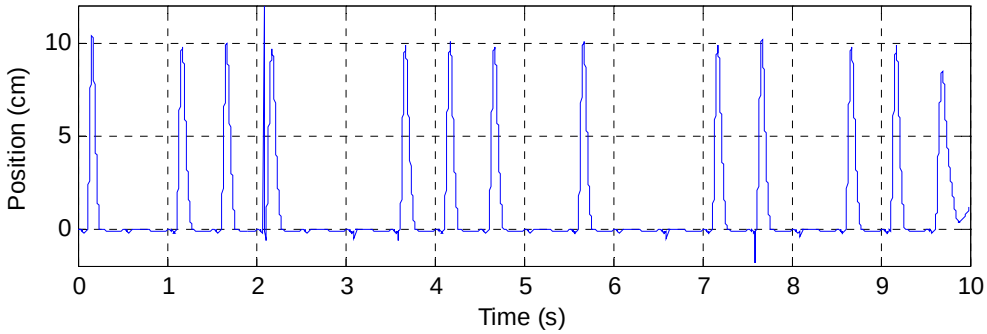

Figure C-18: Position of free piston with 45 ms air valve opening time, 9 ms fuel valve opening time, and 78 PSIG air supply. (run111104_v3.mat)

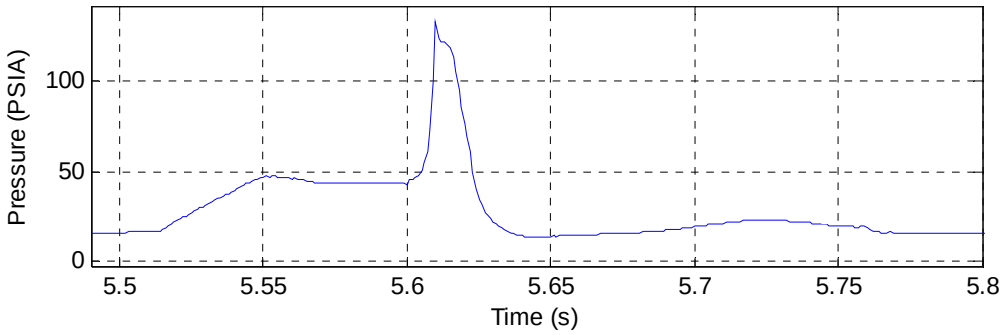

Figure C-19: Up-close view of combustion sample, from Figure C-17. (run111104_v3.mat)

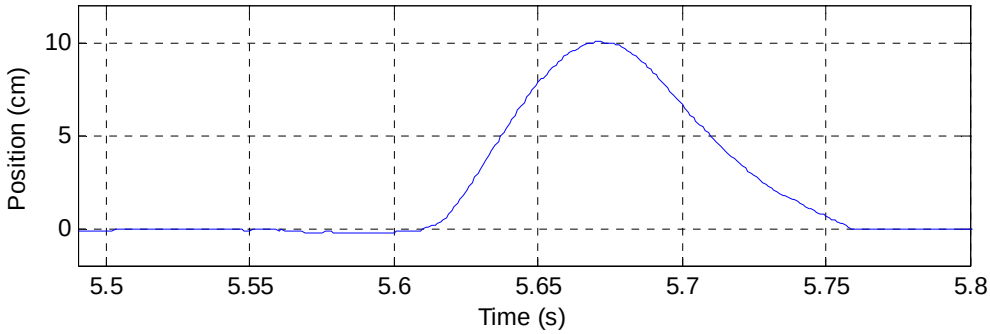

Figure C-20: Up-close view of position profile, from Figure C-18. (run111104_v3.mat)

APPENDIX D

ADDITIONAL EXPERIMENTAL DATA FROM MANUSCRIPT 3 (Final Version of FPC)

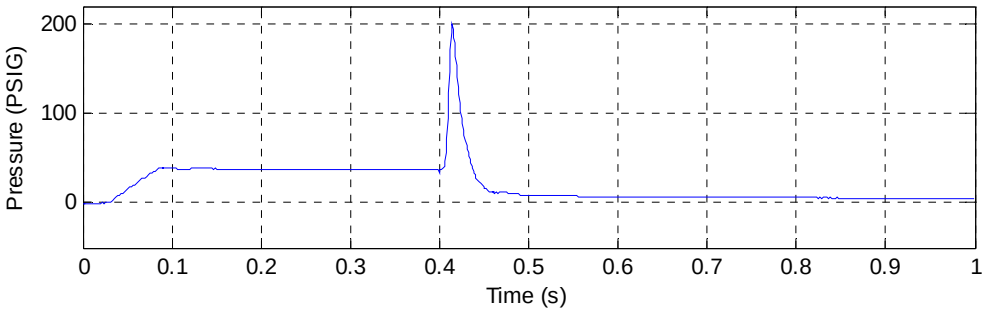

Figure D-1: Combustion Pressure with 70 ms air valve opening time, 13 ms fuel valve opening time, and 78 PSIG air supply. (032305_78psig_supply.mat)

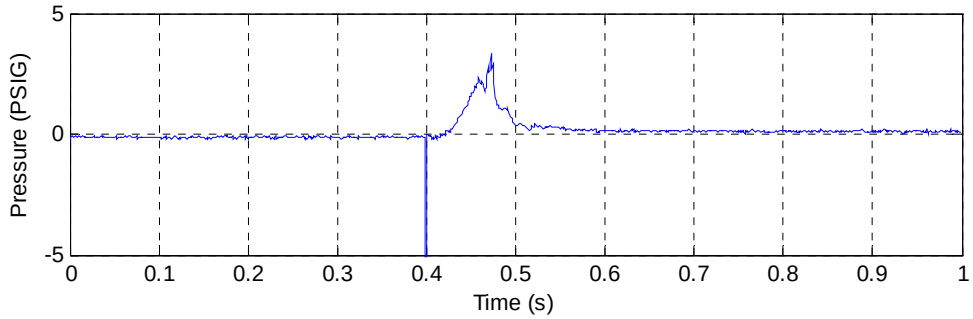

Figure D-2: Pumping Pressure with 70 ms air valve opening time, 13 ms fuel valve opening time, and 78 PSIG air supply. (032305_78psig_supply.mat)

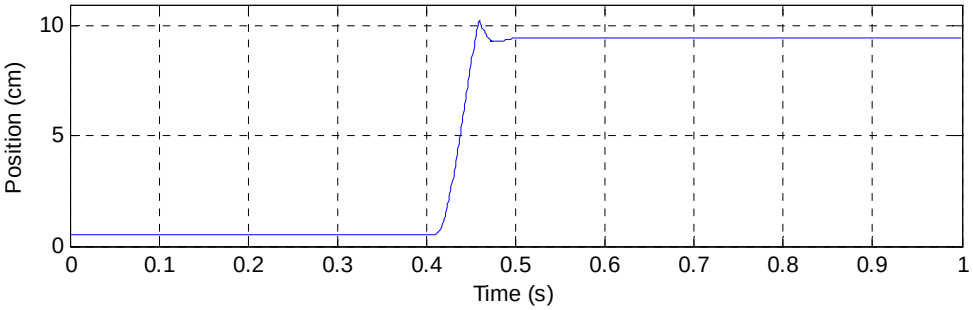

Figure D-3: Position of Free Piston with 70 ms air valve opening time, 13 ms fuel valve opening time, and 78 PSIG air supply. (032305_78psig_supply.mat)

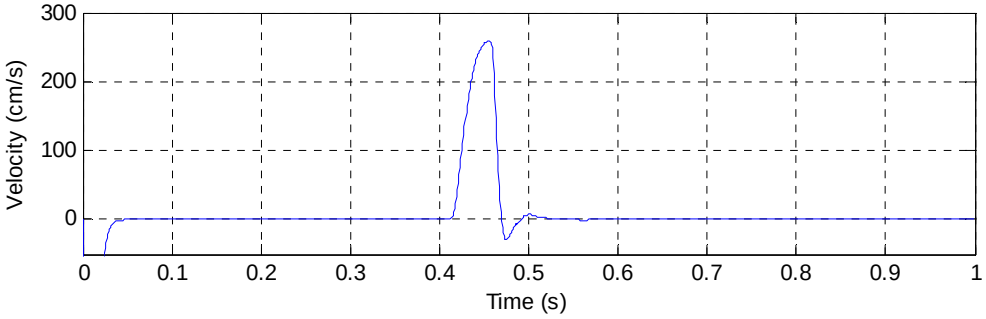

Figure D-4: Velocity of Free Piston with 70 ms air valve opening time, 13 ms fuel valve opening time, and 78 PSIG air supply. (032305_78psig_supply.mat)

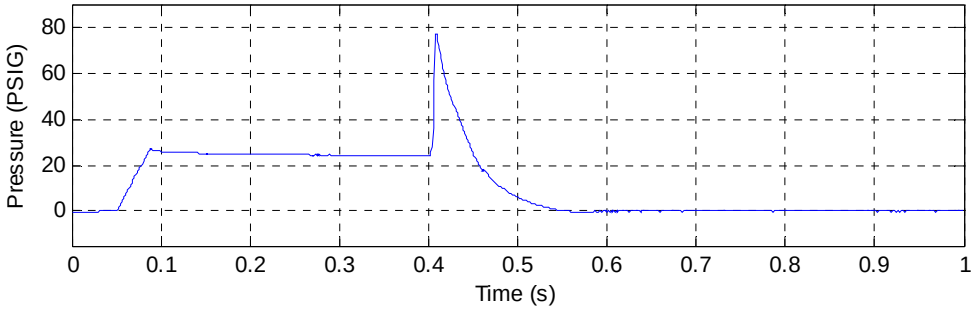

Figure D-5: Combustion Pressure with 45 ms air valve opening time, 13 ms fuel valve opening time, and 78 PSIG air supply. (032405_78psig_supply.mat)

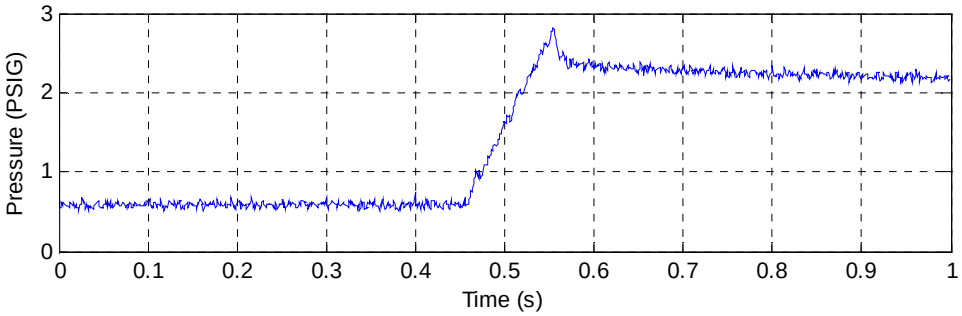

Figure D-6: Pumping Pressure with 45 ms air valve opening time, 13 ms fuel valve opening time, and 78 PSIG air supply. (032405_78psig_supply.mat)

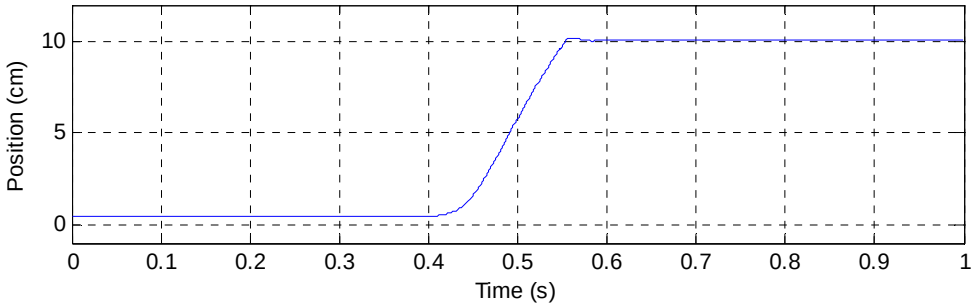

Figure D-7: Position of Free Piston with 45 ms air valve opening time, 13 ms fuel valve opening time, and 78 PSIG air supply. (032405_78psig_supply.mat)

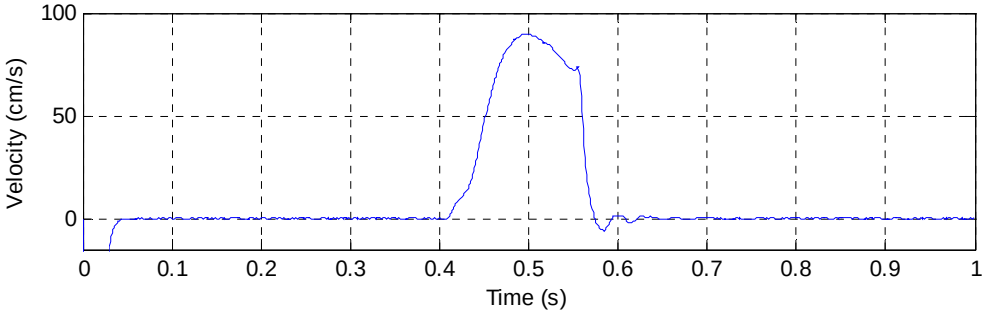

Figure D-8: Velocity of Free Piston with 45 ms air valve opening time, 13 ms fuel valve opening time, and 78 PSIG air supply. (032405_78psig_supply.mat)

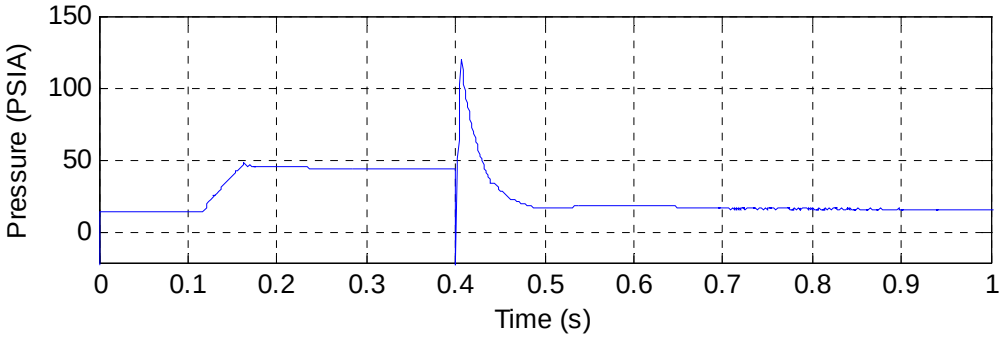

Figure D-9: Combustion Pressure with 59 ms air valve opening time, 9 ms fuel valve opening time, and 78 PSIG air supply. (052305_08.mat)

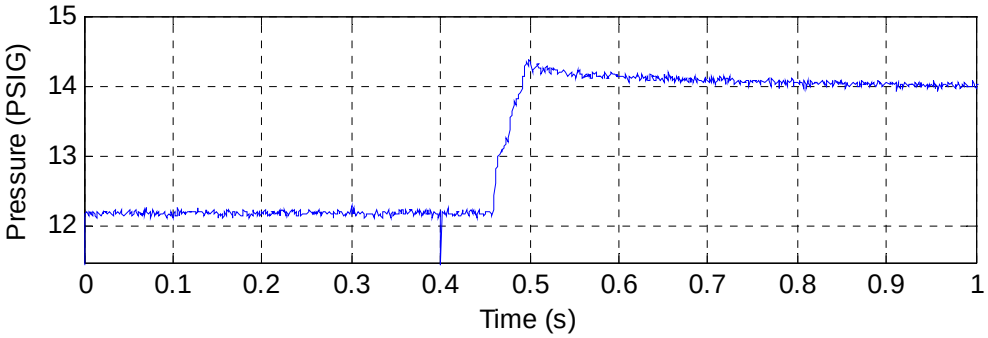

Figure D-10: Pumping Pressure with 59 ms air valve opening time, 9 ms fuel valve opening time, and 78 PSIG air supply. (052305_08.mat)

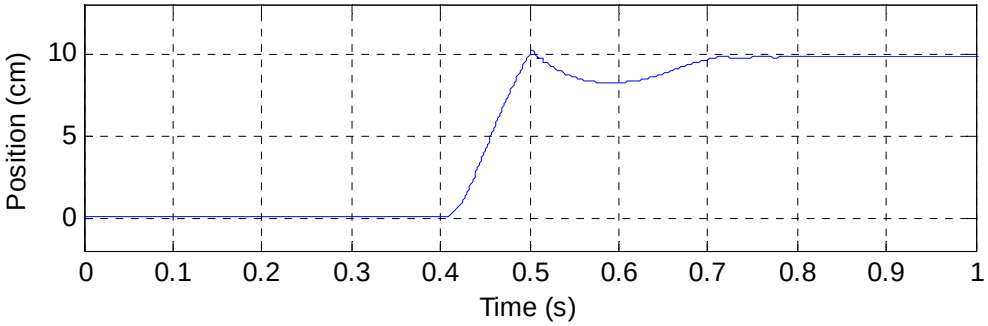

Figure D-11: Position of Free Piston with 59 ms air valve opening time, 9 ms fuel valve opening time, and 78 PSIG air supply. (052305_08.mat)

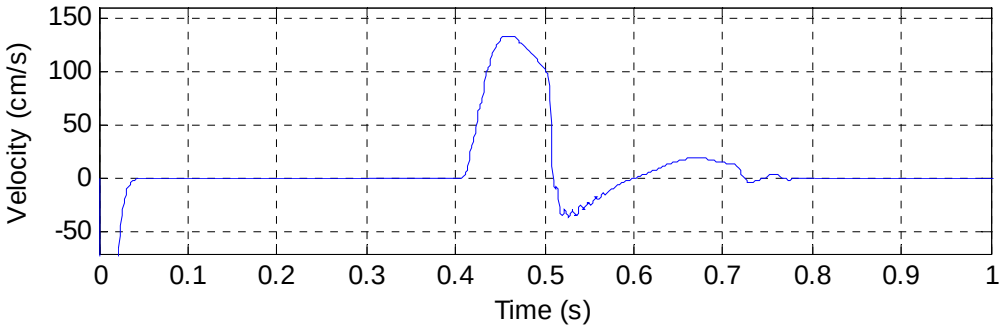

Figure D-12: Velocity of Free Piston with 59 ms air valve opening time, 9 ms fuel valve opening time, and 78 PSIG air supply. (052305_08.mat)

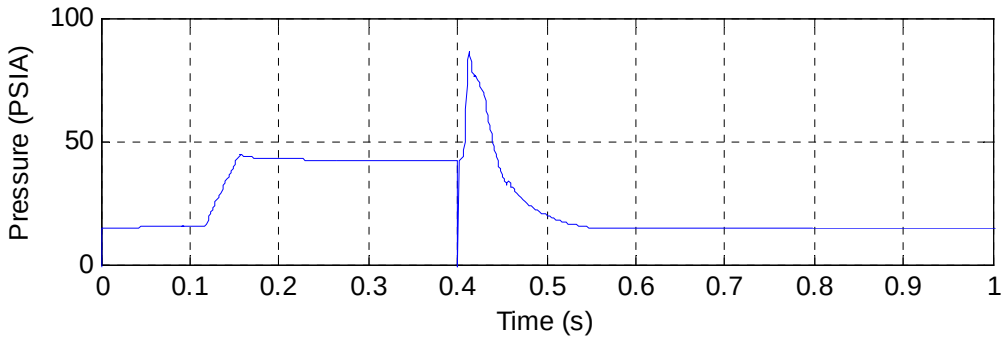

Figure D-13: Combustion Pressure with 53 ms air valve opening time, 8 ms fuel valve opening time, and 78 PSIG air supply. (052405_04.mat)

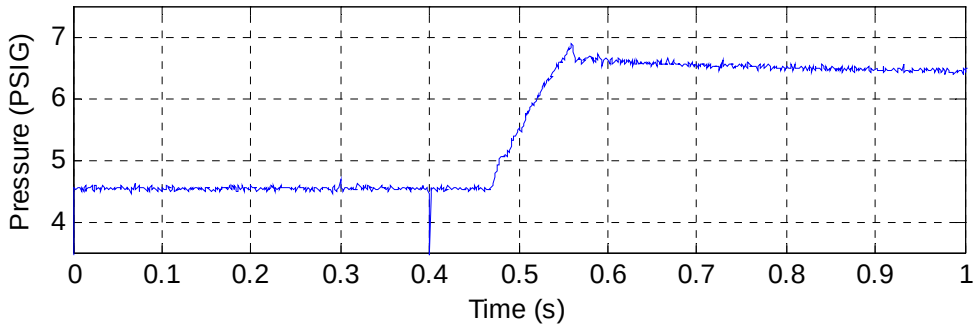

Figure D-14: Pumping Pressure with 53 ms air valve opening time, 8 ms fuel valve opening time, and 78 PSIG air supply. (052405_04.mat)

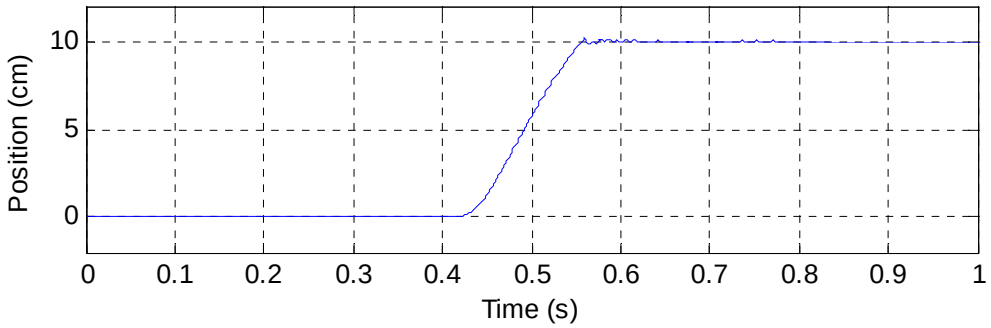

Figure D-15: Position of Free Piston with 53 ms air valve opening time, 8 ms fuel valve opening time, and 78 PSIG air supply. (052405_04.mat)

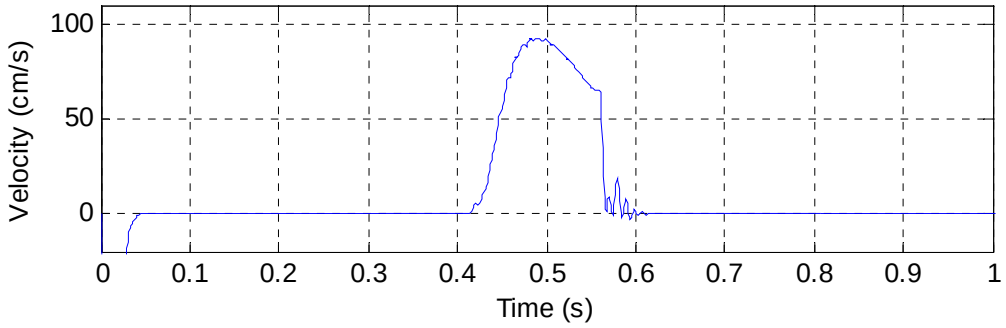

Figure D-16: Velocity of Free Piston with 53 ms air valve opening time, 8 ms fuel valve opening time, and 78 PSIG air supply. (052405_04.mat)

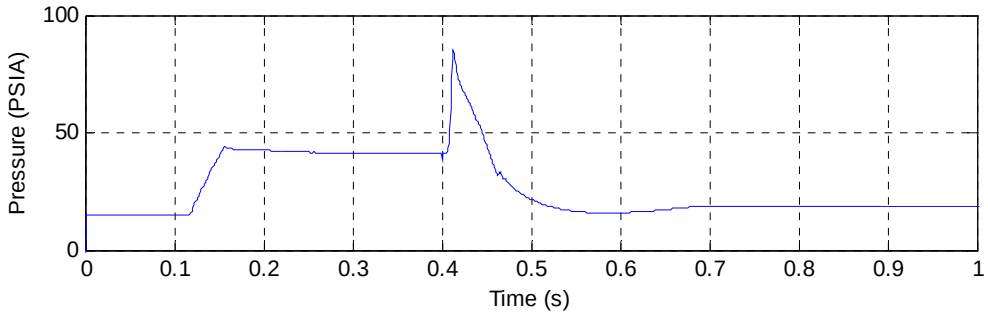

Figure D-17: Combustion Pressure with 53 ms air valve opening time, 8 ms fuel valve opening time, and 78 PSIG air supply. (052405_07.mat)

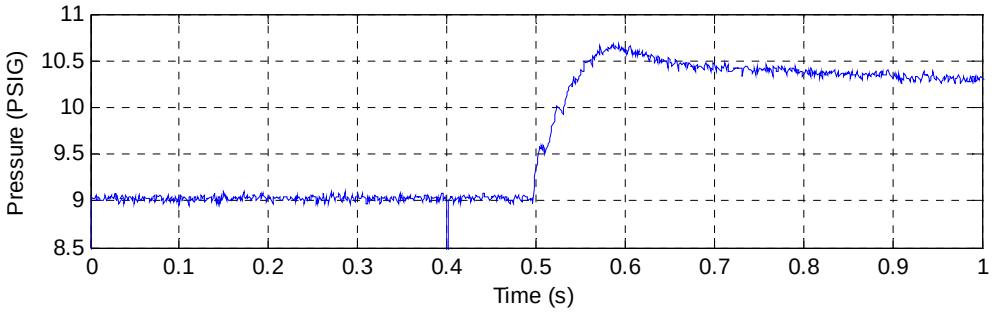

Figure D-18: Pumping Pressure with 53 ms air valve opening time, 8 ms fuel valve opening time, and 78 PSIG air supply. (052405_07.mat)

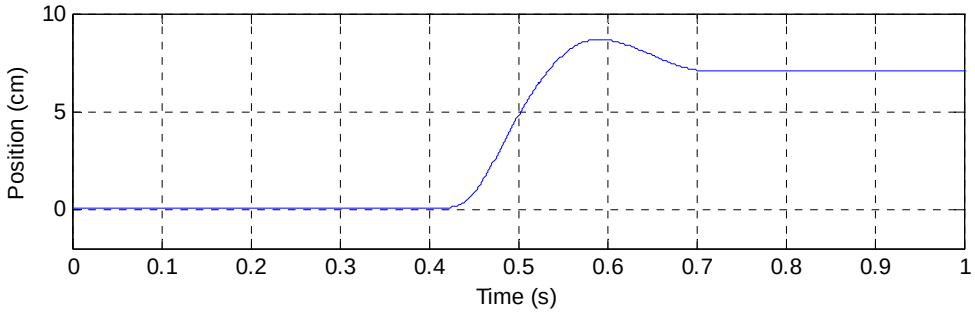

Figure D-19: Position of Free Piston with 53 ms air valve opening time, 8 ms fuel valve opening time, and 78 PSIG air supply. (052405_07.mat)

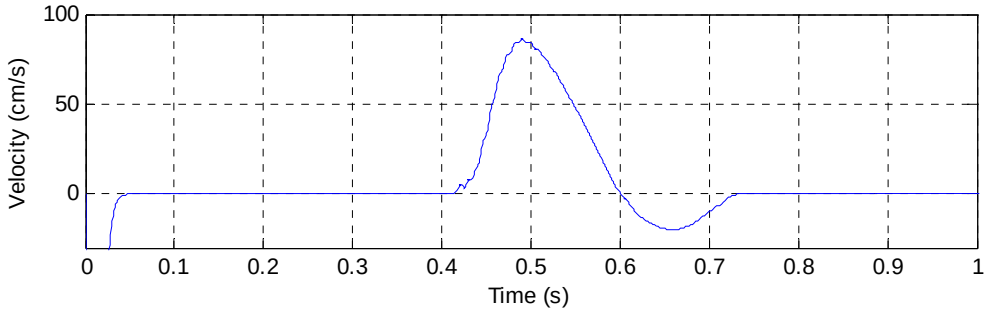

Figure D-20: Velocity of Free Piston with 53 ms air valve opening time, 8 ms fuel valve opening time, and 78 PSIG air supply. (052405_07.mat)

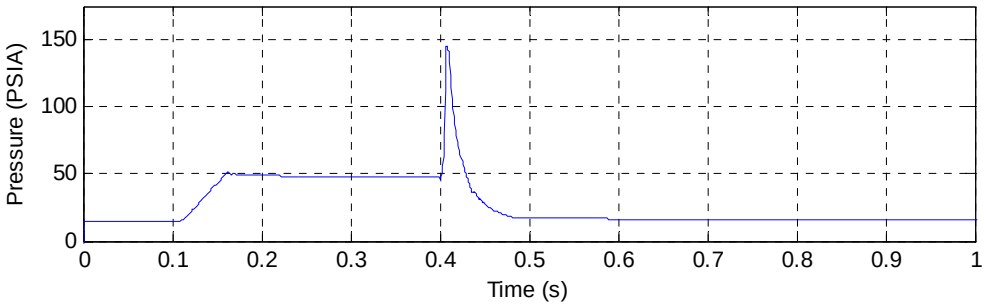

Figure D-21: Combustion Pressure with 59 ms air valve opening time, 9 ms fuel valve opening time, and 78 PSIG air supply. (052405_08.mat)

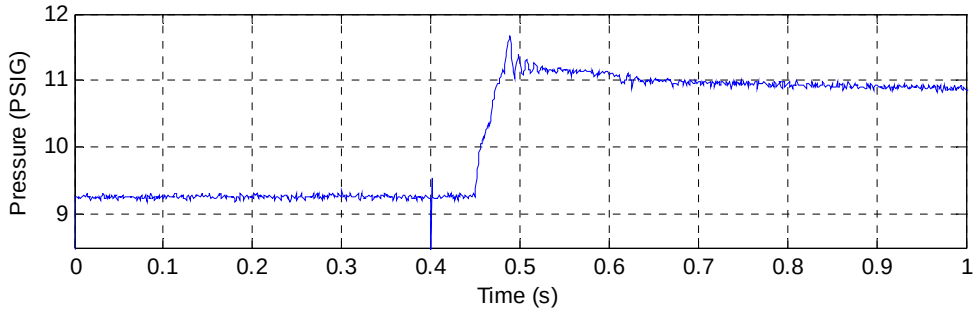

Figure D-22: Pumping Pressure with 59 ms air valve opening time, 9 ms fuel valve opening time, and 78 PSIG air supply. (052405_08.mat)

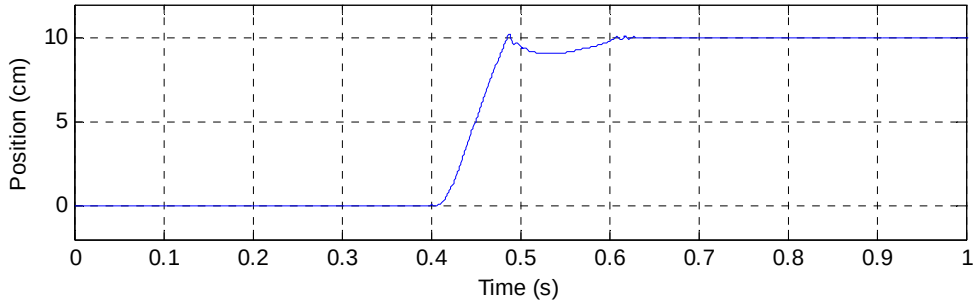

Figure D-23: Position of Free Piston with 59 ms air valve opening time, 9 ms fuel valve opening time, and 78 PSIG air supply. (052405_08.mat)

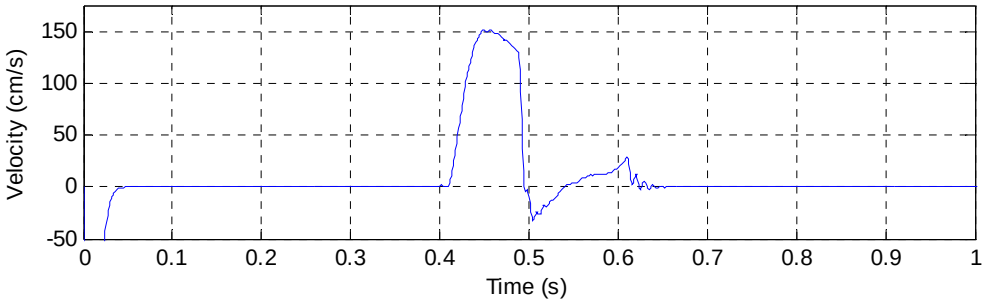

Figure D-24: Velocity of Free Piston with 59 ms air valve opening time, 9 ms fuel valve opening time, and 78 PSIG air supply. (052405_08.mat)

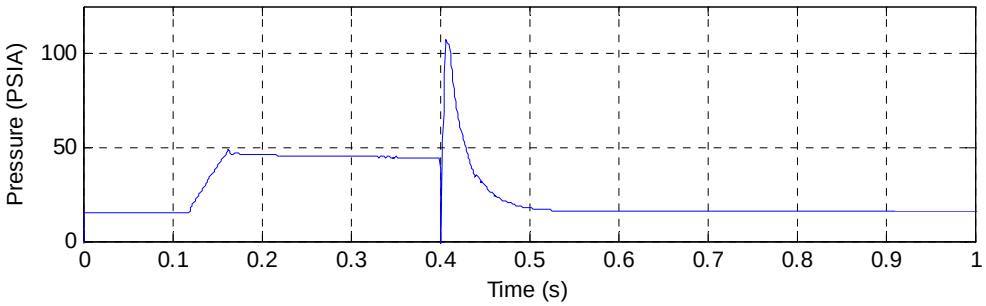

Figure D-25: Combustion Pressure with 59 ms air valve opening time, 9 ms fuel valve opening time, and 78 PSIG air supply. (052405_14.mat)

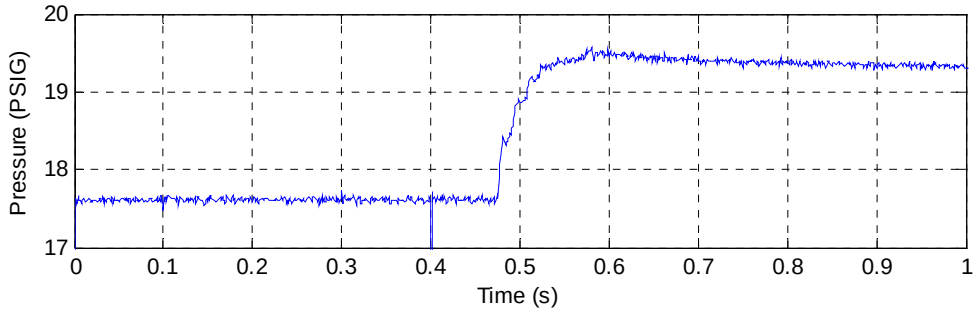

Figure D-26: Pumping Pressure with 59 ms air valve opening time, 9 ms fuel valve opening time, and 78 PSIG air supply. (052405_14.mat)

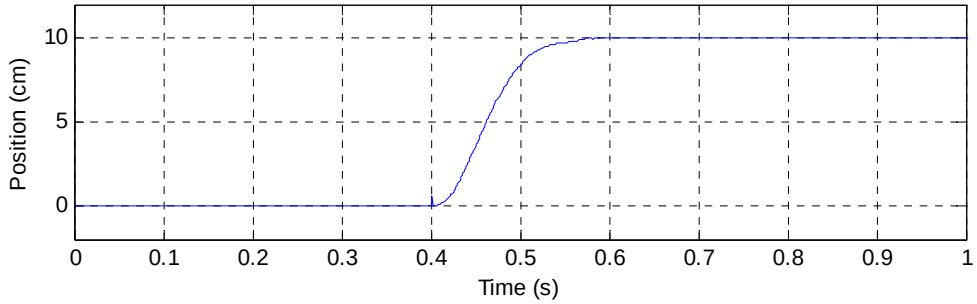

Figure D-27: Position of Free Piston with 59 ms air valve opening time, 9 ms fuel valve opening time, and 78 PSIG air supply. (052405_14.mat)

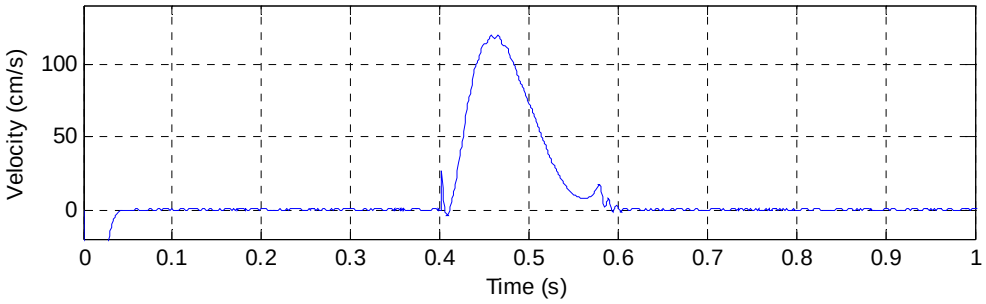

Figure D-28: Velocity of Free Piston with 59 ms air valve opening time, 9 ms fuel valve opening time, and 78 PSIG air supply. (052405_14.mat)

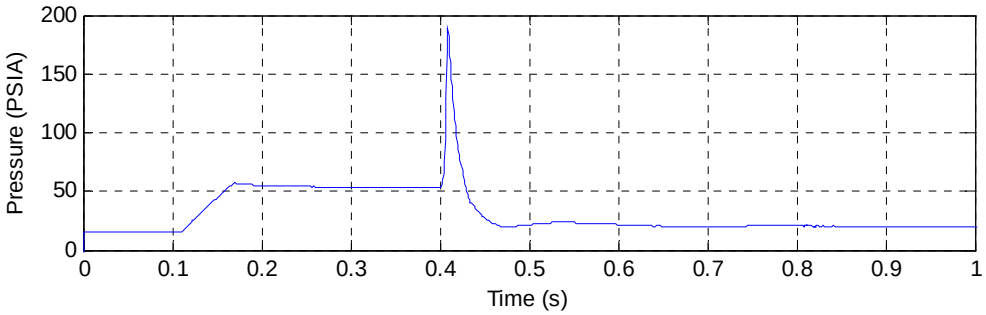

Figure D-29: Combustion Pressure with 67 ms air valve opening time, 10 ms fuel valve opening time, and 78 PSIG air supply. (052405_15.mat)

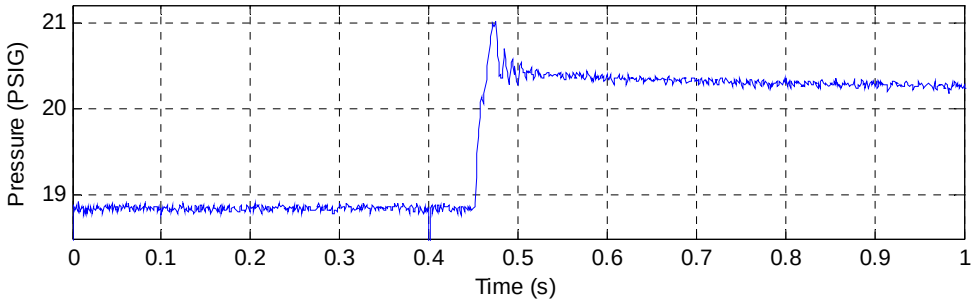

Figure D-30: Pumping Pressure with 67 ms air valve opening time, 10 ms fuel valve opening time, and 78 PSIG air supply. (052405_15.mat)

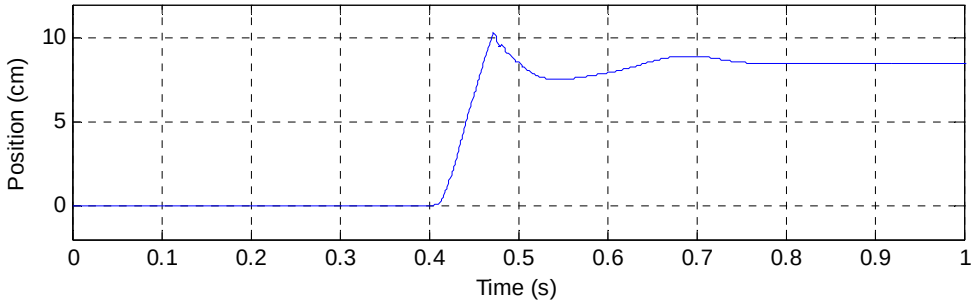

Figure D-31: Position of Free Piston with 67 ms air valve opening time, 10 ms fuel valve opening time, and 78 PSIG air supply. (052405_15.mat)

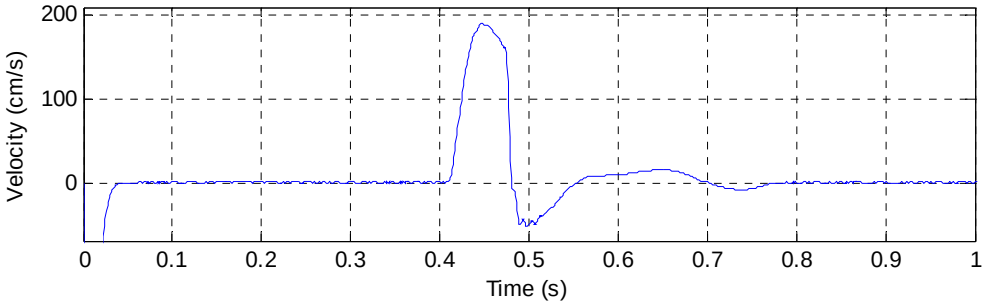

Figure D-32: Velocity of Free Piston with 67 ms air valve opening time, 10 ms fuel valve opening time, and 78 PSIG air supply. (052405_15.mat)

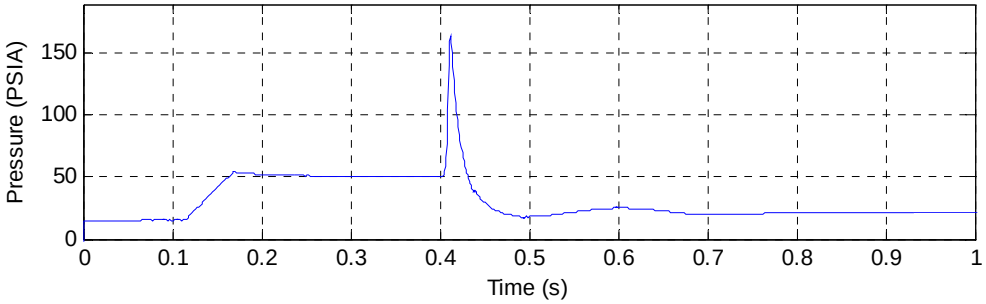

Figure D-33: Combustion Pressure with 67 ms air valve opening time, 10 ms fuel valve opening time, and 78 PSIG air supply. (052405_30.mat)

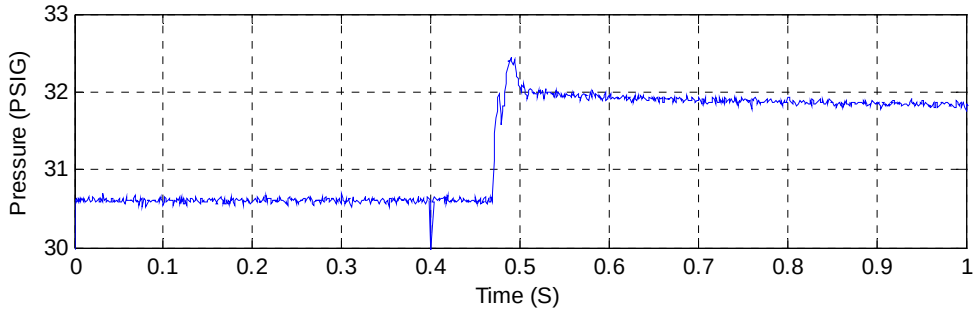

Figure D-34: Pumping Pressure with 67 ms air valve opening time, 10 ms fuel valve opening time, and 78 PSIG air supply. (052405_30.mat)

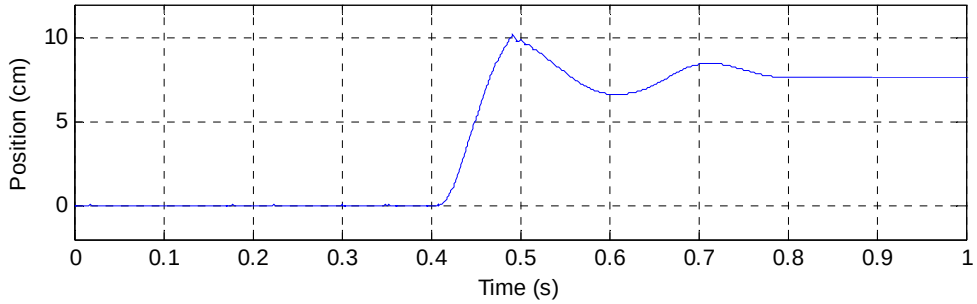

Figure D-35: Position of Free Piston with 67 ms air valve opening time, 10 ms fuel valve opening time, and 78 PSIG air supply. (052405_30.mat)

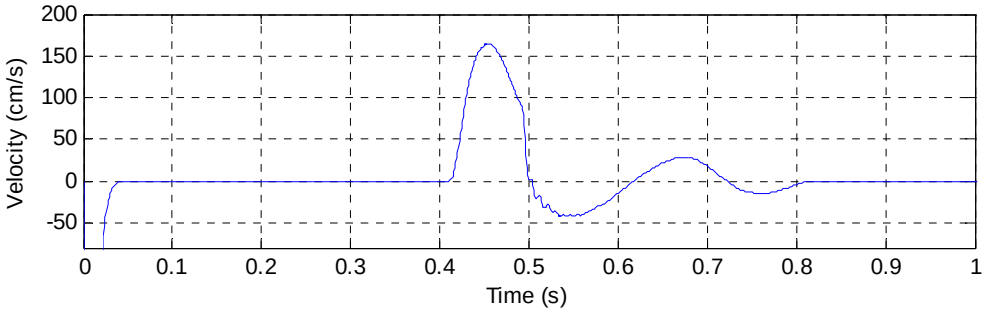

Figure D-36: Velocity of Free Piston with 67 ms air valve opening time, 10 ms fuel valve opening time, and 78 PSIG air supply. (052405_30.mat)